THE UNIVERSITY OF QUEENSLAND

DIVISION OF CIVIL ENGINEERING

REPORT CH63/07

FREE SURFACE, BUBBLY FLOW AND TURBULENCE MEASUREMENTS IN HYDRAULIC JUMPS

AUTHORS: Frédéric MURZYN & Hubert CHANSON

HYDRAULIC MODEL REPORTS

This report is published by the Division of Civil Engineering at the University of Queensland. Lists of recently-published titles of this series and of other publications are provided at the end of this report. Requests for copies of any of these documents should be addressed to the Civil Engineering Secretary.

The interpretation and opinions expressed herein are solely those of the author(s). Considerable care has been taken to ensure accuracy of the material presented. Nevertheless, responsibility for the use of this material rests with the user.

Division of Civil Engineering
The University of Queensland
Brisbane QLD 4072
AUSTRALIA

Telephone: (61 7) 3365 3619
Fax: (61 7) 3365 4599

URL: http://www.eng.uq.edu.au/civil/

First published in 2007 by
Division of Civil Engineering
The University of Queensland, Brisbane QLD 4072, Australia

ISBN No. 9781864998917

The University of Queensland, St Lucia QLD

FREE SURFACE, BUBBLY FLOW AND TURBULENCE MEASUREMENTS IN HYDRAULIC JUMPS

by

Frédéric MURZYN
Visiting Scholar, Department of Civil Engineering, School of Engineering,
The University of Queensland, Brisbane QLD 4072, Australia
Presently: Lecturer, ESTACA Campus Ouest, Parc Universitaire de Laval - Changé
Rue Georges Charpak, BP 76121, 53061 Laval Cedex 9, France
Ph.: (33 2) 43 59 47 15, Fax : (33 2) 43 59 47 19, Email: fmurzyn@estaca.fr

and

Hubert CHANSON
Professor, Department of Civil Engineering, School of Engineering,
The University of Queensland, Brisbane QLD 4072, Australia
Ph.: (61 7) 3365 3619, Fax: (61 7) 3365 4599, Email: h.chanson@uq.edu.au
Url: http://www.uq.edu.au/~e2hchans/

REPORT No. CH 63/07
ISBN 9781864998917
Division of Civil Engineering, The University of Queensland,
August 2007

General view of the hydraulic jump (Flow from right to left): $Fr = 7.6$, $x_1 = 0.75$ m, $d_1 = 0.018$ m

ABSTRACT

The hydraulic jump is the rapid transition from a high-velocity (supercritical regime) to a low-velocity (subcritical regime) open channel flow. It is characterized by the interaction of some strong turbulence with a free surface leading to air entrainment (bubbles, droplets, splashes) with macro-scale vortices, kinetic energy dissipation and a bubbly two-phase flow structure. The aim of this report is to present new free surface and air-water flow measurements in hydraulic jumps with partially-developed inflow conditions for a wide range of inflow Froude numbers (Fr = 3.1 to 8.5, Re= 24,000 to 62,000). New experiments were conducted in a large-size facility using ultrasonic displacement meters to describe the free surface features and a double-tip conductivity probe to study the two-phase flow properties.

The mean and turbulent profiles of the air-water interface were documented. The data were processed in terms of some spectral analysis of the free surface fluctuations and compared with the frequencies of the horizontal oscillations of the toe. The free-surface measurements highlighted large fluctuations in the roller. A peak in free-surface fluctuation intensity was found in the first half of the roller reflecting the dynamic unsteady structure of the free surface in this flow region. This was followed by a gradual decrease in turbulent intensity. The normalized maximum free-surface fluctuation was found to be proportional to the inflow Froude number (Fr). Spectral analyses of the free-surface fluctuations showed dominant frequencies ranging from 0.5 to 4 Hz with decreasing frequencies when increasing Froude number. While the dominant frequencies were nearly constant in the roller, lower values were observed downstream of the roller implying that faster vortical structures developed in the roller itself.

The air-water flow properties were investigated in terms of the distributions of void fraction, bubble count rate, bubble diameter, interfacial velocities, turbulent velocity fluctuations and turbulence time scales. The void fraction measurements (C) showed the presence of an advective diffusion shear layer where the air concentration vertical distributions were successfully compared with an analytical solution of the advective diffusion equation for air bubbles and compared well with earlier studies. The vertical distributions of bubble count rate (F) showed a marked peak (F_{max}), with increased count rates with increasing Froude number. In the air-water shear layer, the maximum bubble count rate (F_{max}) decayed with increasing distance from the jump toe as previously reported. Detailed results were presented concerning the mean bubble chord length, interfacial velocity and turbulent intensity. The vertical distributions of interfacial velocity followed closely a wall jet flow pattern. The turbulence intensity distributions exhibited large values in the jump roller with amplitude up to 400% for the largest Froude number. However the turbulence levels decreased with increasing distance from the jump toe. The probability density functions of bubble chord time exhibited a wide spectrum with a predominance of small bubble chord time for largest Froude numbers. The turbulence time scale data showed an increase with the relative elevation above the bed, as well as some decrease with increasing distance from the toe. Far downstream, nearly homogeneous profiles of turbulent time scales were observed with the smallest time scales.

Simultaneous measurements of free surface and bubbly flow properties suggested some possible correlation between free surface and bubble fluctuations in terms of frequency. Some cross-correlation analysis showed large fluctuations with negative and positive correlations. Some spectral analysis of the cross-correlation function indicated predominant frequencies between 1.2 to 2.3 Hz depending on the distance to the toe. These were in agreement with free-surface fluctuations. A comparative analysis of Froude similar experiments was conducted with Reynolds numbers ranging from 25,000 to 98,000, and inflow depths of 0.012, 0.018 and 0.024 m. The results implied that the experimental data obtained with inflow Reynolds numbers up to 98,000 cannot be extrapolated to large-size prototype structures without significant scale effects in terms of void fraction, bubble count rate and bubble chord time distributions. Te result has important implications in terms of civil, environmental and sanitary engineering structures where the prototype Reynolds numbers range typically from 1E+6 to over 1E+8.

Keywords: Hydraulic jumps, Turbulence, Air-water flow properties, Turbulence scales, Free-surface fluctuations, Froude numbers, Reynolds numbers, Spectral analysis, Physical modelling, Froude similitude, Scale effects.

TABLE OF CONTENTS

NOTATION

The following symbols are used in this report:

C	void fraction defined as the volume of air per unit volume of air;
C_{max}	maximum void fraction in the air bubble diffusion layer;
ch_{mbc}	mean bubble chord length (m)
D_t	turbulent diffusivity (m^2/s) of air bubbles in air-water flow;
D^*	dimensionless turbulent diffusivity: $D^* = \frac{D_t}{U_1 d_1}$;
d_{asw}	distance (m) above still water;
d_c	critical flow depth (m): $d_c = \sqrt[3]{q^2/g}$;
d_1	flow depth (m) measured perpendicular to the flow direction at the upstream gate;
d_2	flow depth (m) measured perpendicular to the flow downstream of the hydraulic jump;
F	bubble count rate (Hz), or bubble frequency (number of detected air bubbles per unit time);
F_{fs}	free-surface fluctuation frequency (Hz);
F_{max}	maximum bubble count rate (Hz) at a given cross-section;
F_{toe}	hydraulic jump tie oscillation frequency (Hz);
Fr	Froude number: $Fr = U_1/\sqrt{gd_1}$
g	gravity constant: g = 9.80 m/s^2 in Brisbane, Australia;
h	vertical step height(m);
L_r	roller length (m);
L_{scale}	geometric scaling ratio defined as the ratio of prototype to model dimensions;
Mo	Morton number defined as : $Mo = g\,\mu^4/(\rho\,\sigma^3)$
N	inverse of the exponent of the velocity power law;
N_{ab}	number of air bubbles per record;
Q	water discharge (m^3/s);
q	water discharge per unit width (m^2/s);
Re	Reynolds number: $\mathrm{Re} = \rho U_1 d_1/\mu$;
R_{xx}	normalised auto-correlation function (reference probe);
R_{xz}	normalised cross-correlation function between two probe output signals;
$(R_{xz})_{max}$	maximum cross-correlation coefficient between two probe output signals;
St	Strouhal number : $St = F_{toe} d_1/U_1$
Tu	turbulence intensity defined as: $Tu = \frac{u'}{V}$;
T	average air-water interfacial travel time between the two probe sensors (s);
T_{xx}	auto-correlation integral time scale (s): $T_{xx} = \int_{\tau=0}^{\tau=\tau(R_{xx}=0)} R_{xx}\,d\tau$;
$T_{0.5}$	characteristic time lag τ (s) for which $R_{xx} = 0.5$;
U_1	depth-averaged flow velocity upstream the hydraulic jump (m/s): $U_1 = q/d_1$;

U_2 depth-averaged flow velocity downstream the hydraulic jump (m/s): $U_2 = q / d_2$;

u' root mean square of longitudinal component of turbulent velocity (m/s);

V interfacial velocity (m/s);

V_c critical flow velocity (m/s): $V_c = \sqrt{g\, d_c}$;

V_{max} 1- maximum velocity (m/s) at outer edge of boundary layer;
2- maximum velocity (m/s) in the wall jet;

W channel width (m);

We Weber number;

x longitudinal distance from the upstream gate (m);

x_1 longitudinal distance from the gate to the jump toe (m);

y distance (m) measured normal to the channel bed;

y_{Cmax} distance (m) normal to the jet support where $C = C_{max}$;

y_{Fmax} distance (m) normal to the jet support where $F = F_{max}$;

y_{Vmax} distance (m) from invert where $V = V_{max}$;

y_{30} characteristic depth (m) where $C = 0.30$;

y_{50} characteristic depth (m) where $C = 0.50$;

y_{60} characteristic depth (m) where $C = 0.60$;

y_{80} characteristic depth (m) where $C = 0.80$;

$y_{0.5}$ distance (m) normal to invert where $V = V_{max} / 2$;

y_* distance (m) measured normal to the channel bed corresponding to boundary between turbulent shear layer and mixing layer

z transverse distance (m) from the channel centreline;

Greek symbols

δ boundary layer thickness (m) defined in term of 99% of the free-steam velocity: $\delta = y_{V=0.99V_{max}}$;

Δx longitudinal distance (m) between probe sensors (double-tip conductivity probe);

η free surface level (m) of the jump above channel bottom;

η' root mean square of the free surface level fluctuation (m);

$\Delta\eta$ maximum fluctuation of the free surface motion (m);

μ dynamic viscosity of water (Pa.s);

ν kinematic viscosity of water (m^2/s);

ρ density (kg/m^3) of water;

σ surface tension between air and water (N/m);

τ time lag (s);

$\tau_{0.5}$ characteristic time lag τ (s) for which $R_{xz} = 0.5(R_{xz})_{max}$;

Subscript

air air flow;

c	critical flow conditions;
max	maximum;
xx	auto-correlation of reference probe signal;
xz	cross-correlation;
1	upstream flow conditions;
2	downstream flow conditions;
50	flow conditions where $C = 0.50$;

Abbreviations

P / D	partially-developed inflow conditions;
rms	root mean square.

DEDICATION

Frédéric MURZYN and Hubert CHANSON dedicate this report to the memory of the late Professor D. Howell PEREGRINE (1938-2007) who passed away on 20 March 2007 ([1]). Professor Howell PEREGRINE did his Ph.D. at the University of Cambridge under the supervision of Professor T. Brooke BENJAMIN and he graduated in 1965. He joined the Mathematics Department at the University of Bristol (UK) in 1964. He worked there until his official retirement in 2004, and he was still an active researcher after his retirement. The extra-ordinary contribution of Professor PEREGRINE to fluid dynamics encompassed 57 journal articles which were cited more than 1,880 times in the last 40 years, yielding a h-index of 22 (Ref. Web of Science™).

Photograph of Howell PEREGRINE (© University of Bristol, 2006. Photo by Paul GROOM)

Professor Howell PEREGRINE was influential in the study of the interactions between turbulence and free-surface, which encompassed the present collaborative project. Both Frédéric MURZYN and Hubert CHANSON had many exchanges with Professor PEREGRINE on various topics including tidal bores, whirlpools, free-surface turbulence interactions and air bubble entrainment.

[1] Obituary. Professor D. Howell Peregrine. 30 December 1938 - 20 March 2007, by H.K. MOFFATT, *Journal of Fluid Mechanics*, Vol. 580, 2007, pp.1-2.

Professor PEREGRINE was truly instrumental in facilitating a close collaboration between applied mathematicians, coastal engineers, hydraulic engineers and mechanical engineers.

The report describes a series of detailed experimental measurements of turbulence properties in the bubbly flow region of hydraulic jumps. This topic captivated Professor D. Howell PEREGRINE. The experiments were conducted in Brisbane, Australia between May and June 2007. The report was published by the Division of Civil Engineering at the University of Queensland as part of the Hydraulic Model Series under the reference Report CH63/07 with the ISBN 9781864998917.

"Whilpools at Naruto, one of the sixty odd famous placed of Japan" by Hiroshige ANDO (1853-1856) - Modern reproduction in traditional style

1. INTRODUCTION

A hydraulic jump is the sudden transition from a supercritical open channel flow regime to a subcritical regime. It is characterised by a highly turbulent flow with macro-scale vortices, some significant kinetic energy dissipation, a two-phase flow region and some strong turbulence interactions with a free surface leading to splashes and droplet formation. Figures 1.1A and 1.1B show a sketch of a hydraulic jump flow with typical vertical distributions of void fraction and bubble count rate in the roller, together with the relevant notations used in the present report.

Fig. 1.1 - Air entrainment in a hydraulic jump with partially-developed inflow conditions

(A) Definition sketch

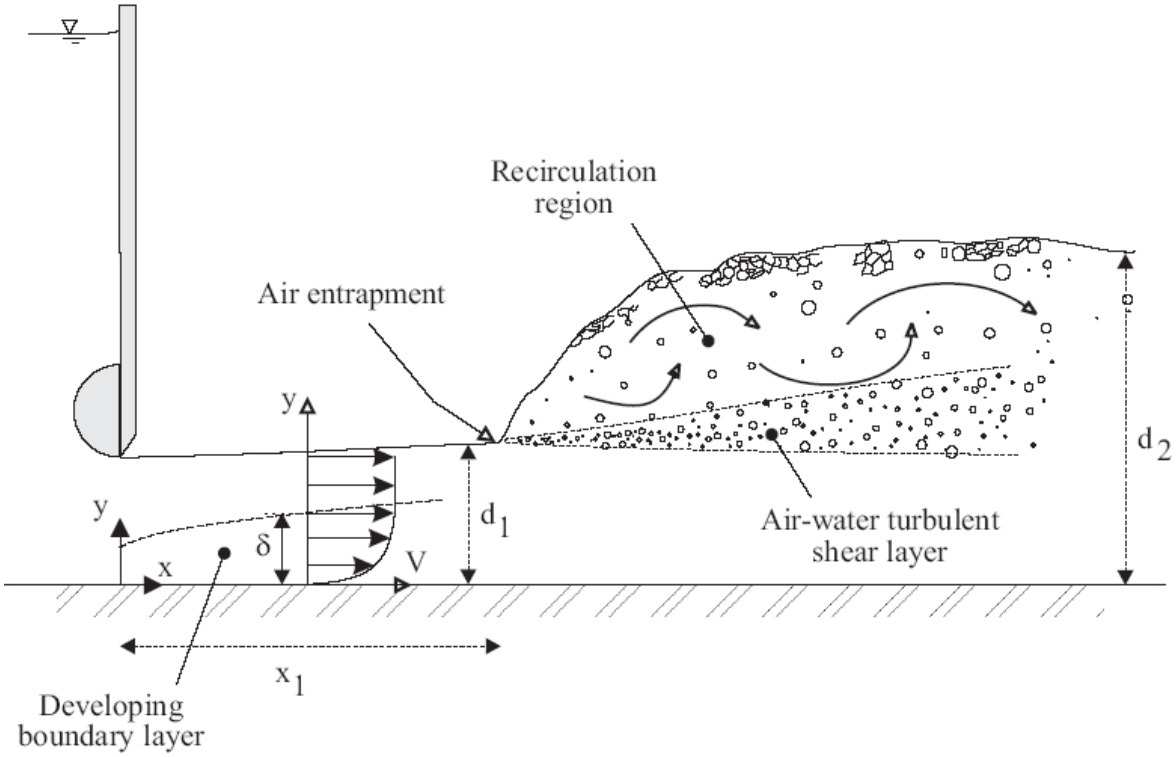

(B) Vertical distributions of void fraction *C* and bubble count rate *F*

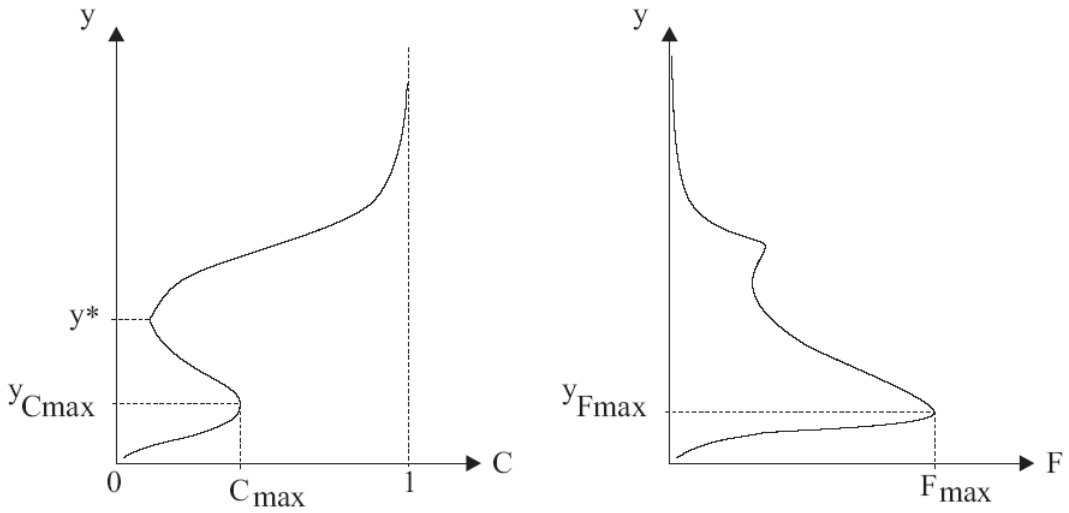

A hydraulic jump is defined by its inflow Froude number Fr :

$$Fr = \frac{U_1}{\sqrt{g d_1}} \tag{1.1}$$

where U_1 is the inflow velocity, d_1 is the inflow depth and g is the gravity acceleration. In a hydraulic jump, this number is always greater than unity (BELANGER 1828, HENDERSON 1966, CHANSON 2004).

Air bubble entrainment in a hydraulic jump starts for $Fr > 1$ to 1.3 (CHANSON 1997, MURZYN et al. 2007). The air entrainment is caused by the strong interaction between turbulence and free surface which generates disturbances of the air-water interface and vortex formation leading to some air entrapment. Generally, air bubble entrainment takes place when the turbulent stresses overcome the surface tension (ERVINE and FALVEY 1987, CHANSON 2007b). The physical mechanisms involved in this process are an important research topic in fluid mechanics as they have strong implications in terms of mixing processes with environmental applications, turbulence development, and oxygen transfer and air/sea gas exchanges. Furthermore, experimental studies in hydraulic jumps are relevant to the understanding of air entrainment in plunging jets, self-aerating flows and breaking waves with many applications in terms to sediment transport, coastal engineering, chemical and pollutant dispersion ...

Void fraction measurements in hydraulic jumps were first conducted by RAJARATNAM (1962). RESCH and LEUTHEUSSER (1972) performed hot-film probe measurements in the bubbly flow region and showed some effects of the upstream flow conditions. CHANSON (1995) highlighted the significance of maximum air concentration in the turbulent shear layer in hydraulic jumps with partially-developed inflow conditions. CHANSON and BRATTBERG (2000) showed that it decayed with increasing downstream distance from the jump toe. Some accurate analysis of the vertical void fraction profiles measured in the roller allowed to distinguish two regions: The first one extends from the bottom of the channel to a well-defined position $y = y^*$ (Fig. 1.1B). On this region ($y < y^*$), the void fraction profile satisfies a diffusion equation as shown by CHANSON (1997) and experimentally verified by MURZYN et al. (2005) with optical probes. This region ($y < y^*$) is the turbulent shear layer (Fig 1.1A). A second region extends from y^* up to the free surface. The air content is strongly dominated by interfacial aeration and large amplitude free surface motion. In this region ($y > y^*$), MURZYN et al (2005) suggested that void fraction profiles are well-described by a Gaussian error function. CHANSON (2006,2007c) developed the first systematic study of dynamic similarity and scale effects affecting the two-phase flow properties in hydraulic jumps.

Turbulence measurements in hydraulic jumps were conducted by several researchers, including ROUSE et al (1959), RESCH and LEUTHEUSSER (1972,1972b), CHANSON and BRATTBERG (1997, 2000), LIU et al (2004), MOUAZE et al. (2005), CHANSON (2006, 2007) and KUCUKALI and CHANSON (2007). These studies focused either on turbulence levels or on turbulence length and time scales developing at the free surface. MOUAZE et al (2005) identified some turbulent length scales associated with the free surface fluctuations along the hydraulics jumps using wire

gages and video analysis. Their experimental works were limited to low Froude numbers ($2 < Fr < 4.8$) while the study of CHANSON and BRATTBERG (2000) covered two Froude numbers ($Fr = 6.3$ & 8.5). CHANSON (2007,2007c) covered large Froude numbers ($Fr = 5$ to 8.6) and presented integral turbulent length and time scale data. KUCUKALI and CHANSON (2007) and GUALTIERI and CHANSON (2007) investigated respectively the air-water turbulence length and time scales, and the effect of Froude number on air entrainment in hydraulic jumps. Table 1.1 compares the flow conditions of recent experimental studies.

The present study aims to examine accurately the free surface motion as well as the air-water flow properties in hydraulic jumps with relatively large (inflow) Froude numbers ($3.1 < Fr < 8.5$). The experimental facility and instrumentation are described in section 2. The main results are presented in sections 3 and 4, and discussed in section 5.

Table 1.1 - Experimental conditions of previous and present investigations in hydraulic jumps

Reference (1)	Flow conditions (2)	Measurement technique(s) (3)	Comments (4)
MOSSA and TOLVE (1998)	Fr=6.42 to 7.3 Re=52,000 to 62,000 U_1=2.85 to 3.12m/s d_1=0.0185 to 0.020m x_1=0.90m P/D inflow conditions	Video-imaging CCD 10^5 pixels with 16.8 10^6 levels of grey pixels	W = 0.40m
CHANSON and BRATTBERG (1997,2000)	Fr=6.33 and 8.48 Re=33,000 to 44,000 U_1=2.34 and 3.14m/s d_1=0.014m x_1=0.50m P/D inflow conditions	+ Pitot-Prandtl tube, 3.3mm external diameter + Double-tip conductivity probe, 0.025mm inner electrode, 8mm tip spacing	W = 0.25m
MURZYN et al. (2005)	Fr=2.0 to 4.8 Re=46,000 to 88,000 U_1=1.50 to 2.19 m/s d_1=0.021 to 0.059 m	Double-tip optical fiber probe, 0.010mm sensor diameter, 1mm tip spacing	W = 0.30m
CHANSON (2006, 2007)	Fr=5.0 to 8.4 Re=25,000 to 95,000 U_1=1.85 to 3.9m/s d_1=0.013 to 0.029m x_1=0.5 and 1.0m P/D inflow conditions	Two single-tip conductivity probes (0.35mm inner electrode)	W = 0.25m
	Fr=5.1 and 8.6 Re=68,000 to 98,000 U_1=2.6 & 4.15m/s d_1=0.026 and 0.024m P/D inflow conditions		W = 0.50m
GUALTIERI and CHANSON (2007)	Fr=5.2 to 14.3 Re=24,000 to 58,000 U_1=1.86 to 4.9m/s d_1=0.012 to 0.013m x_1=0.5m P/D inflow conditions	Single-tip conductivity probe (0.35mm inner electrode)	W = 0.25 m
KUCUKALI and CHANSON (2007)	Fr=4.7 to 8.5 Re=50,000 to 98,000 U_1=2.28 to 4.12m/s d_1=0.024m x_1=1.0m P/D inflow conditions	Conductivity probes + single tip probe, 0.35mm inner electrode + double-tip probe, 0.25mm inner electrode, 7.0mm tip spacing Ultrasonic displacement meters	W = 0.50m
Present study	Fr=3.1 to 8.5 Re=23,750 to 64,100 U_1=1.32 to 3.56m/s d_1=0.018m x_1=0.75m P/D inflow conditions	Conductivity probes + single tip probe, 0.35mm inner electrode + double-tip probe, 0.25mm inner electrode, 7.0mm tip spacing Ultrasonic displacement meters	W = 0.50m

2. EXPERIMENTAL SET-UP, INSTRUMENTATION AND FLOW CONDITIONS

2.1 EXPERIMENTAL SET-UP

New experiments were performed in a horizontal rectangular flume at the Gordon McKAY Hydraulics Laboratory of University of Queensland (Fig 2.1). The channel width was 0.50 m. The sidewall height and flume length were respectively 0.45 m and 3.2 m. The sidewalls were made of glass and the channel bed was PVC. This channel was previously used by CHANSON (2005,2006,2007) and KUCUKALI and CHANSON (2007). Photographs of the experimental facility are shown in Figure 2.1 and in Appendix A.

Fig. 2.1 - Photographs of the experimental channel for hydraulic jump measurements at the Gordon McKAY Hydraulics Laboratory

(A) General view : Fr = 8.3, d_1 = 0.018 m, flow from left to right

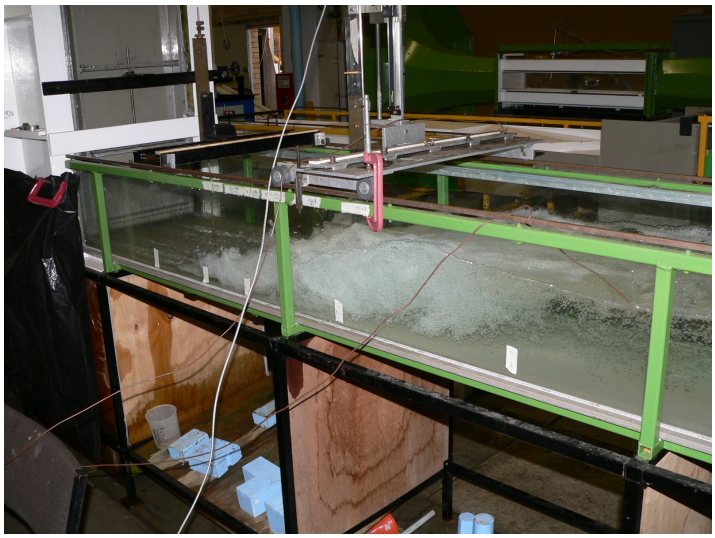

(B) Side view of the experiment : Fr = 7.6, d_1 = 0.018 m, Re = 57,250, flow from left to right

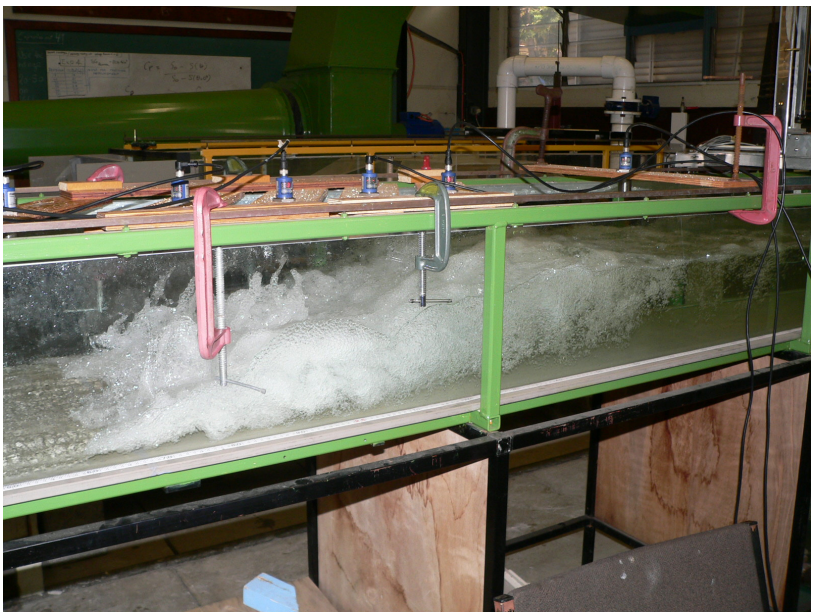

(C) Looking upstream: Fr = 8.3, d_1 = 0.018 m, Re = 62,250, flow from right to left

(D) Side view: Fr = 8.3, d_1 = 0.018 m, Re = 62,250, flow from right to left

2.2 INSTRUMENTATION

The water discharge was measured with a Venturi meter located in the supply line and which was calibrated on-site with a large V-notch weir. The discharge measurement was accurate within ±2%. The clear-water flow depths were measured using rail mounted point gages with a 0.2 mm accuracy. The inflow conditions were controlled by a vertical gate with a semi-circular rounded shape (∅ = 0.3 m) (Fig. 1A). The upstream gate aperture was fixed during all experiments (d_1 = 0.018 m) and all the experiments were performed with partially-developed inflow conditions.

2.2.1 Free surface measurements using ultrasonic displacement meters

The free surface data were measured using six ultrasonic displacement meters Microsonic™. These included five Mic+25/IU/TC with 0.18 mm accuracy and 50 ms response time, and one Mic+35/IU/TC sensor with 0.18 mm accuracy and 70 ms response time. Further informations on the sensors are reported in Appendix B. The displacement meters were mounted above the flow at a fixed location for all sets of experiments and they scanned downward the air-water flow interface (Fig. 2.2). In Figure 2.2B, the distances between all acoustic sensors (S1 to S6) are drawn at scale. Each probe signal output was scanned at 50 Hz per sensor for 10 minutes.

Fig. 2.2 - Ultrasonic displacement meters above the flow during measurements

(A) Side view photograph with flow from left to right

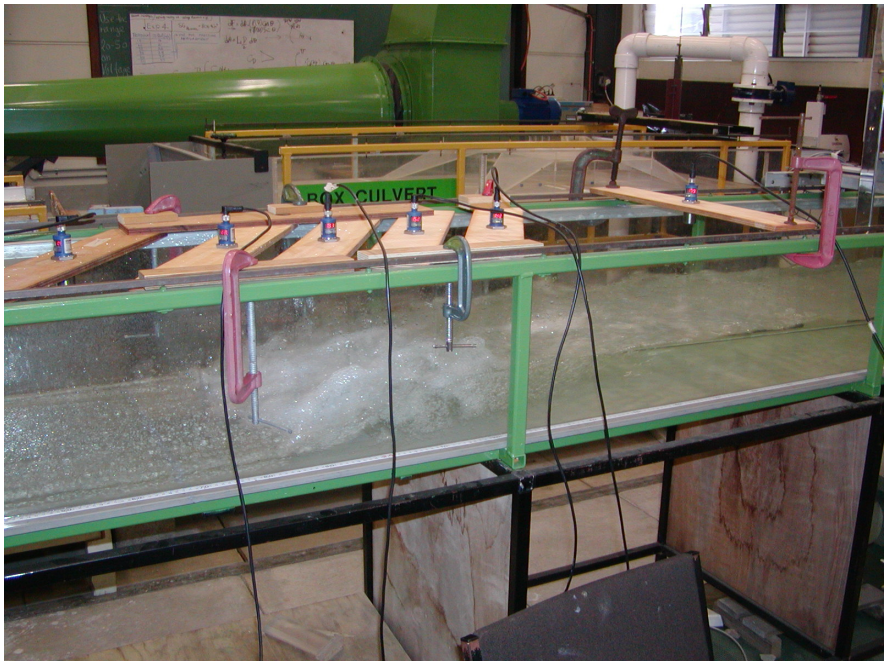

(B) Sketch of the experimental set-up with the sensor locations

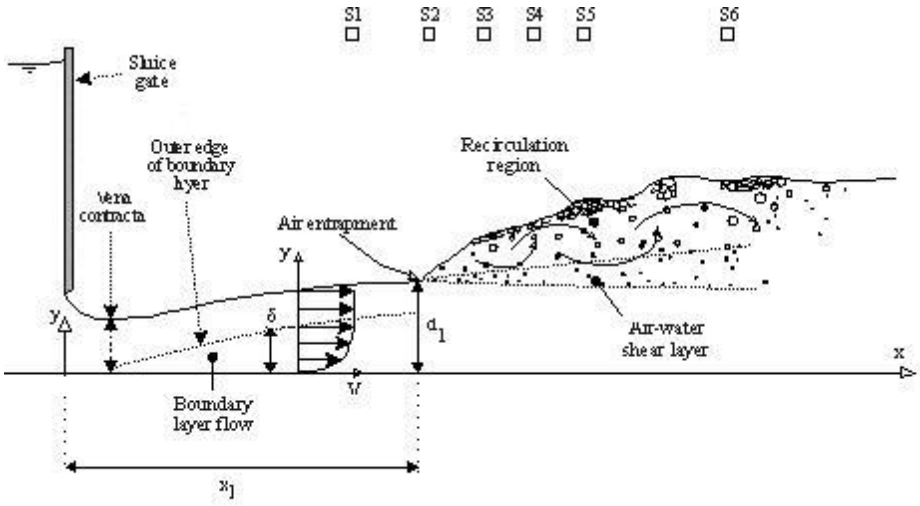

Fig. 2.3 - Examples of calibration curves for the acoustic displacement meters

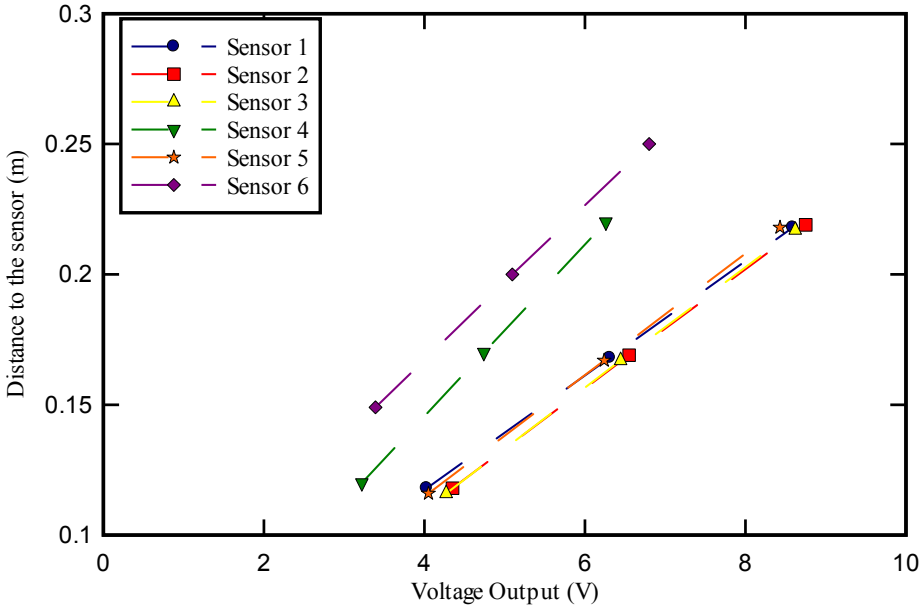

The principle of the acoustic displacement meters is based upon an acoustic beam emitted in air by the sensitive part of the acoustic displacement meter. The beam propagates downward perpendicular to the free-surface. Once it hits the air-water interface, the beam is reflected back to the sensor. From the knowledge of the sound celerity in air, a simple measure of the travel time provides the distance between the sensor and the free surface. Before each experiment, the sensors were calibrated. Some typical example of the linear relationship between voltage output and distance from sensor is shown in Figure 2.3. During the experiments, some erroneous data could be recorded for a number of reasons. Examples included :

- When the free surface was not horizontal. The acoustic beam did not reflect back to the receiver;
- When the free surface was a bubbly flow/foam region. CHANSON et al. (2002) tested an ultrasonic displacement meter Keyence™ UD300 in a bubbly column with up to 10% void fraction suggesting that the ultrasonic probe readings corresponded to about y_{50} to y_{60} where y_{xx} is the elevation where the void fraction is xx% . Recently, KUCUKALI and CHANSON (2007) suggested that response of these acoustics displacement meters corresponded to the range y_{60} to y_{80};
- When some "out of range" measurements were made. This happened when the distance between the sensor and the free surface was too large or too small. The problem was mainly encountered for the upstream ultrasonic displacement meter. In this case, the output voltage was saturated and the corresponding data were filtered as it did not represent true signal;
- When measurements were made in the roller or downstream of the toe for largest Froude numbers. In this case, some data errors were caused by bubbles, water splashes and droplets coming into contact with the sensitive part of the acoustic displacement meter.

Herein, the data were filtered to remove and replace erroneous points (Fig. 2.4). Figure 2.4 shows

an example of both original and filtered signals. In most cases, less than 7% of the data samples were also removed. For two data sets only, up to 20% were removed due to the large number of droplets impacting the ultrasonic displacement meter sensor. This happened for the largest Froude number.

Fig. 2.4 - Acoustic displacement meter data filtering - Flow conditions: Fr = 4.2, d_1 = 18 mm, x_1 = 0.75 m, sensor S4

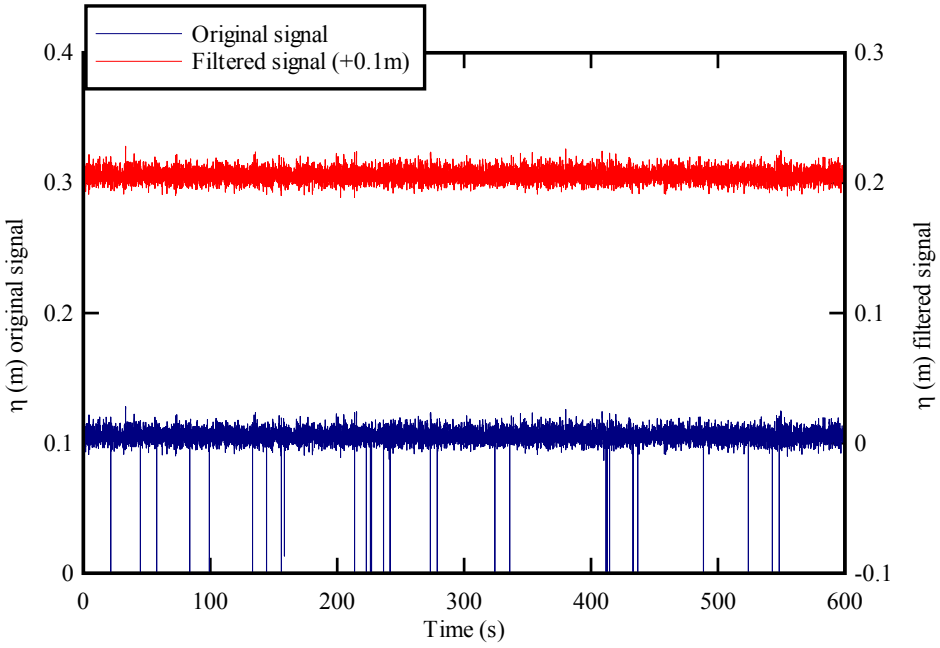

2.2.2 Air-water flow measurements using conductivity probes

The air-water flow properties were measured with a double-tip conductivity probe (Fig. 2.5). The probe was equipped with two identical sensors with an inner diameter of 0.25 mm. The distance between probe tips was Δx = 7.0 mm (Fig. 2.6). The probe was manufactured at the University of Queensland. It was previously used in several studies, including CHANSON (2005b), CAROSI and CHANSON (2006), CHANSON and CAROSI (2007), and KUCUKALI and CHANSON (2007).

The conductivity probe is a phase-detection intrusive probe designed to pierce the bubbles (Fig. 2.6). It is based on the difference in electrical resistance between air and water (CROWE at al. 1998, CHANSON 2002). Herein the dual-tip probe was excited by an electronic system (Ref. UQ82.518) designed with a response time of less than 10 μs. During the experiments, each probe sensor was sampled at 20 kHz for 45 s and the recorded output signal was a voltage ranging from 0 (air) to 4.5 V (water) (Fig. 2.7). Depending upon the Froude number, three to four vertical profiles were recorded at different cross-sections downstream of the jump toe. Each vertical profile contained at least 30 points. The displacement and the position of the probe in the vertical direction were controlled by a fine adjustment system connected to a Mitutoyo™ digimatic scale unit with a vertical accuracy Δy of less than 0.1 mm.

Fig. 2.5 - Dual-tip conductivity probe - Flow conditions: Fr = 7.6, d_1 = 0.018 m, y = 0.108 m, shutter speed: 1/250 s, flow from bottom right to top left

Fig. 2.6 - Sketch of the dual-tip conductivity probe developed at the University of Queensland - (Top) Side view; (Bottom) View in elevation

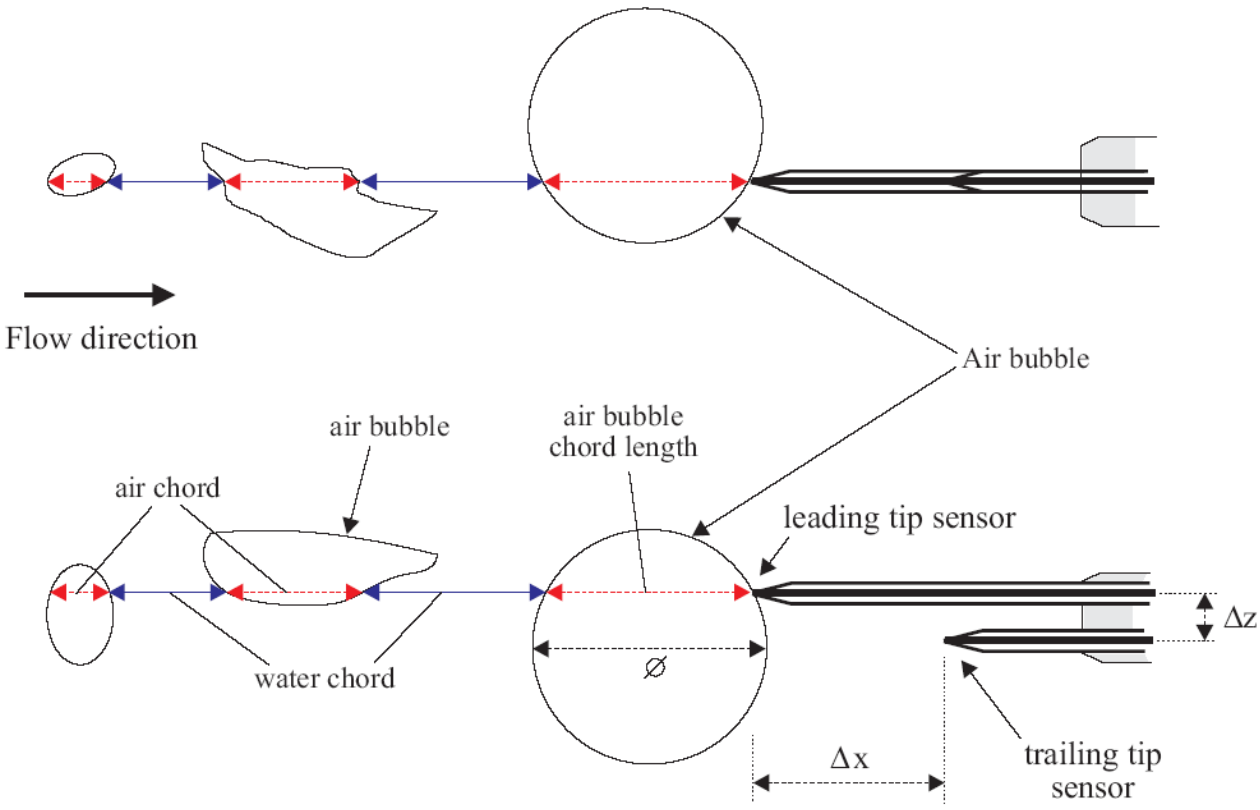

Fig. 2.7 - Signal output of a conductivity probe sensor with single threshold - Flow conditions: Fr = 5.1, d_1 = 0.018 m, x-x_1 = 0.09 m, y = 0.083 m, C = 0.19, F = 14 Hz

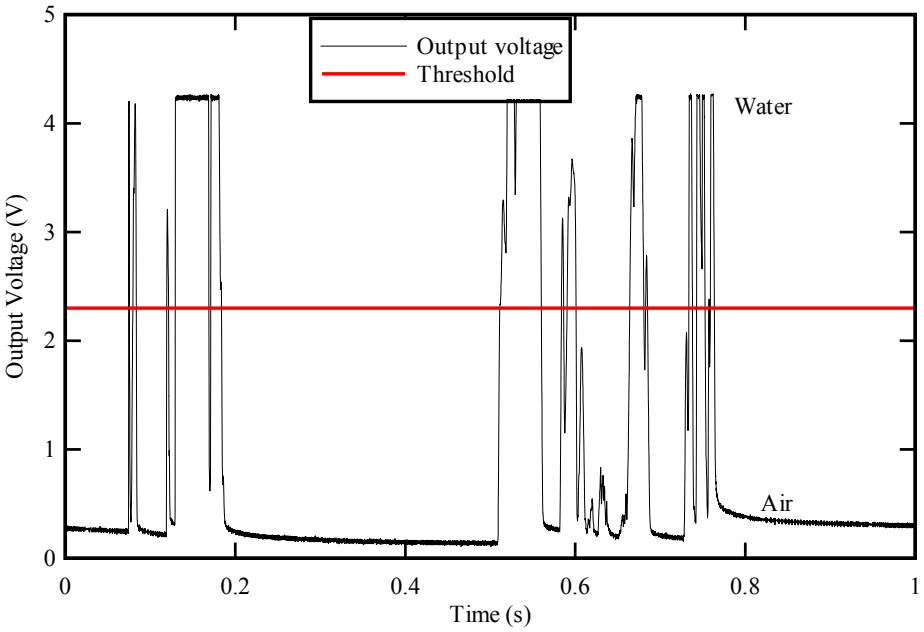

The analysis of the probe voltage output was based upon a single threshold technique, with a threshold set between 45% and 55% of the air–water voltage range. Below this threshold, the probe was in air whereas it was in water for larger voltage output voltages (Fig. 2.7). The error on the void fraction was expected to be less than 1% using this technique. The single-threshold technique is a robust method that is well-suited to free-surface flows (CHANSON and CAROSI 2006a).

A number of air-water flow properties may be derived from the signal analysis. These include the void fraction C defined as the volume of air per unit volume of air and water, the bubble count rate or bubble frequency F defined as the number of bubbles impacting the probe tip per second, and the air chord time distribution where the chord time is defined as the time spent by the bubble on the probe tip. The air-water interfacial velocities V were estimated as $V = \Delta x/T$ where Δx is the longitudinal distance between both tips (Δx = 7.0 mm here) and T is the average air-water interfacial time between the two probe sensors (CROWE et al. 1998, CHANSON 1997,2002) (Fig. 2.6 and 2.8). T was deduced from a cross-correlation analysis (Fig. 2.8 Right). The turbulence level Tu characterised the fluctuations of the air-water interfacial velocity between the probe sensors (CHANSON and TOOMBES 2002, CHANSON 2002). It was deduced from the shapes of the cross-correlation R_{xz} and auto-correlation R_{xx} functions :

$$Tu = 0.851 \frac{\sqrt{{\tau_{0.5}}^2 - {T_{0.5}}^2}}{T} \quad (2.1)$$

where $\tau_{0.5}$ is the time scale for which the normalised cross-correlation function is half of its maximum value such as $R_{xz}(T+\tau_{0.5}) = (R_{xz})_{max}/2$, $(R_{xz})_{max}$ is the maximum cross-correlation coefficient for $\tau = T$, $T_{0.5}$ is the time for which the normalized auto-correlation function equals 0.5

(Fig. 2.8). These notations are summarized on Figure 2.8.

The analysis of the signal auto-correlation function provided further information (CHANSON 2004b, CHANSON and CAROSI 2006a). The integral time scale T_{xx} represented a time scale relative to the longitudinal bubbly flow structures (Fig. 2.8). It was defined as:

$$T_{xx} = \int_{\tau=0}^{\tau=\tau(R_{xx}=0)} R_{xx} d\tau \quad (2.2)$$

where τ is the time lag and R_{xx} is the normalised auto-correlation function of the probe signal. T_{xx} was a characteristic time of the large eddies advecting the air-water interfaces in the longitudinal direction (MURZYN 2002, CHANSON 2007, CHANSON and CAROSI 2007).

In the present report, the data processing of correlation functions were conducted on the raw probe output signals. Indeed, any analysis based upon thresholded signals tends to ignore the contributions of the smallest air-water particles (CHANSON and CAROSI 2006a,2006b). Thus, all original files of 900,000 samples (sampling frequency of 20 kHz for 45 s) were segmented into 15 non-overlapping segments of 60,000 samples each. At a given position, the results in terms of turbulence intensities and integral time scales were averaged values over the 15 non-overlapping sub-segments.

Fig. 2.8 - Sketch of the auto and cross-correlation functions derived from the dual-tip probe signals

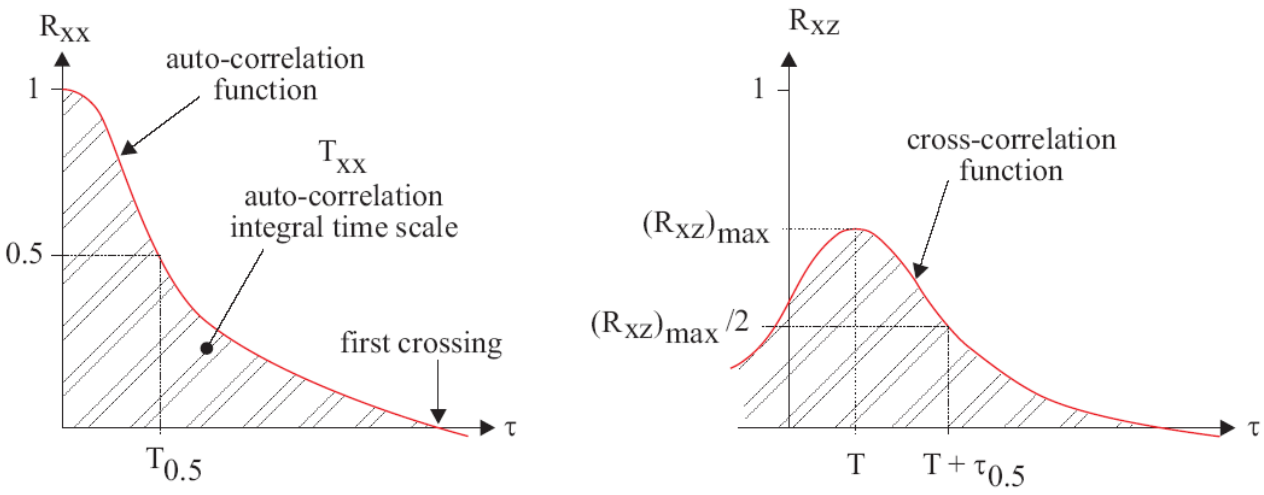

2.3 FREE-SURFACE MEASUREMENTS: A SHORT DISCUSSION ON THEIR ACCURACY

The measurements of free-surface fluctuations may be conducted with different methods. Two modern techniques are the wire gage and the acoustic displacement sensor. The first kind of probe is used in coastal engineering to measure wave height and/or period (e.g. MURZYN 2002). It is particularly accurate for periodic waves in absence of wave breaking. It may give some interesting result on the free surface turbulence length and time scales in different flows such as hydraulic jumps and jet beneath a free surface (MOUAZE et al 2005, MURZYN et al 2007). When the flow becomes strongly turbulent with large variations of the air-water interface associated with bubbles, splashes and droplets (hydraulic jumps with high Froude numbers, breaking waves), the output signal must be considered with some caution because the sensitive part of the probe is not

continuously immersed. Further most sensors have a dynamic response that is generally lower than 12 Hz (MURZYN et al. 2007). In some circumstances, this may not be large enough to describe accurately the rapid fluctuations of the free surface.

The second technique is based upon acoustic displacement sensors. It is more accurate in terms of the dynamic response. In our experiments, the sensor manufacturer specified with a response time less than 50 ms and the data rate was 50 Hz. Furthermore, the acoustic displacement meter is a non intrusive technique contrary to the wire gage. Thus, it does not disturb the flow. While the acoustic displacement sensor seems a well-defined measurement technique in hydraulic jumps, two questions remain nonetheless: what do these sensors exactly measure and what is their accuracy ? A first answer was given by KUCUKALI and CHANSON (2007). They suggested that the water level detected by these sensors corresponds to void fractions between 60 and 80%. This is in relatively good agreement with the earlier results of CHANSON et al (2002). In the present study, a similar comparison between displacement sensor outputs and void fraction profiles was conducted and the results will be discussed in the next chapter. The main conclusion suggested that acoustic sensors were well-suited to free surface measurements in hydraulic jumps with large Froude numbers and rapid fluctuations of the air-water interfaces.

Nowadays, newer measurement techniques are developed to characterise monophase turbulent flows with PIV (AMADOR et al., 2006) as well as complex two-phase flows with optical techniques (RYU et al. 2005, MURZYN et al. 2007). The first technique brings new interesting information on the velocity field (mean and turbulent) and turbulence shear stresses. Although it is more accurate for one-phase flow, it can also be used in multiphase flows but still limited to low void fractions ($C < 5\%$). It seems to be a promising technique which will certainly be improved in the next few years. The second technique is based on a measurement of the refractive index of the fluid. It is well-suited for measurements in hydraulic jumps and gives high quality results even for very-low void fraction down to $C \approx 0.001$ (MURZYN et al. 2007).

2.4 EXPERIMENTAL FLOW CONDITIONS

Several experimental flow conditions were tested. The foot of the jump, or jump toe, was always fixed at $x_1 = 0.75$ m. All sets of experiments were carried out with the same upstream rounded gate opening $d_1 = 0.018$ m. This will be taken as the upstream flow depth as well since the gate contraction coefficient was basically unity. Based on previous experiments made with the same experimental facility (CHANSON 2005), the inflow was characterised by a partially-developed boundary layer.

Two main series of measurements were conducted. The first series aimed to study the free surface properties using the acoustic displacement meters. The second series was related to the air-water flow analysis using a dual-tip conductivity probe. A summary of the flow conditions is given in Tables 2.1 and 2.2 where Q is the water discharge, x_1 is the position of the toe downstream of the upstream gate, d_1 is the upstream flow depth, U_1 is the upstream mean velocity, Fr is the Froude number, and Re is the corresponding Reynolds number :

$$\mathrm{Re} = \rho \frac{U_1 d_1}{\mu} \qquad (2.3)$$

where ρ and μ are respectively is the density and dynamic viscosity of water. In Table 2.1, S_1 to S_6 refer to the positions (x-x_1) of the six acoustic displacement meters. In Table 2.2, x-x_1 is the longitudinal position downstream of the toe where the vertical profiles were made using the dual-tip conductivity probe (Fig. 2.2B). The majority of the tests corresponded to a "steady jump" according to the traditional classification ([1]) and which is least sensitive to variation in tailwater depths, with a rate of energy dissipation from 45 to 70% and is regarded the best economical design. Full details of the data sets are given in the Appendices B and C. Note that some small oscillations of the toe were noticed and recorded during measurements. This point will be discussed in Chapter 3.

In the next part, the free surface results (mean profiles, turbulent fluctuations and frequency range) are presented first. Then, the air-water flow properties and simultaneous measurements with conductivity probe and acoustic sensors are discussed.

Table 2.1 - Experimental conditions for free surface measurements

	Q (m^3/s)	x_1 (m)	d_1 (m)	U_1 (m/s)	Fr	Re	x-x_1 S_1 (m)	x-x_1 S_2 (m)	x-x_1 S_3 (m)	x-x_1 S_4 (m)	x-x_1 S_5 (m)	x-x_1 S_6 (m)
1	0.012	0.75	0.018	1.32	3.1	23,750	-0.20	0.06	0.24	0.41	0.58	1.06
2	0.016	0.75	0.018	1.77	4.2	31,850	-0.20	0.06	0.24	0.41	0.58	1.06
3	0.020	0.75	0.018	2.21	5.3	39,800	-0.20	0.06	0.24	0.41	0.58	1.06
4	0.024	0.75	0.018	2.70	6.4	48,600	-0.20	0.06	0.24	0.41	0.58	1.06
5	0.028	0.75	0.018	3.17	7.6	57,050	-0.20	0.06	0.24	0.41	0.58	1.06
6	0.032	0.75	0.018	3.56	8.5	64,100	-0.20	0.06	0.24	0.41	0.58	1.06

Note : S_i :acoustic displacement sensor i (Fig. 2.2B).

Table 2.2 - Experimental conditions for air-water flow measurements

	Q (m^3/s)	x_1 (m)	d_1 (m)	U_1 (m/s)	Fr	Re	x-x_1 (m)	x-x_1 (m)	x-x_1 (m)	x-x_1 (m)
1	0.019	0.75	0.018	2.12	5.1	38,150	0.075	0.150	0.225	-
2	0.029	0.75	0.018	3.18	7.6	57,250	0.225	0.300	0.450	-
3	0.031	0.75	0.018	3.47	8.3	62,250	0.225	0.300	0.450	0.600

[1] For example, CHOW (1959), HENDERSON (1966), CHANSON (2004).

3. EXPERIMENTAL RESULTS

3.1 FREE SURFACE RESULTS

A basic characteristic of the hydraulic jump is the free surface profile and its fluctuations. Although the free-surface is well-defined upstream of the toe (nearly flat), it becomes strongly turbulent downstream of the impingement point with large vertical fluctuations and a bubbly/foamy structure (Fig. 2.1). In the roller, high amplitude motions and strong fluctuations in time and space occurred with increasing amplitude with increasing inflow Froude number. The aim of this first part is to investigate the free surface features in terms of mean and turbulent profiles, as well as the free-surface fluctuation frequencies. The measurements were performed using the acoustic displacement meters. The results are compared with some pertinent studies (Table 3.1).

Table 3.1 - Experiments measurements of hydraulic jump free-surface fluctuations

Reference	x_1 (m)	d_1 (m)	Fr	Re	W (m)	Instrumentation
MADSEN (1981)	0.1	0.024	2	23,000	0.15	Resistance gage.
MOSSA and TOLVE (1998)	0.9	0.020	6.4	57,000	0.45	PIV and photography.
MOUAZE et al. (2005)	0.35	0.059	1.98	88,230	0.30	Wire gages.
		0.032	3.65	64,965		
CHANSON (2006)	0.5	0.013	8.5	38,000	0.25	Visual observations.
	1.0	0.028	4.6	69,000		
		0.029	5.0	77,000		
		0.029	6.7	100,000		
		0.025	7.5	94,000		
	1.0	0.027	5.1	68,000	0.50	
		0.028	6.9	100,000		
		0.027	7.3	98,000		
		0.024	8.6	98,000		
KUCUKALI & CHANSON (2007)	1.0	0.024	4.7	54,335	0.50	Acoustic displacement meters.
			5.0	57,800		
			5.8	67,050		
			6.9	79,770		
			8.5	98,265		
Present study	0.75	0.018	3.1	23,750	0.50	Acoustic displacement meters.
			4.2	31,850		
			5.3	39,800		
			6.4	48,600		
			7.5	57,050		
			8.5	64,100		

Note : Hydraulic jumps with partially-developed inflow conditions

3.1.1 Mean profiles

Visual observations showed that the air-water interface exhibited small amplitude motions for the lowest Froude number, whereas it became strongly turbulent for the larger Froude numbers with large air packets and splashes projected above the air-water interface. For example, some droplets were even ejected out of the channel. This can be seen on photographs presented in Figure 2-1 and Appendix A.

Figure 3.1 presents some results obtained in terms of the mean free surface profile for six sets of experiments with inflow Froude numbers ranging from 3.1 to 8.5. In Figure 3.1, the position of the toe corresponds to $(x\text{-}x_1)/d_1 = 0$, where x is the longitudinal distance from the gate, x_1 is the jump toe position and d_1 is the inflow depth. Upstream, the free surface profile was flat with very-small fluctuations. First, let us notice that the upstream flow depths were between 0.017 m and 0.020 m which were close to the upstream gate aperture (d_1 = 0.018 m). The difference of about 10% was satisfactory considering the uncertainties of the sensors and the expected contraction coefficient of unity for the upstream rounded gate.

Second, downstream of the jump toe, a regular increase of the mean water level was noted. This pattern was in accordance with visual observations during the experiments and photographic evidences (App A). For inflow Froude numbers less than and up to Fr = 6.4, the jump roller surface was followed by a flat region where the flow was less turbulent: i.e., with large scale motion and low fluctuation frequencies. For these jumps (i.e. Fr < 6.5), the roller length (L_r) was estimated where L_r was defined as the distance over which the mean free surface level increased monotonically. The results are presented on Figure 3.2. The present data were in agreement with the experiments of MURZYN et al (2007) (1.9 < Fr < 4.8) and the correlation of HAGER et al (1990) developed for 2.5 < Fr < 8.

Fig. 3.1 - Dimensionless mean free surface profile (η/d_1) measurements in hydraulic jumps (Fr = 3.1 to 8.5)

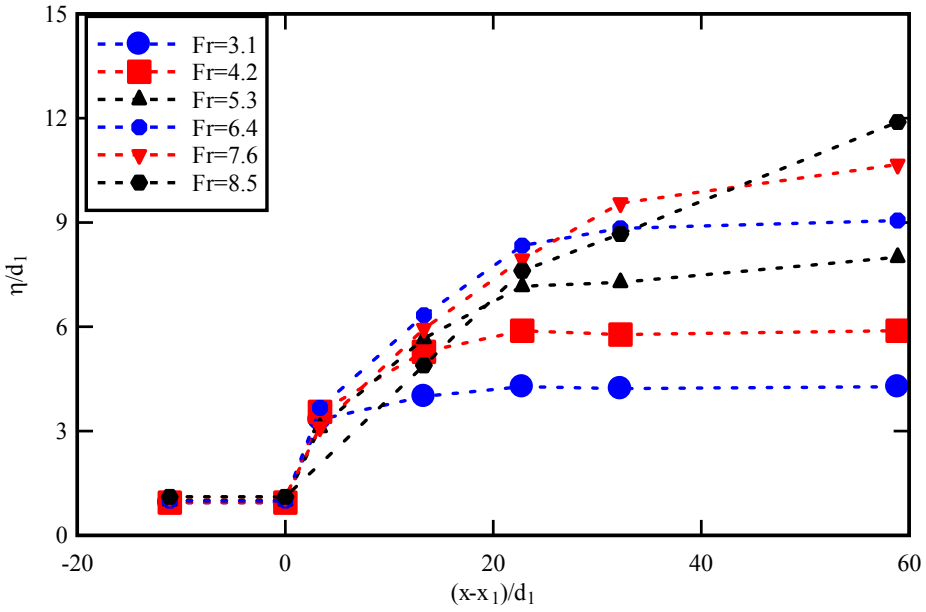

Fig. 3.2 - Measurements of dimensionless hydraulic jump roller length L_r/d_1 for Fr < 6.5 - Comparison with the correlations of HAGER et al. (1990) and MURZYN et al. (2007)

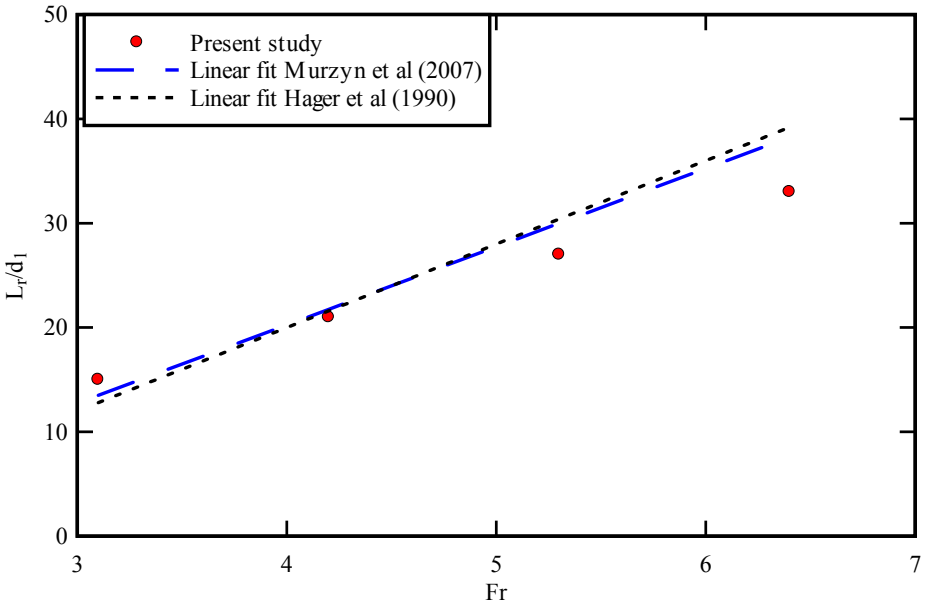

3.1.2 Turbulent fluctuations of the free-surface

The free surface fluctuations were investigated and some results are given in Figure 3.3. Figure 3.3 presents the dimensionless standard deviation of the water depth η'/d_1 as a function of the dimensionless distance from the jump toe $(x\text{-}x_1)/d_1$.

Upstream of the toe, the turbulent fluctuations η' were very small. Immediately downstream of the jump toe (i.e. $(x\text{-}x_1)/d_1 > 0$), a marked increase in free-surface fluctuation was recorded for all Froude numbers, reaching a maximum value η'_{max} which increased with increasing Froude number (Fig. 3.4). Further downstream, the free-surface fluctuations decayed with increasing distance from the jump foot. This pattern was consistent with the earlier studies of MOUAZE et al. (2005) and KUCUKALI and CHANSON (2007). It is characteristic of a dissipative area. Far downstream, the turbulence levels were small, with magnitudes comparable to those observed upstream of the impingement point.

The peak of turbulent fluctuations was observed in the first half of the roller (Fig. 3.3). This was in agreement with the findings of MOUAZE et al. (2005) who observed an intense turbulent area with a length of about 30% of the roller length. In that region, the flow is characterized by strong turbulence production, large recirculation vortices and coherent structures reaching the free surface. For Fr = 8.5, the highest fluctuations were close to 1.5 times the inflow depth ($1.5d_1$) whereas it was only about $0.3d_1$ for Fr = 3.1 (Fig. 3.4). This finding highlighted that the free surface motion became more turbulent with increasing inflow Froude number. In Figure 3.4, the present results are compared with the data of MADSEN (1981), MOUAZE et al. (2005) and KUCUKALI and CHANSON (2007) (Table 3-1). All the data collapsed into a monotonic curve best fitted by :

Fig. 3.3 - Dimensionless profiles of free surface fluctuations η'/d_1 in hydraulic jumps for several experimental conditions (Fr = 3.1 to 8.5)

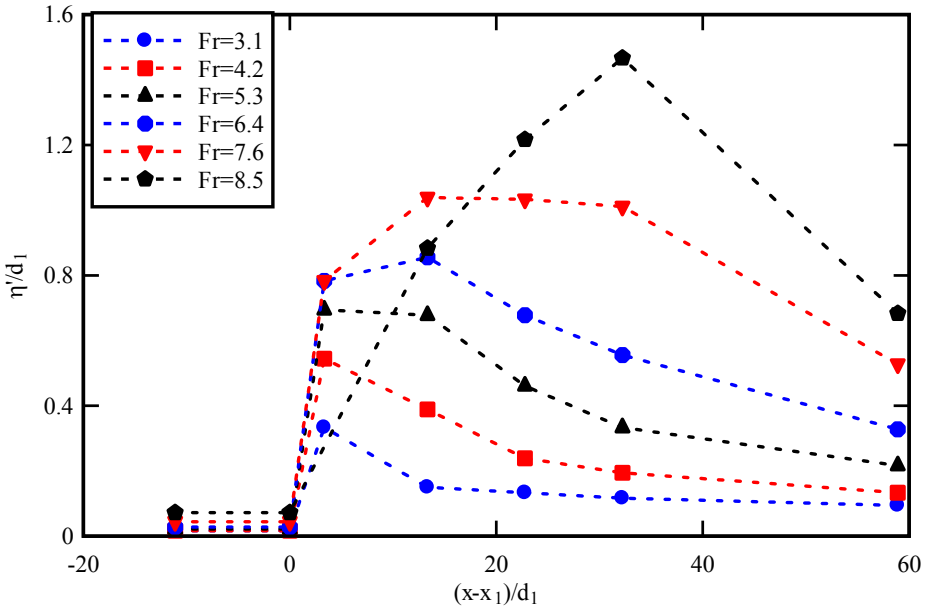

Fig. 3.4 - Maximum of turbulent fluctuations $(\eta'/d_1)_{max}$ in hydraulic jumps as a function of Froude number Fr - Comparison with the data of MADSEN (1981), MOUAZE et al. (2005) and KUCUKALI and CHANSON (2007), and Equation (3.1)

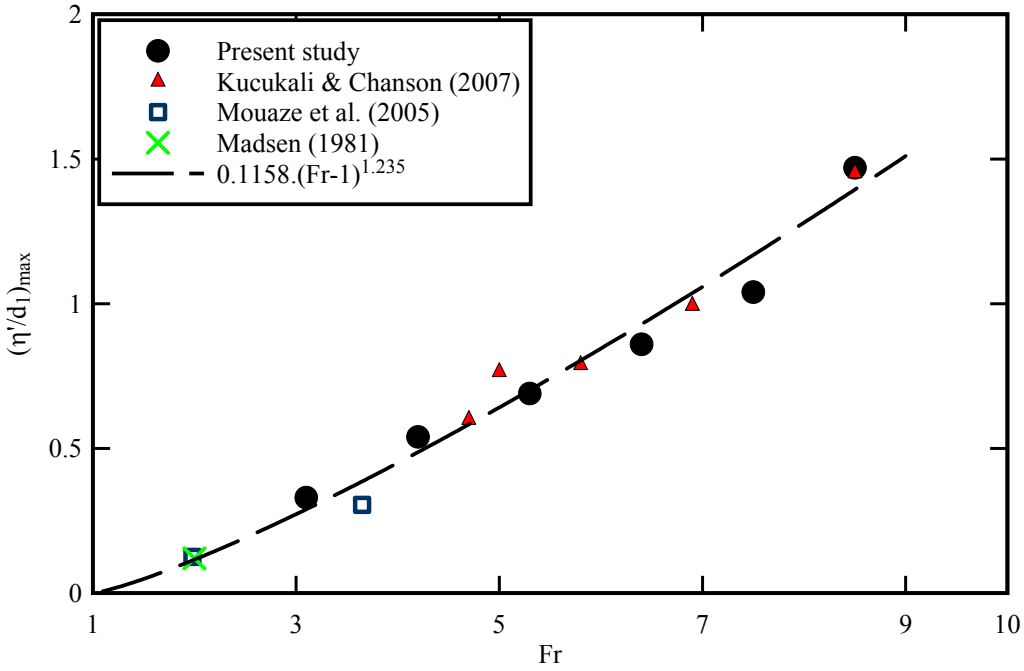

$$\left(\frac{\eta'}{d_1}\right)_{max} = 0.116(Fr-1)^{1.235} \quad (3.1)$$

with a normalised correlation coefficient of 0.985. For comparison, KUCUKALI and CHANSON (2007) proposed a linear fit :

$$\left(\frac{\eta'}{d_1}\right)_{max} = 0.22Fr - 0.46 \quad (3.2)$$

Equation (3.1) is compared with the experimental data in Figure 3.4.

3.1.3 Detection of the air-water interface

The present data were further analysed to bring new information on the free surface fluctuation characteristics in hydraulic jumps. Figure 3.5 presents the dimensionless relationship between the turbulent fluctuations $(\eta'/d_1)_{max}$ and the maximum amplitude of the free surface $(\Delta\eta/d_1)$. $\Delta\eta$ was the maximum free-surface fluctuation recorded during the 600 s sampling duration: $\Delta\eta = \eta_{max} - \eta_{min}$. The results indicated that the largest turbulent fluctuations were closely linked to the most important free surface amplitudes according to a well-defined linear trend. This behaviour was consistent with visual observations during the experiments.

A main point of interest was linked with the signal output from the acoustic displacement meters: i.e., their ability and accuracy to detect a "free surface position". Although previous studies gave some gross indication (CHANSON et al. 2002, KUCUKALI and CHANSON 2007), no definitive answer was available. Thus, a comparative analysis was conducted between the acoustic displacement meter and void fraction data. The latter were measured with the conductivity probe (see next paragraph). The mean depth recorded with the acoustic displacement meter was compared with the void fraction profile measured with the leading tip of the dual-tip conductivity probe. Some results are presented on Figure 3.6A where y^* is defined as the boundary between the turbulent shear layer and the upper part of the flow dominated by free surface strong fluctuations. The definition of y^* is sketched in Figure 3.6B. Figure 3.6A shows that the "free-surface" measurement η of the acoustic displacement sensor was slightly above the characteristic location y^* for all investigated Froude numbers. This suggests that the interface location measured by the acoustic sensor was within the recirculation region (Fig. 1.1). This region was typically a thin layer ($\eta > y^*$) where the void fraction was basically larger than 20%, rapidly reaching 90% and more. The present description is thought to be a more physical measure of the free-surface location in hydraulic jumps because it refers to a specific region of the flow. Altogether, however, the present results were in relatively good agreement with the experimental work of KUCUKALI and CHANSON (2007).

Fig 3.5 - Maximum turbulent fluctuations $(\eta'/d_1)_{max}$ as a function of maximum fluctuation of the free surface $(\Delta\eta/d_1)$

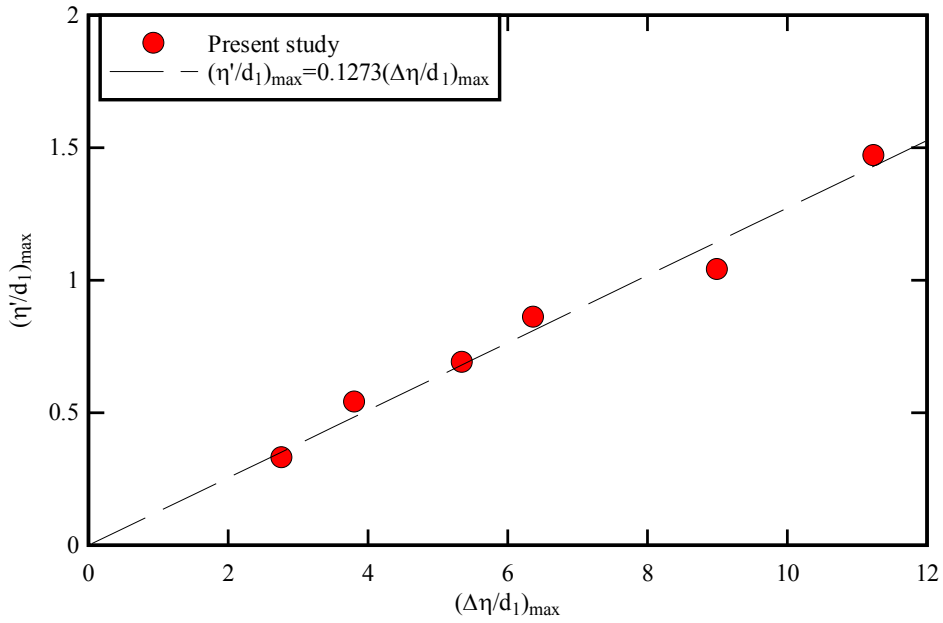

Fig 3.6 - Comparison of free surface and void fraction measurements using acoustic displacement sensor and dual-tip conductivity probe

(A) Experimental results

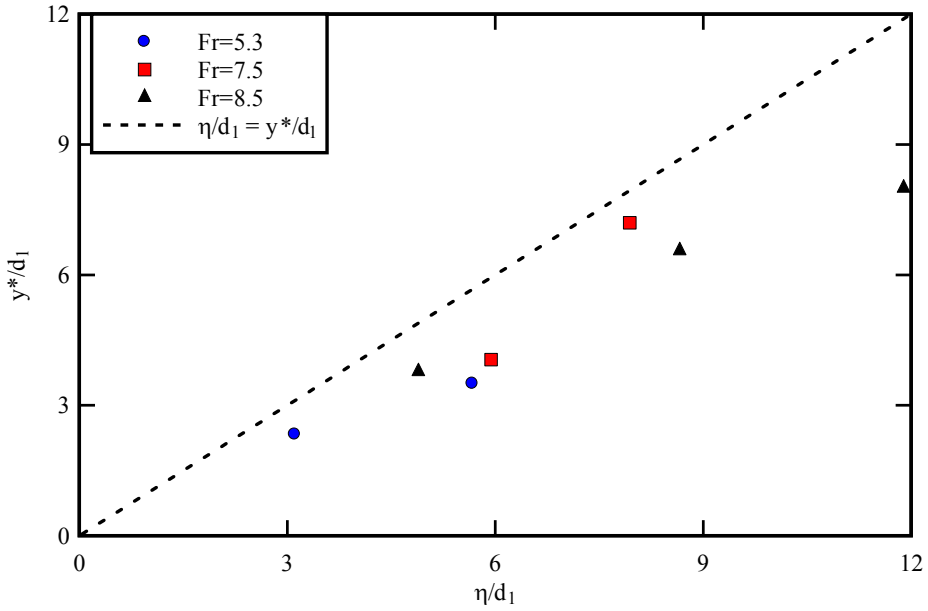

(B) Definition sketch of the vertical distribution of void fraction

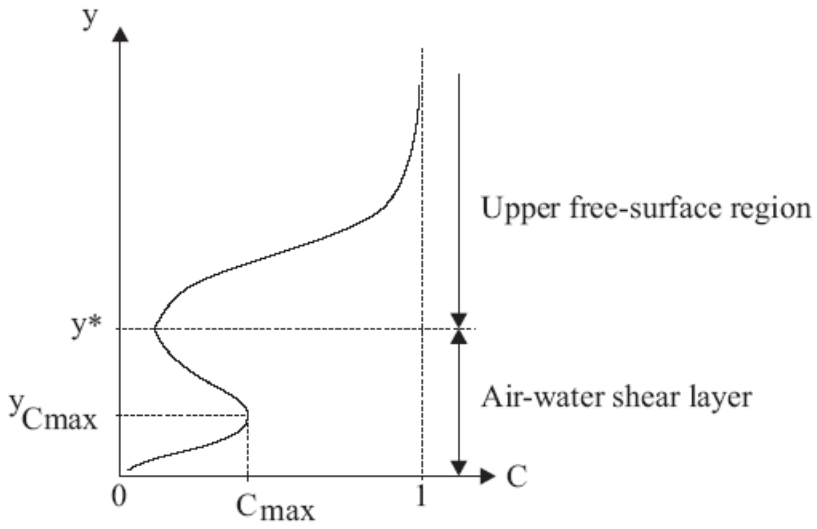

3.1.4 Frequency range in hydraulic jumps

Free-surface fluctuations

Some spectral analyses of the free-surface fluctuations were performed ([1]). The data processing provided new information on the time scales of the flow next to the upper free-surface. A typical Fast Fourier Transform (FFT) of a sensor output signal is presented in Figure 3.7. Both the raw and smoothed FFT data are shown ([2]). In the followings, the smooth FFT results were used in order to clearly identify the most important frequency(ies) occurring at the given position downstream of the impingement point. For example, in Figure 3.7, a peak is clearly marked at F_{fs} = 3 Hz depicting the main frequency of the free surface fluctuations at $(x\text{-}x_1)/d_1$ = 13.3 (acoustic sensor S3) for Fr = 4.2. This approach was applied to all flow conditions and the results yielded the dominant frequencies of the free-surface fluctuations in the hydraulic jumps. The results are presented on Figure 3.8, where the main frequency data are plotted as a function of the dimensionless distance from the jump toe $(x\text{-}x_1)/L_r$ where L_r is the roller length. The graph includes experimental results obtained both in the roller ($(x\text{-}x_1)/L_r < 1$) and downstream of the roller ($(x\text{-}x_1)/L_r > 1$).

Figure 3.8 indicates that the main frequency range was between 1 and 4 Hz ([3]). For a given inflow Froude number, the free-surface fluctuation frequency appeared to be constant in the roller ($(x\text{-}x_1)/L_r < 1$) while it decreased downstream for ($(x\text{-}x_1)/L_r > 1$). Downstream of the jump, the free surface dynamic was dominated by low frequency motions associated with largest time scales. The results (Fig. 3.8) seemed to be in good agreement with the flow visualizations. Note that the highest observed frequency was recorded in the hydraulic jump roller ($(x\text{-}x_1)/L_r < 1$) : $(F_{fs})_{max}$ = 4 Hz

[1] Calculations performed using the software DPlot™ {http://www.dplot.com/}.

[2] Smoothing window of 20 points.

[3] The finding was obtained independently of the sampling rate : i.e., 50 Hz for 20 min. (Section 3), or 5,000 Hz for 12 s (Section 4).

Fig. 3.7 - Spectral analysis of the free-surface fluctuations: raw FFT (Left) and smoothed FFT (right) of the free surface fluctuations - Flow conditions : $Fr = 4.2$, $d_1 = 0.018$ m, $x_1 = 0.75$ m, x-x_1 = 0.24 m (sensor S3)

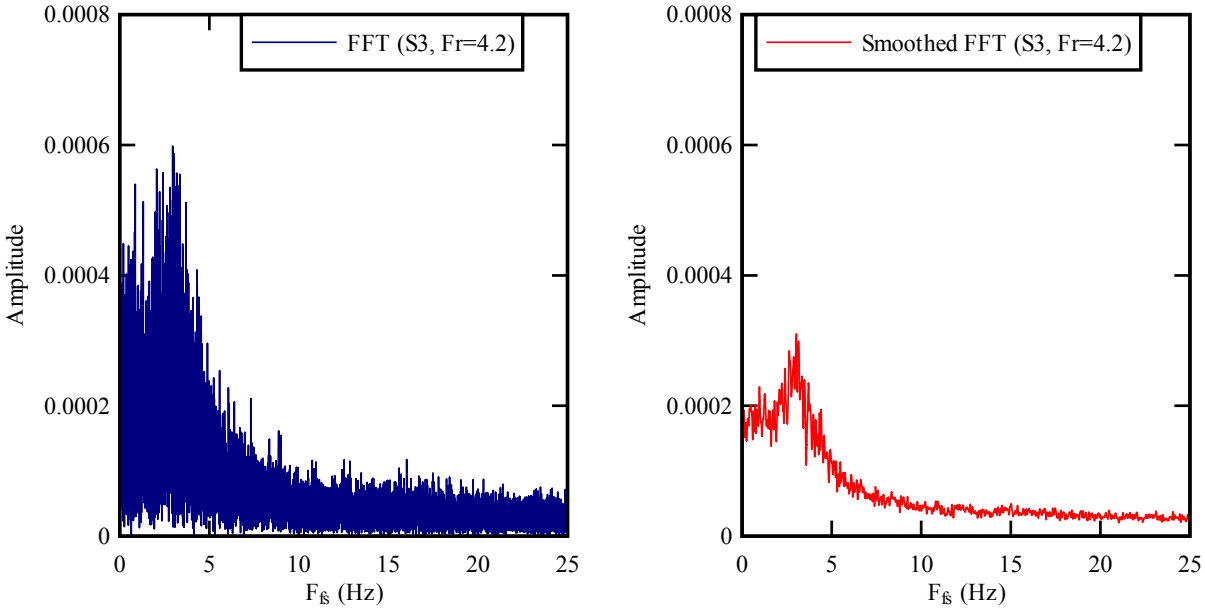

Fig. 3.8 - Main free surface frequencies of the free-surface fluctuations in hydraulic jumps

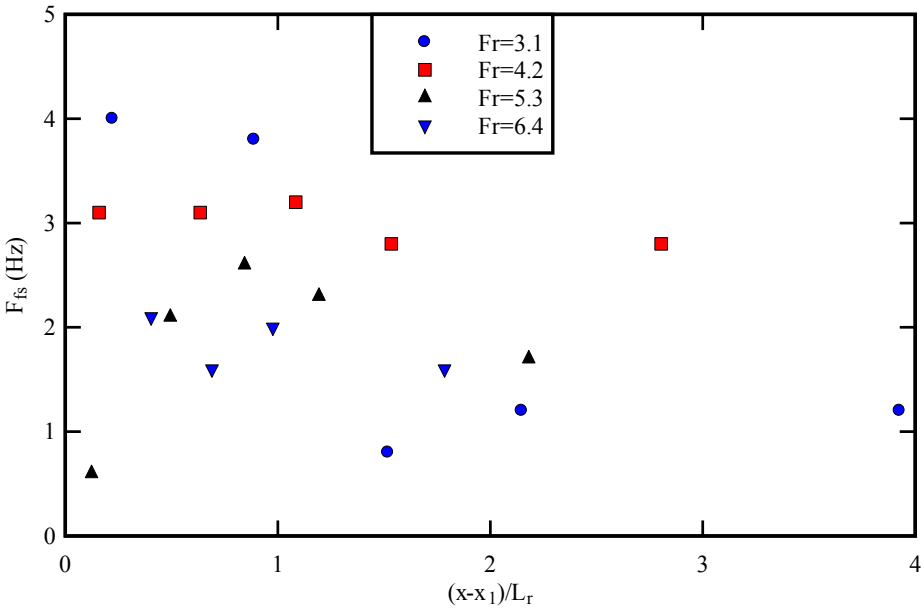

Jump toe oscillations

During the present experiments, the horizontal oscillations of the jump toe were recorded. These oscillations had relatively small amplitudes and their frequencies were estimated visually. The results are listed in Table 3.2, and the dimensionless data are plotted in Figure 3.9 in terms of the

Strouhal number defined as

$$St = \frac{F_{toe}\ d_1}{U_1} \tag{3.3}$$

where F_{toe} is the toe oscillation frequency and U_1 is the inflow velocity. The Strouhal number St is a dimensionless term characterising the oscillations of a physical system. The results were compared with the dimensionless free-surface fluctuation frequencies (Fig. 3.8) and with two earlier studies of jump toe oscillations (Table 3.2). The comparison is presented in Figure 3.9. The present jump toe data were close to the findings of MOSSA and TOLVE (1998) and CHANSON (2006) (Fig. 3.9 and Table 3.2).

The jump toe oscillation frequencies were consistently smaller than the free-surface fluctuation frequencies for a given Froude number (Fig. 3.9). In Figure 3.9, the free-surface frequency F_{fs} is the mean frequency observed above the roller ($(x\text{-}x_1)/L_r < 1$) for a given Froude number (Fig. 3.8). The comparative results indicated that the Strouhal number $F_{toe}d_1/U_1$ of the toe oscillations was nearly constant independently of the Reynolds number, whereas the Strouhal number $F_{fs}d_1/U_1$ of the roller surface fluctuations decreased with increasing Reynolds number (Fig. 3.9). These results were in agreement with the earlier findings of MOSSA and TOLVE (1998).

Table 3.2 - Experimental observations of jump toe longitudinal oscillations

Reference	x_1 (m)	d_1 (m)	Fr	Re	W (m)	F_{toe} (Hz)	St
MOSSA and TOLVE (1998)	0.90	0.020	6.4	57,000	0.45	0.67	0.0047
CHANSON (2006)	0.5	0.013	8.5	38,000	0.25	1.27	0.0055
	1.0	0.028	4.6	69,000		0.59	0.0069
		0.029	5.0	77,000		0.75	0.0081
		0.029	6.7	100,000		1.18	0.0096
		0.025	7.5	94,000		1.27	0.0086
	1.0	0.027	5.1	68,000	0.50	1.25	0.013
		0.028	6.9	100,000		1.47	0.011
		0.027	7.3	98,000		1.59	0.011
		0.024	8.6	98,000		2.0	0.011
Present study	0.75	0.018	5.1	38,300	0.50	0.47	0.0040
			7.6	57,070		0.68	0.0038
			8.3	62,300		0.77	0.0039

Note : Hydraulic jumps with partially-developed inflow conditions

Fig. 3.9 - Comparison between the dimensionless hydraulic jump toe oscillation frequency $F_{toe}d_1/U_1$ and dimensionless free-surface fluctuation frequency F_{fs} d_1/U_1 - Comparison with the jump toe oscillation data of MOSSA and TOLVE (1998) and CHANSON (2006)

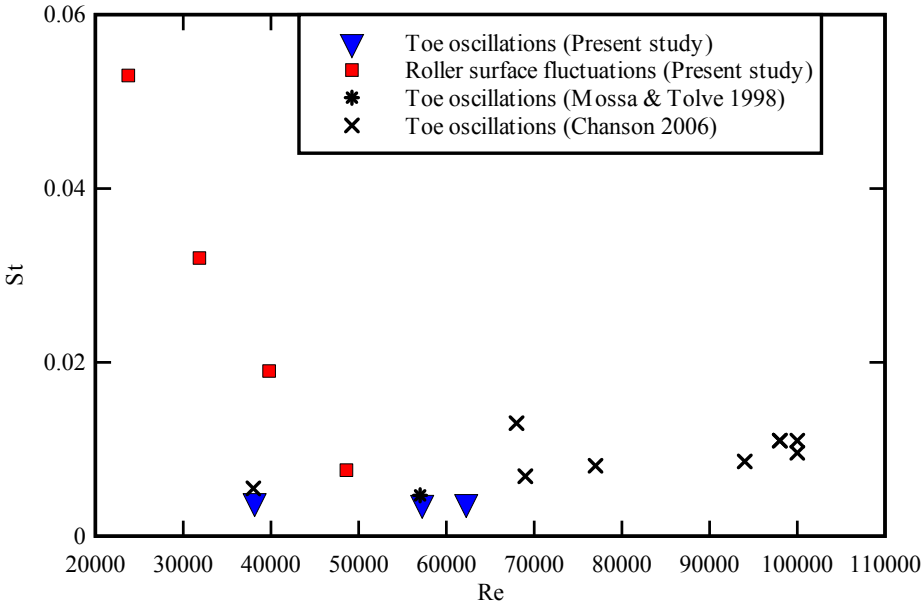

3.2 AIR WATER FLOW PROPERTIES

Hydraulic jumps are characterised by strong air bubble entrainment, spray and splashing (Fig. 2.1). Although many experimental studies investigated air entrainment in hydraulic jumps such as RAJARATNAM (1962, 1965), RESCH and LEUTHEUSSER (1972), CHANSON (1995, 1997, 2006, 2007), CHANSON and BRATTBERG (2000), MURZYN et al. (2005), KUCUKALI and CHANSON (2007), GUALTIERI and CHANSON (2007), there is still a lack of information and knowledge on many two-phase flow properties including turbulence characteristics in the roller, influence of Froude and Reynolds numbers on void fraction, bubble frequency. The aim of this sub-section is the investigation of the air-water flow structure and features. First some basic results are presented in terms of void fraction vertical profiles, bubble frequency and bubble size. These results can be used as the boundary conditions of the experiments. Then new results are exposed. They include mainly interfacial velocities, turbulent intensities, probability density function of bubble chord times and turbulence time scales. Table 3.3 summarises the experimental flow conditions, while key findings are summarised in Appendix D.

Table 3.3 - Detailed air-water flow measurements in hydraulic jumps with phase-detection intrusive probes

Reference	x_1 (m)	d_1 (m)	Fr	Re	W (m)	Instrumentation / Probe	Sensor size (mm)	Sampling rate (Hz)	Sampling time (s)
CHANSON & BRATTBERG (1997,2000)	0.5	0.014	6.3 8.5	35,500 43,700	0.25	Dual-tip conductivity	0.025	20,000	10
MURZYN et al. (2005)	0.35	0.059 0.046 0.032 0.021	2.0 2.4 3.7 4.8	88,000 75,000 65,000 46,000	0.30	Dual-tip optical fibre	0.010	< 1 MHz	120
CHANSON (2006)	1.0	0.024	5 8.5	68,000 98,000	0.5	Single-tip conductivity	0.35	20,000	45
KUCUKALI & CHANSON (2007)	1.0	0.024	4.7 5.8 6.9	54,000 67,000 80,000	0.50	Single-tip conductivity	0.35	10,000	48
			6.9	80,000		Dual-tip conductivity	0.25	10,000	48
Present study	0.75	0.018	5.1 7.6 8.3	38,000 57,000 62,000	0.50	Dual-tip conductivity	0.25	20,000	45

Note : Hydraulic jumps with partially-developed inflow conditions

3.2.1 Basic results

In hydraulic jumps, air bubble entrainment occurred at the intersection of the supercritical flow with the roller. Bubbles and air packets were entrained at the flow singularity formed by the impingement point (Fig. 1.1 & 2.2B). These were dispersed and advected downstream in a turbulent shear flow characterised by a range of relevant turbulent time and length scales. In the jump roller, two regions were identified. The lower part was dominated by the developing turbulent shear layer where air bubbles were broken up into small bubbles and entrained in this high shear stress region (Fig 1.1A and 3.6B). Above the turbulent shear layer, the upper free-surface region was characterized by large air contents, splashes and recirculation areas, with large eddies and a wavy free surface pattern.

The basic results included the void fraction profiles in hydraulic jumps. For Fr = 5.1 to 8.3, several vertical measurement profiles were conducted at different longitudinal positions $4.1 < (x\text{-}x_1)/d_1 < 34$ (Table 2.2). Figure 3.10 presents some typical results. In the developing shear layer, the data compared favourably with an analytical solution of the advective diffusion equation for air bubbles (CHANSON 1997) :

$$C = C_{max} \exp\left(- \frac{\left(\frac{y - y_{C\max}}{d_1} \right)^2}{4 D^* \left(\frac{x - x_1}{d_1} \right)} \right) \quad (3.4)$$

where C_{max} is the maximum void fraction in the shear layer, y_{Cmax} is the vertical elevation of the maximum void fraction C_{max}, D^* is a dimensionless turbulent diffusivity : $D^* = D_t/(U_1 d_1)$, D_t is the air bubble turbulent diffusivity which averages the effects of turbulent diffusion of longitudinal velocity gradient. Equation (3.4) is compared with some data in Figure 3.10. The results illustrated the Gaussian distributions of void fraction in the developing shear region.

The good agreement between Equation (3.4) and turbulent shear layer data was previously observed in hydraulic jumps with partially-developed inflow conditions, including a re-analysis of the data of RESCH and LEUTHEUSSER (1972) and CHANSON (1995), and the newer studies of CHANSON and BRATTBERG (2000), MURZYN et al. (2005), CHANSON (2006, 2007) and KUCUKALI and CHANSON (2007).

The peak of void fraction C_{max} was clearly marked for all investigated conditions (Table 3.3). At a given position downstream of the toe, C_{max} increased with increasing Froude number, while, for a given Froude number, it decreased with the distance from the jump toe. The present data are shown in Figure 3.11. A good agreement was observed with the results of KUCUKALI and CHANSON (2007), and with their correlation :

$$C_{max} = 0.07\, Fr\, \exp\left(-0.064\,\frac{x - x_1}{d_1}\right) \qquad (3.5)$$

Equation (3.5) is compared with the present data in Figure 3.11.

Fig. 3.10 - Dimensionless distributions of void fraction along the hydraulic jump - Comparison with Equation (3.4)
(A) $Fr = 5.1$

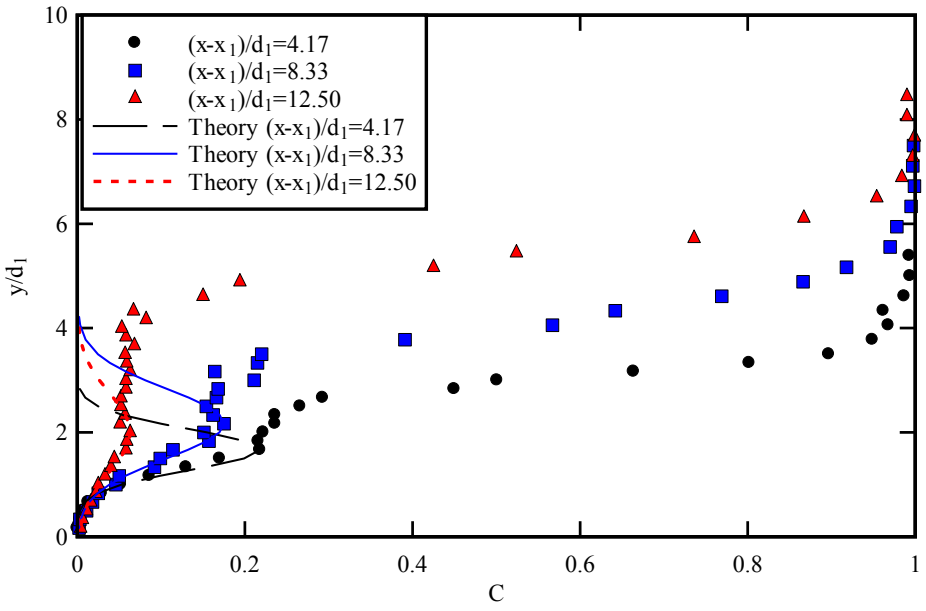

(B) *Fr* = 7.6

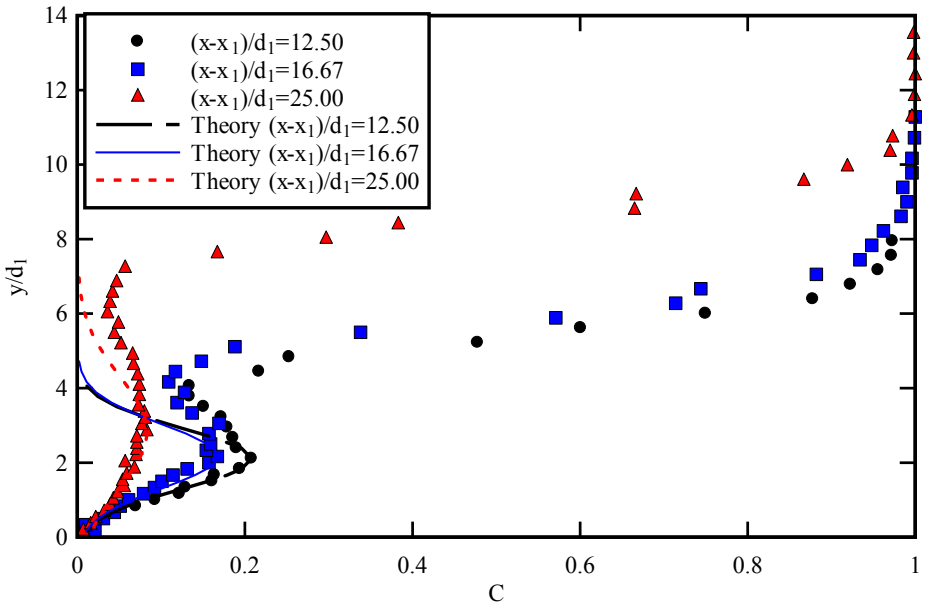
(x-x1)/d1=12.50
(x-x1)/d1=16.67
(x-x1)/d1=25.00
Theory (x-x1)/d1=12.50
Theory (x-x1)/d1=16.67
Theory (x-x1)/d1=25.00
y/d1
C
0
2
4
6
8
10
12
14
0.2
0.4
0.6
0.8
1

(C) *Fr* = 8.3

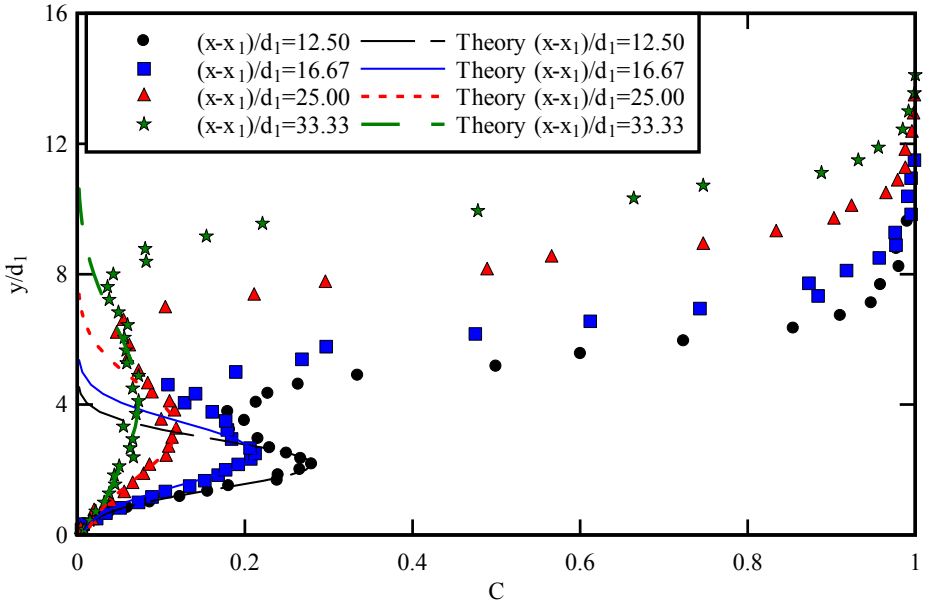
(x-x1)/d1=12.50
(x-x1)/d1=16.67
(x-x1)/d1=25.00
(x-x1)/d1=33.33
Theory (x-x1)/d1=12.50
Theory (x-x1)/d1=16.67
Theory (x-x1)/d1=25.00
Theory (x-x1)/d1=33.33
y/d1
C
0
4
8
12
16
0.2
0.4
0.6
0.8
1

Fig. 3.11 - Dimensionless longitudinal distributions of maximum void fraction in the shear layer C_{max} - Comparison with the data of KUCUKALI and CHANSON (2007) and Equation (3.5)

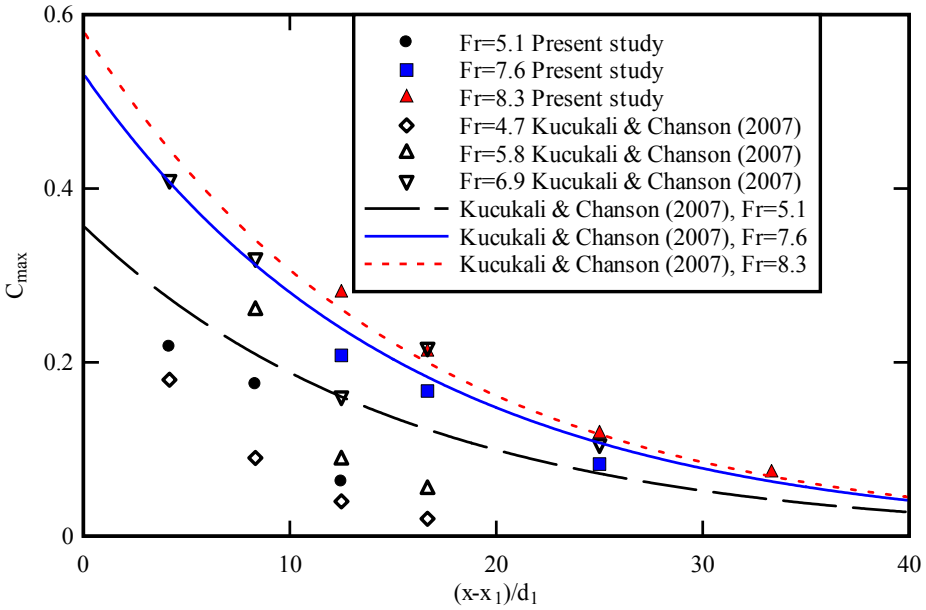

Fig. 3.12 - Dimensionless longitudinal distributions of y_{Cmax}/d_1 - Comparison with the data of KUCUKALI and CHANSON (2007) and the correlation of CHANSON and BRATTBERG (1997,2000) (Equation 3.6)

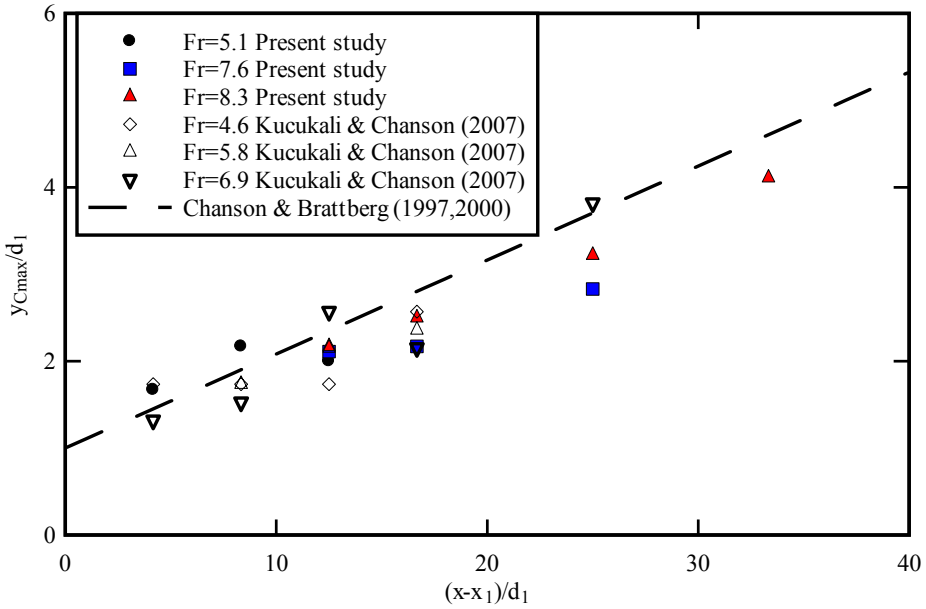

For a given Froude number, the vertical elevation of the maximum void fraction y_{Cmax}/d_1 increased with increasing distance from the toe (Fig. 3.12). This was linked with smaller shear stress and

larger buoyancy effects inducing some bubble de-aeration. The present results compared well with the data of KUCUKALI and CHANSON (2007), and with the findings of CHANSON and BRATTBERG (1997, 2000):

$$\frac{y_{C\max}}{d_1} = 1 + 0.11\frac{x - x_1}{d_1} \quad (3.6)$$

Equation (3.6) was compared successfully with a range of studies and it is shown in Figure 3.12.

Figure 3.13 presents some typical vertical distributions of dimensionless bubble count rate $F\ d_1/V_1$ where d_1 and U_1 are respectively the upstream flow depth and velocity. Note however the different scales of the horizontal and vertical axes of Figures 3.13A, 3.13B and 3.13C. The bubble count rate F is defined the number of air bubbles detected by the probe leading sensor per unit time and it is proportional to the specific air-water interface area. All the data exhibited a major peak of bubble count rate F_{max} in the developing shear region. This feature was previously documented by CHANSON and BRATTBERG (2000), MURZYN et al. (2005) and CHANSON (2007). KUCUKALI and CHANSON (2007) suggested that this peak in bubble count rate was linked with "high levels of turbulent shear stresses that break up the entrained air bubbles into finer air entities". The maximum bubble count rate F_{max} increased with increasing Froude number. For Fr = 5.1, F_{max} reached 55 Hz whereas it was nearly 124 Hz for Fr = 8.3 (Fig. 3.14). For a given Froude number, F_{max} decreased with an increasing distance from the impingement point as shown on Figures 3.14 and 3.15. Note that the vertical distributions of bubble count rate highlighted a second, smaller peak in the upper part of the flow. This is seen in Figure 3.13 and sketched in Figure 1.1B. It could be related to break up of air packets entrapped from above the free surface by large fluctuations of the air/water interface.

Fig. 3.13 - Dimensionless distributions of bubble count rate $F\ d_1/U_1$ in the hydraulic jump roller
(A) Fr = 5.1

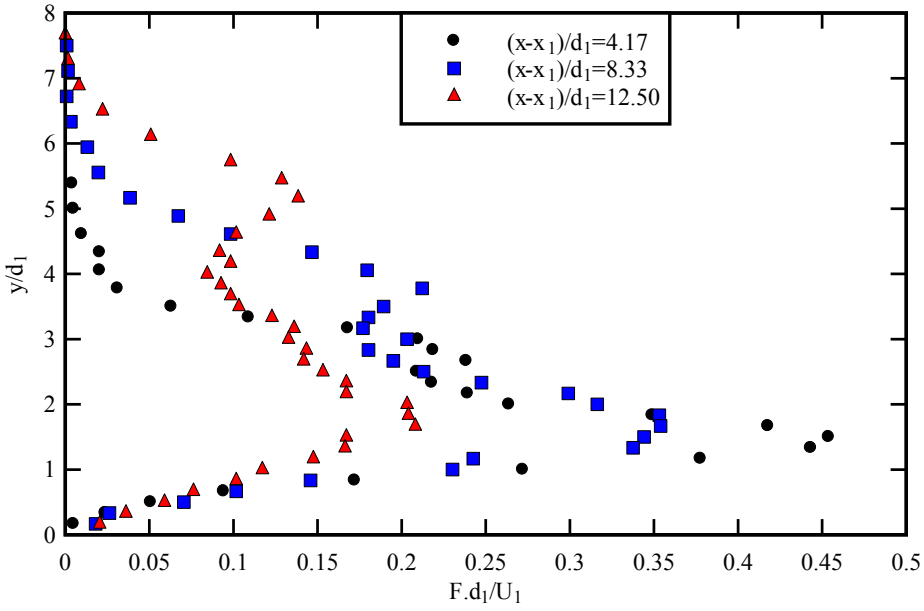

(B) *Fr* = 7.6

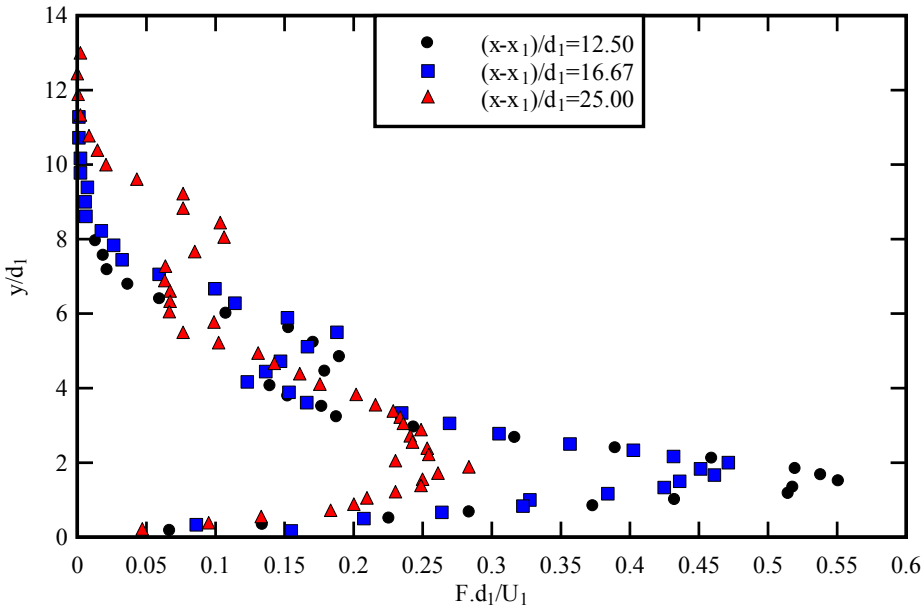
(x-x1)/d1=12.50
(x-x1)/d1=16.67
(x-x1)/d1=25.00
y/d1
F.d1/U1
0
2
4
6
8
10
12
14
0
0.05
0.1
0.15
0.2
0.25
0.3
0.35
0.4
0.45
0.5
0.55
0.6

(C) *Fr* = 8.3

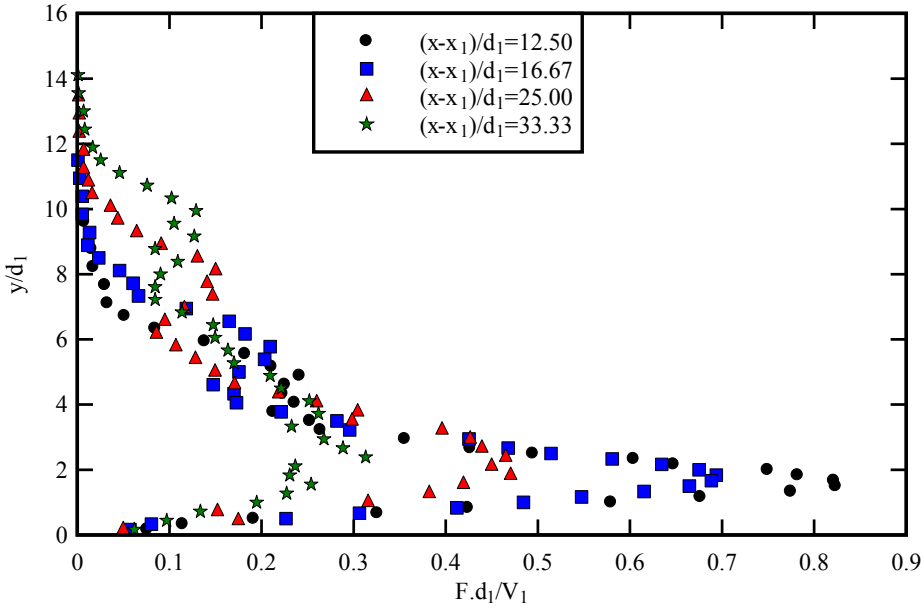
(x-x1)/d1=12.50
(x-x1)/d1=16.67
(x-x1)/d1=25.00
(x-x1)/d1=33.33
y/d1
F.d1/V1
0
2
4
6
8
10
12
14
16
0
0.1
0.2
0.3
0.4
0.5
0.6
0.7
0.8
0.9

Fig. 3.14 - Longitudinal distributions of maximum bubble count rate F_{max} in the hydraulic jump shear layer (Present study)

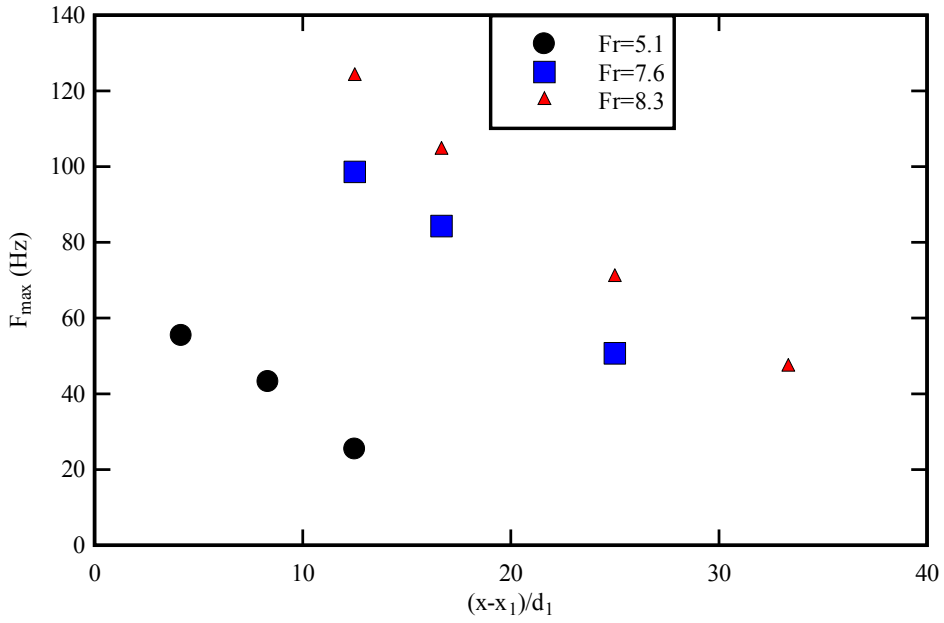

The dimensionless maximum bubble count rate data $F_{max}\ d_1/U_1$ were compared with earlier results (Fig. 3.15). The data showed consistently a longitudinal decay in maximum bubble count rate with increasing dimensionless distance downstream of the jump toe. Some data scatter is noted in Figure 3.15 that might be related to some difference in instrumentation and probe sensor sizes (Table 3.3). The present data however agreed well with the experimental results of CHANSON and BRATTBERG (2000), and their empirical correlation:

$$\frac{F_{max}\ d_1}{U_1} = 0.117\ Fr\ \exp\left(-0.0415\frac{x-x_1}{d_1}\right) \quad (3.7)$$

Equation (3.7) is compared with the present data in Figure 3.15.

In the present study, the location of maximum bubble count rate F_{max} was always observed beneath the location of maximum void fraction C_{max} in the shear layer such that :

$$d_1 < y_{Fmax} < y_{Cmax} \quad (3.8)$$

This finding was first reported by CHANSON and BRATTBERG (2000). CHANSON (2006) argued that it could be caused by a double diffusion process where vorticity and air bubbles diffuse at a different rate and in a different manner downstream of the impingement point. This situation would mean some dissymmetric turbulent shear stress. The result is illustrated in Figure 3.16 where y_{Fmax}/d_1 is plotted as a function y_{Cmax}/d_1 for a range of experimental data.

Fig. 3.15 - Longitudinal distributions of dimensionless maximum bubble count rate in the hydraulic jump shear layer F_{max} d_1/U_1 - Comparison with the data of CHANSON and BRATTBERG (1997,2000), CHANSON (2006) and KUCUKALI and CHANSON (2007), and with Equation (3.7)

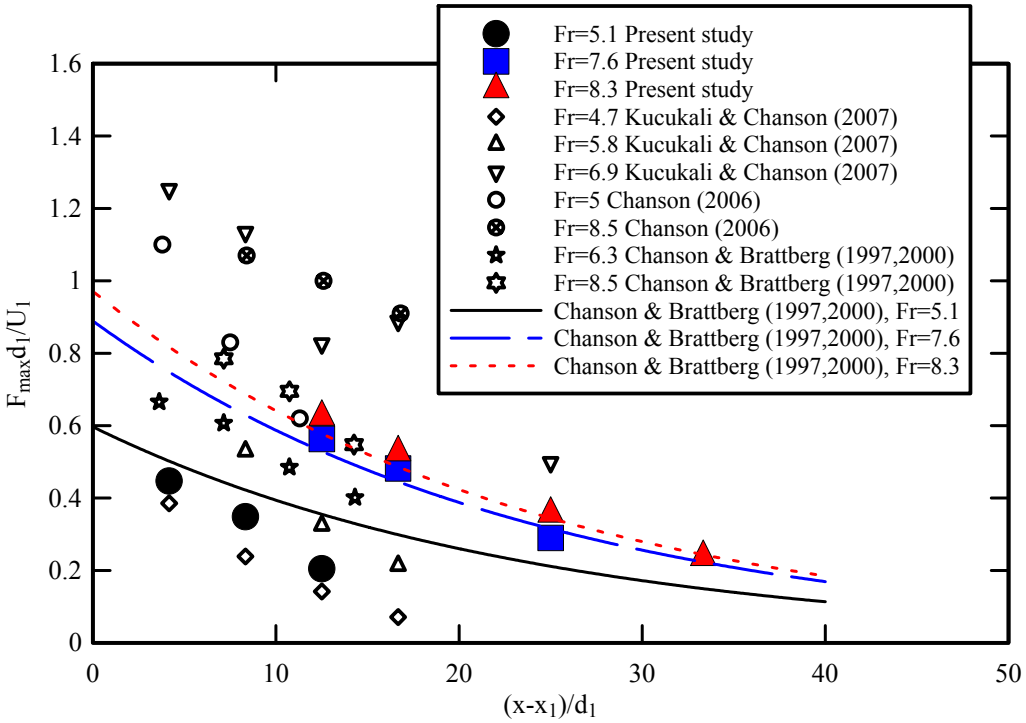

Fig. 3.16 - Dimensionless relationship between y_{Fmax}/d_1 and y_{Cmax}/d_1 in hydraulic jumps - Comparison between the present results and the data of CHANSON and BRATTBERG (2000), CHANSON (2006) and KUCUKALI and CHANSON (2007)

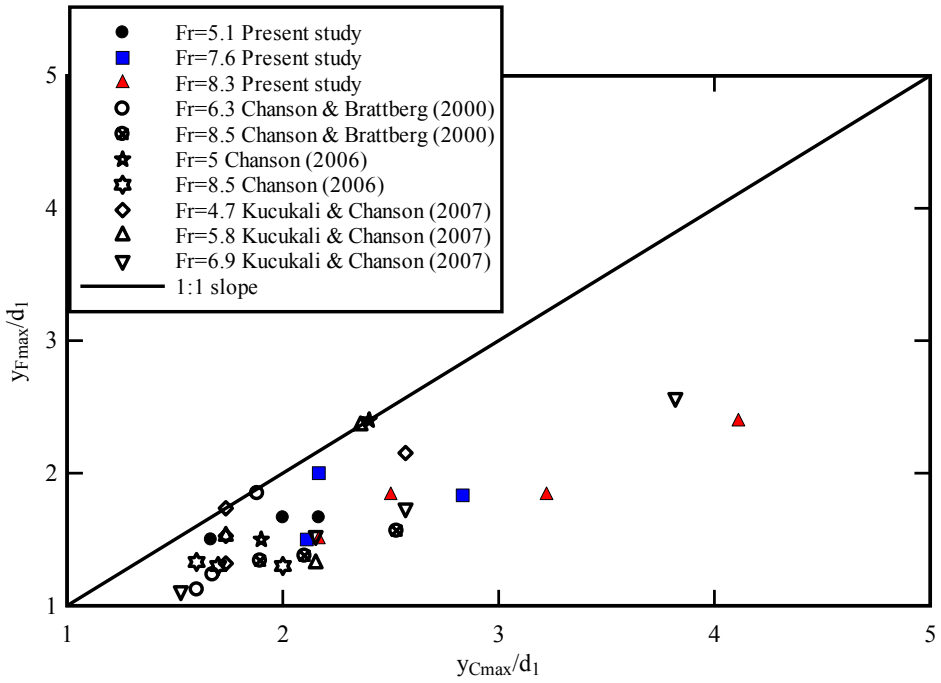

Typical mean bubble chord length data are presented on Figure 3.17. Note that the horizontal axes have dimensional units (mm), and the same scales are used for both horizontal and vertical axes in each graph. The results are limited to the mean bubbles chord lengths in the jump roller. The measurements at large void fractions were not presented. All the results showed millimetric mean bubble chord sizes in the jump roller. Flow visualizations and high-shutter speed photography taken during experiments tended to confirm the findings.

The vertical distributions of mean bubble chords showed systematically an increase in mean bubble chord with increasing vertical elevation above the bed (Fig. 3.17). At a given position $(x\text{-}x_1)/d_1$, the smallest air bubbles were found close to the channel bed in regions of high shear. At a given elevation y/d_1, the mean bubble chord size decreased with increasing distance from the jump toe $(x\text{-}x_1)/d_1$.

The order of magnitude of the present observations were in agreement with those published by MURZYN et al. (2005), CHANSON (2006,2007) and KUCUKALI and CHANSON (2007). MURZYN et al. (2005) reported Sauter mean diameter ranging from 2 mm to 10 mm in the developing shear layer for Fr = 2.0 to 4.8. KUCUKALI and CHANSON (2007) gave median bubble chord sizes between 0.5 mm and 2 mm for Fr = 6.9.

Fig. 3.17 - Vertical distributions of mean bubble chord length ch_{mbc} in the hydraulic jump roller
(A) Fr = 5.1

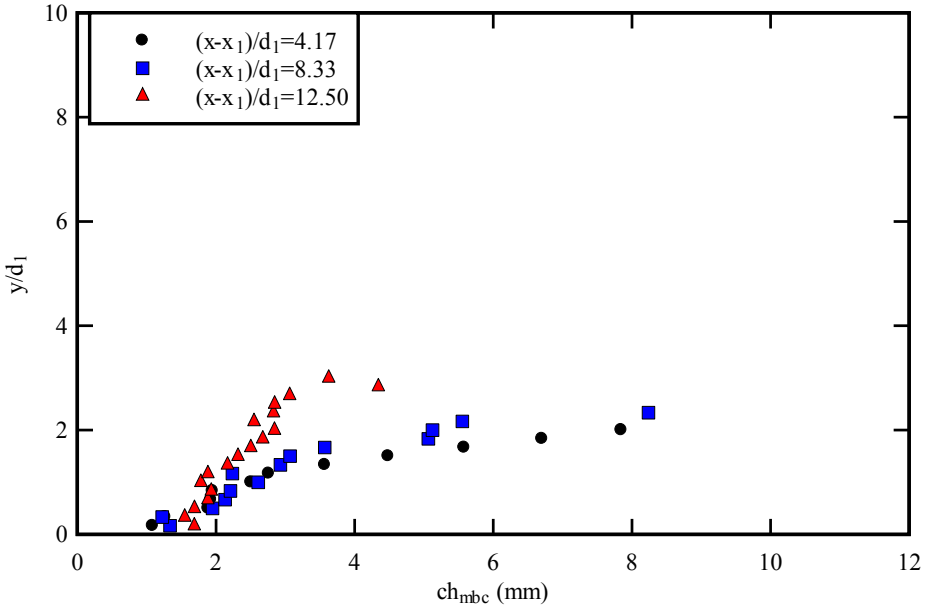

(B) Fr = 7.6

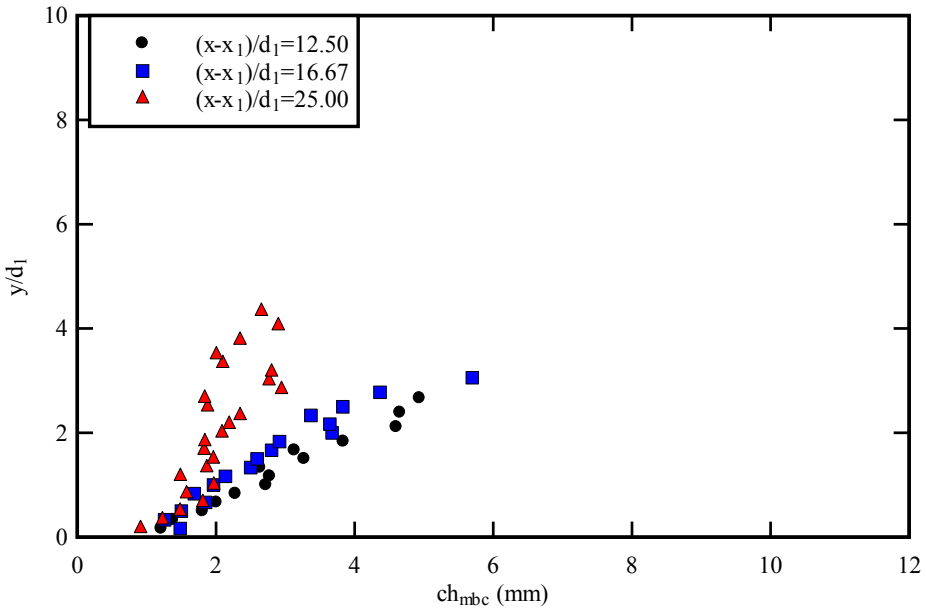

(C) Fr = 8.3

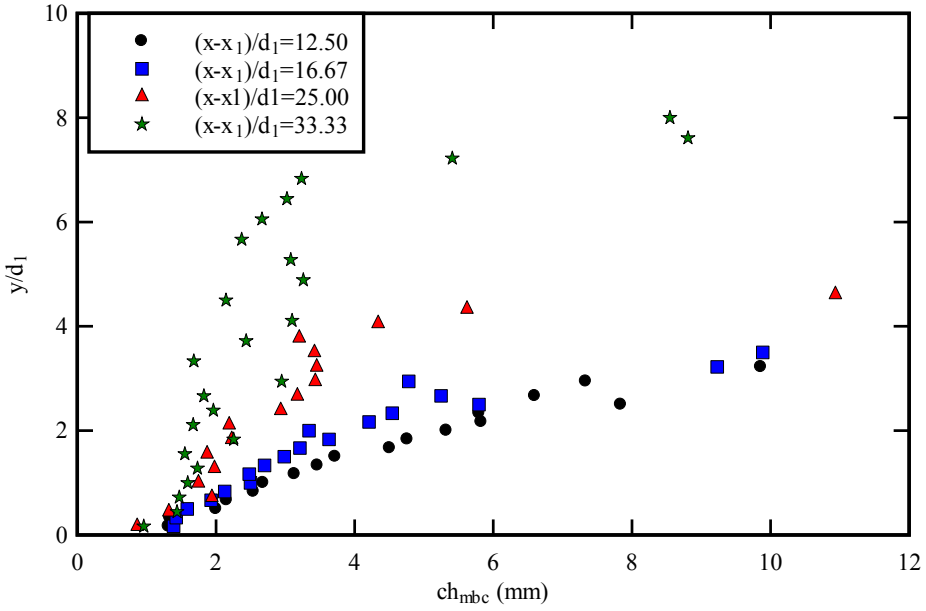

3.2.2 Interfacial velocity and turbulence intensity

Interfacial velocity

Air-water velocity measurements were conducted with the dual-tip conductivity probe based upon the mean travel time between the probe sensors and the distance between both tips (Δx = 7.0 mm). All the data are reported in Appendix C. Importantly, these measurements were restricted to the air-

water flow regions where the velocity was positive and the probe sensors were aligned with the flow streamlines. In the recirculation region, the results were meaningless because of negative velocities. Furthermore, this intrusive technique disturbed the flow and the leading sensor might induce wake effects leading to some erroneous data.

Figure 3.18 presents typical dimensionless distributions of interfacial velocities V/V_{max} in the hydraulic jump roller, where V_{max} is the maximum velocity measured in the cross-section. At the channel bed, the no-slip condition imposed $V(y=0) = 0$. At a given position $(x\text{-}x_1)/d_1$, the velocity profiles showed the development of a boundary layer next to the bed. This thin fluid layer was characterised by a rapid increase in dimensionless interfacial velocity V/V_{max} from 0 for $y = 0$ to 1 at $y = y_{Vmax}$. Above (i.e. $y > y_{Vmax}$), a gradual decrease in velocity was observed (Fig. 3.18). All the velocity profiles exhibited a similar shape despite some data scattering. The data suggested further that the boundary layer thickness grew with the distance to the toe, while the maximum interfacial velocity decreased with increasing distance from the jump toe $(x\text{-}x_1)/d_1$. Following the work of RAJARATNAM (1965) in monophase flows, CHANSON and BRATTBERG (2000) showed that the dimensionless distributions of interfacial velocities were best fitted by some wall jet equations :

$$\frac{V}{V_{max}} = \left(\frac{y}{y_{V\,max}}\right)^{\frac{1}{N}} \quad \text{for } \frac{y}{y_{V\,max}} < 1 \quad (3.9)$$

$$\frac{V}{V_{max}} = \exp\left(-\frac{1}{2}\left[1.765\left(\frac{y - y_{V\,max}}{y_{0.5}}\right)\right]^2\right) \quad \text{for } 1 < \frac{y}{y_{V\,max}} < 3 \text{ to } 4 \quad (3.10)$$

where V_{max} is the maximum velocity measured at $y = y_{Vmax}$, $y_{0.5}$ is the vertical elevation where $V = V_{max}/2$ and N is a constant ($N \approx 6$). Equations (3.9) and (3.10) are compared with the data in Figures 3.18B and 3.18C. The present results followed closely the wall jet velocity profile, despite some data scatter caused by the unsteady and fluctuating nature of the flow.

The maximum velocity data V_{max} showed a gradual decrease with increasing distance from the jump toe. They compared favourably with the observations of CHANSON and BRATTBERG (2000) and KUCUKALI and CHANSON (2007) (Fig. 3.19). All the data followed closely the empirical correlation :

$$\frac{V_{max}}{U_1} = \exp\left(-0.02875\frac{x - x_1}{d_1}\right) \quad (3.11)$$

with a normalised correlation of 0.877. Equation (3.11) is compared with the experimental data in Figure 3.19.

Fig. 3.18 - Dimensionless distributions of interfacial velocity V/V_{max} in hydraulic jump - Comparison with Equations (3.9) and (3.10)

(A) $Fr = 5.1$

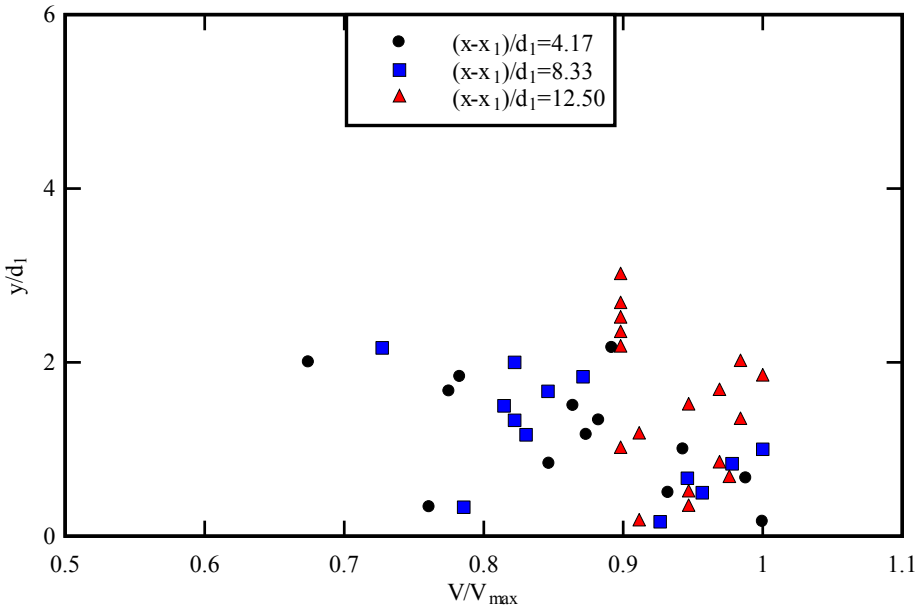

(B) $Fr = 7.6$

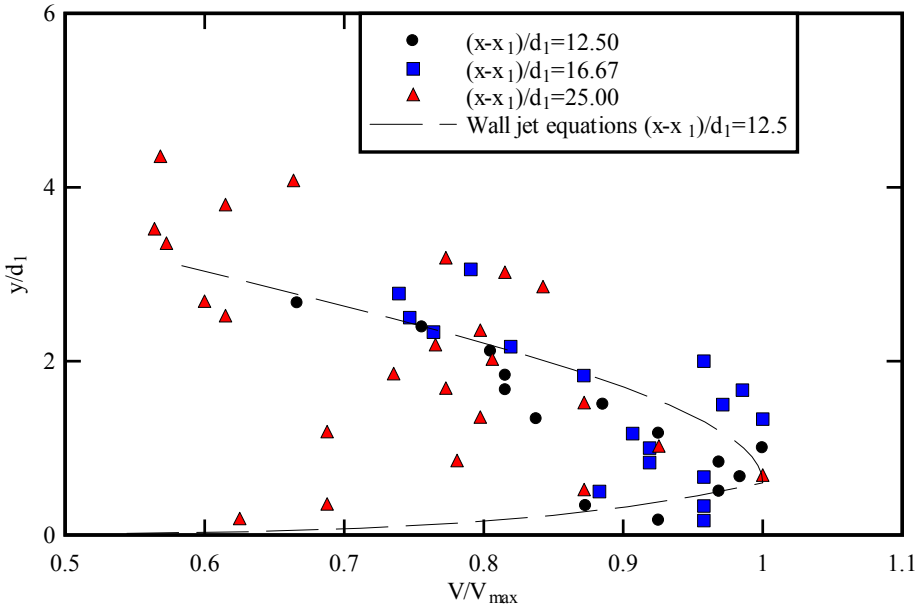

(C) Fr = 8.3

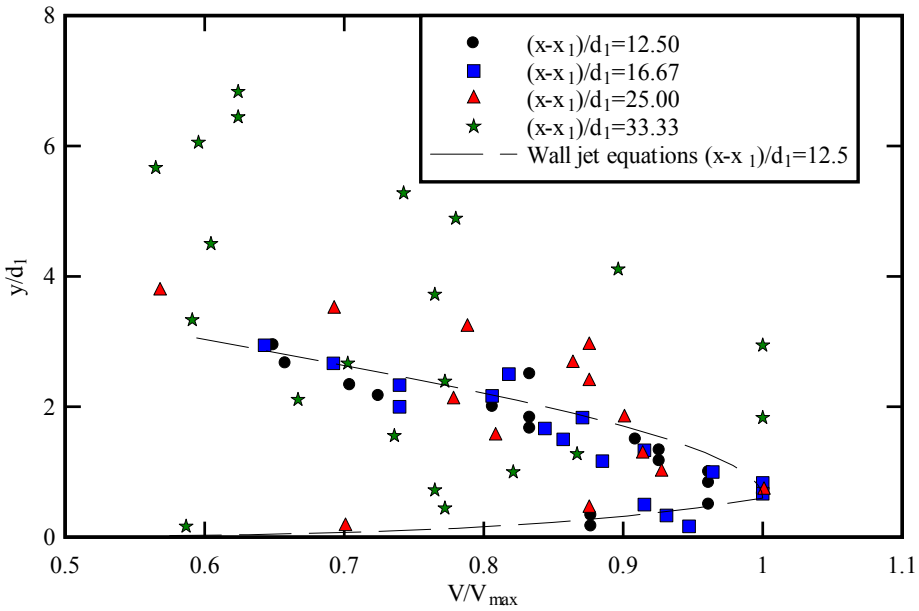

Fig. 3.19 - Longitudinal distribution of dimensionless maximum velocity V_{max}/U_1 in hydraulic jumps - Comparison with the data of CHANSON and BRATTBERG (2000) and KUCUKALI and CHANSON (2007), and Equation (3.11)

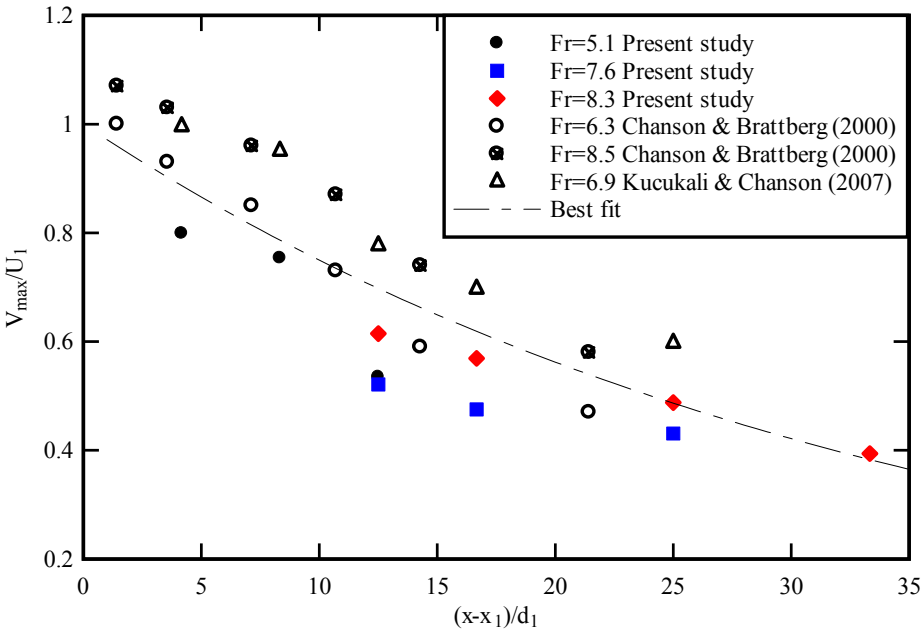

Turbulence intensity

The turbulence intensity was derived from a cross-correlation analysis between the two probe sensor signals (paragraph 2.2.2, Eq. (2-1)). From a theoretical point of view, this approach was

based on the relative width of the auto- and cross-correlation functions (CHANSON and TOOMBES 2002). The turbulence level *Tu* characterised the fluctuations of the interfacial velocity. Figure 3.20 presents typical distributions of the turbulence intensities in hydraulic jumps. The data are presented in Appendix C. The results showed very high levels of turbulence up to 400%. The turbulence levels increased with increasing distance from the bed y/d_1 and with increasing Froude number. At a given relative water depth y/d_1, *Tu* decreased with increasing distance from the jump toe $(x-x_1)/d_1$. Far downstream, the vertical profiles showed a homogeneous vertical distribution over the whole water depth with relatively lower turbulence levels (*Tu* < 100%). The present results were consistent with those obtained by KUCUKALI and CHANSON (2007) in terms of the order magnitude, while the present investigation covered a wider range of flow conditions (Table 3.3). The present data set brings new information on the internal structure of the flow in terms of turbulence intensity in a complex two-phase flow.

Fig. 3.20 - Dimensionless distributions of streamwise turbulence intensity *Tu* in hydraulic jumps
(A) *Fr* = 5.1

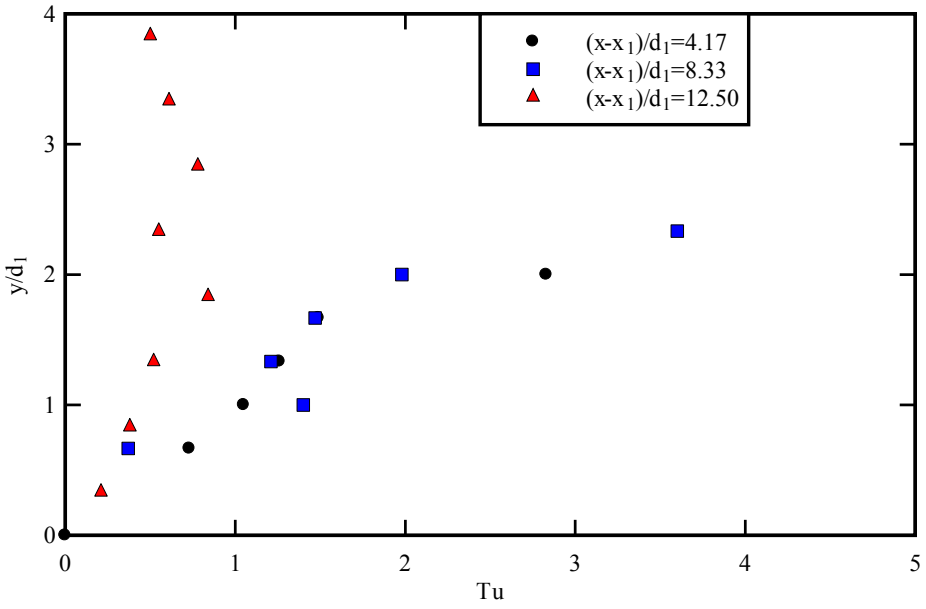

(B) *Fr* = 7.6

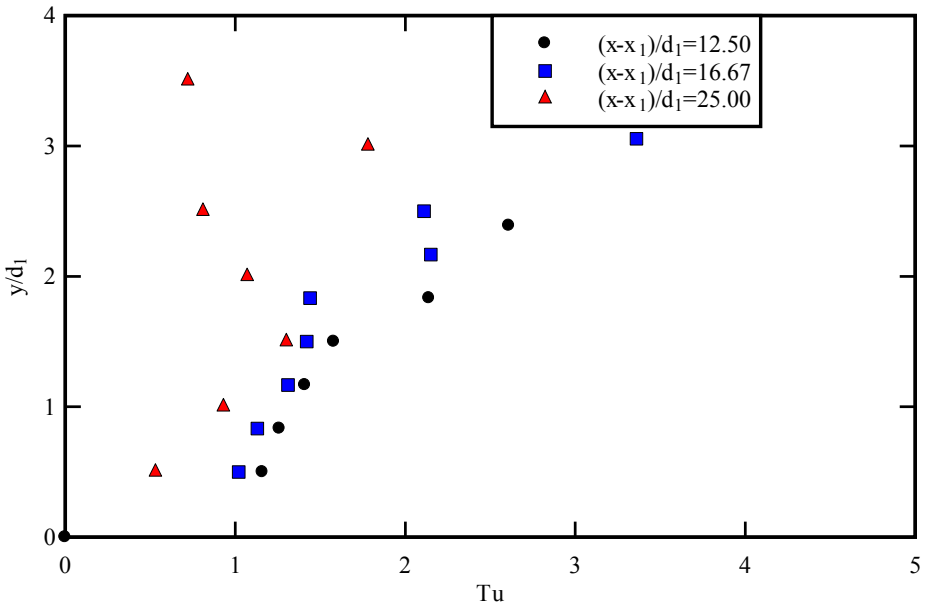

(C) *Fr* = 8.3

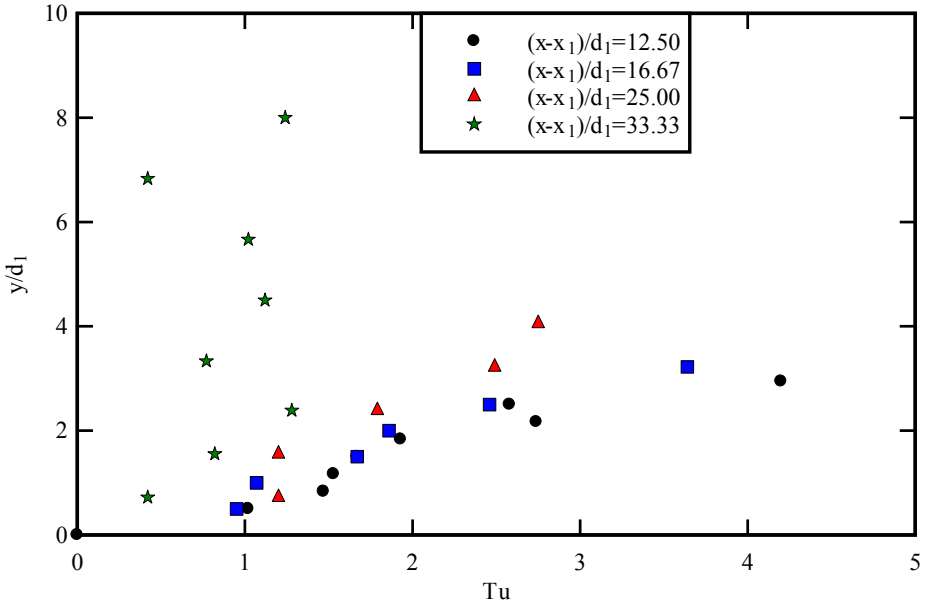

3.2.3 Time scales of turbulence

Further properties of the bubbly flow were deduced from the dual-tip conductivity probe signal output with an advanced signal processing (paragraph 2.2.2). The data processing of the signal output may provide information on turbulence structure and its properties. Particularly, a further analysis of autocorrelation function (TENNEKES and LUMLEY 1997) may be undertaken on

leading and trailing tip output signals. Herein the focus was on the autocorrelation function characteristics of the leading tip output signal and the autocorrelation time scales of turbulence T_{xx}. Using the technique developed by CHANSON (2006,2007) and CHANSON and CAROSI (2007), the auto-correlation coefficient function $R_{xx}(\tau)$ was calculated and its integration led to T_{xx} (Eq. (2.2)). Figure 3.21 presents a typical auto-correlation coefficient. The flow conditions are listed in the figure caption. The complete data set of autocorrelation time scales is presented in Appendix C. The auto-correlation function data showed a well-known and well-defined shape which allowed calculation of the auto-correlation time scale. The integral time scale T_{xx} characterised the streamwise coherence of the two-phase flow. It was also a rough estimate of the longest longitudinal connection in the air-water flow structure. Figure 3.22 presents some typical vertical distributions of auto-correlation time scales ($5.1 \leq Fr \leq 8.3$) for different distances downstream of the toe. Note that the horizontal scale is dimensional (units: seconds). The median auto-correlation time scales were between 3 and 5 ms, that was close the data of CHANSON (2006,2007) and KUCUKALI and CHANSON (2007) (Table 3.4).

Figure 3.21 - Example of an auto-correlation function in the hydraulic jump roller - Flow conditions: $Fr = 5.1$, $d_1 = 0.018$ m, $(x\text{-}x_1)/d_1 = 12.5$, $y/d_1 = 0.83$, $C = 0.029$, $F = 21$ Hz, $V = 1.43$ m/s

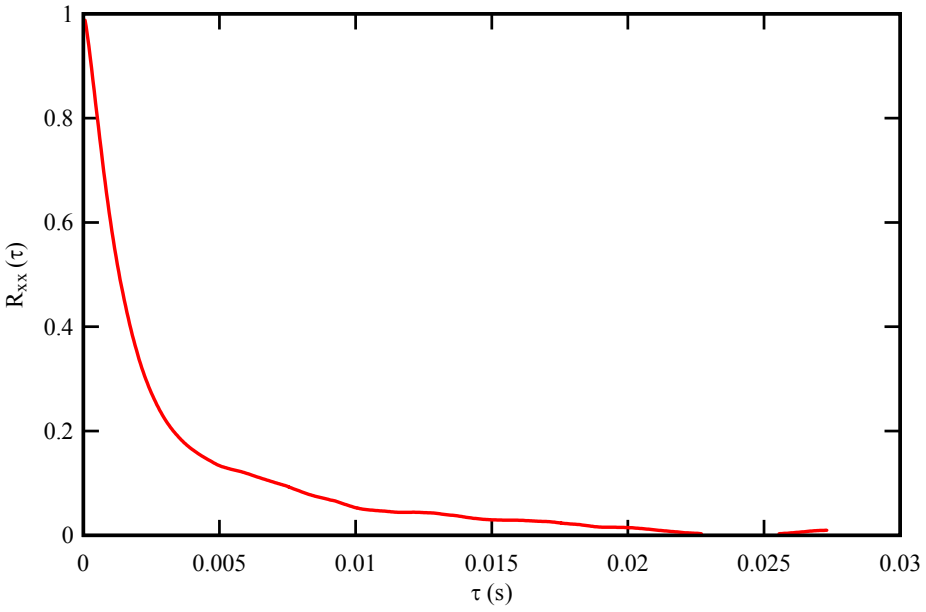

Figure 3.23 shows some distribution of dimensionless auto-correlation time scale $T_{xx}U_1/d_1$. The results showed that the integral time scale increased with increasing vertical elevation above the bed suggesting that the largest structures developed in the turbulent shear layer. At a given relative depth y/d_1, T_{xx} tended to decrease with increasing distance from the jump toe. Furthermore, towards the downstream end of the roller, the vertical distributions of dimensionless auto-correlation time scale $T_{xx}U_1/d_1$ became nearly homogeneous and roughly constant over the whole water column:

e.g., $T_{xx}U_1/d_1 \approx 0.7$ in Figure 3.23B at $(x\text{-}x_1)/d_1 = 25$. The smallest integral time scales were observed close to the channel bed. It was likely that the boundary condition (presence of the bottom) prevented the vortex stretching and development of large-scale structures. The free surface played similarly a role with a lesser influence. Figure 3.23C presents further a comparison with some data of CHANSON (2006,2007) for a similar Froude number and dimensionless distances from the jump toe. That study was conducted at a larger Reynolds number in the same facility (Table 3.3). The agreement between the two data sets was good (Fig. 3.23C).

Table 3.4 - Median auto-correlation time scales in hydraulic jump flows

Reference	d_1	W	Fr	$(x\text{-}x_1)/d_1$	T_{xx} (median)
		m			ms
CHANSON (2006,2007)	0.0265	0.50	5.1	3.77	3.8
				7.55	6.5
				11.32	4.8
	0.02385	0.50	8.6	4.19	3.5
				8.39	3.1
				12.58	4.6
				16.77	5.1
	0.0245	0.25	7.9	4.08	8.8
				8.16	4.7
KUCUKALI and CHANSON (2007)	0.024	0.50	4.7	4.17	21.9
				8.33	7.3
				12.50	4.4
				16.67	3.5
	0.024	0.50	5.8	8.33	13.9
				12.50	8.5
				16.67	4.2
Present study	0.018	0.50	5.1	4.17	4.0
				8.33	5.3
				12.5	4.6
	0.018	0.50	7.6	12.5	4.9
				16.67	4.8
				25.0	4.0
	0.018	0.50	8.3	12.5	4.7
				16.67	4.8
				25.0	5.1
				33.33	3.3

Fig. 3.22 - Vertical distributions of auto-correlation time scale T_{xx} in hydraulic jumps
(Left) Fr = 5.1
(Right) Fr = 8.3

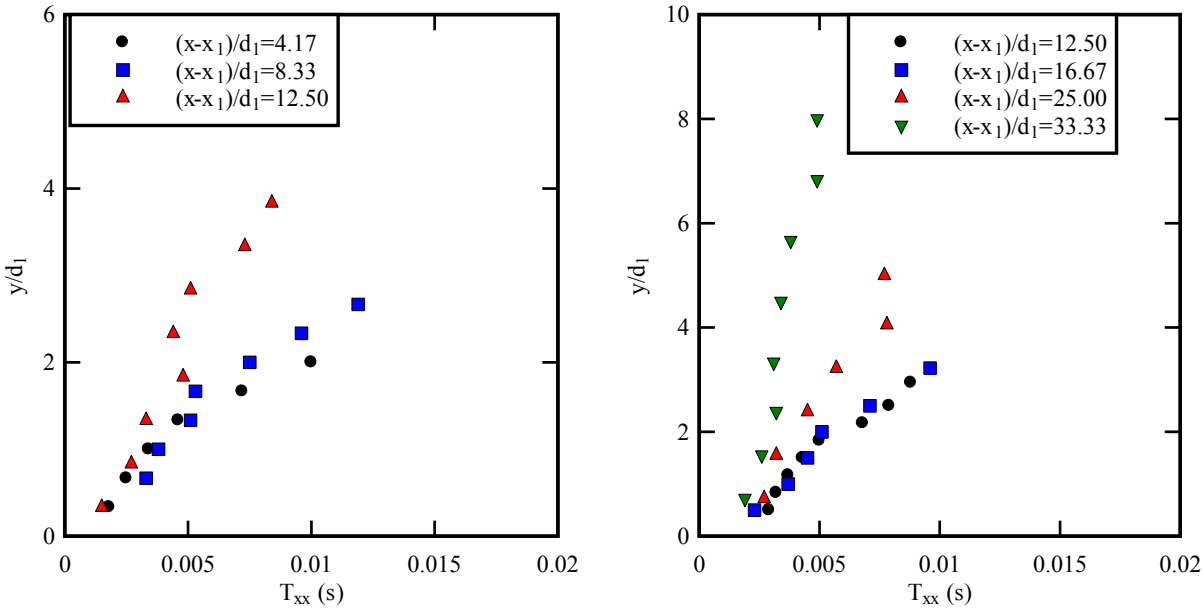

Fig. 3.23 - Vertical distribution of dimensionless auto-correlation time scale $T_{xx}U_1/d_1$ in hydraulic jumps - Comparison with the data of CHANSON (2006,2007)
(A) Fr = 5.1

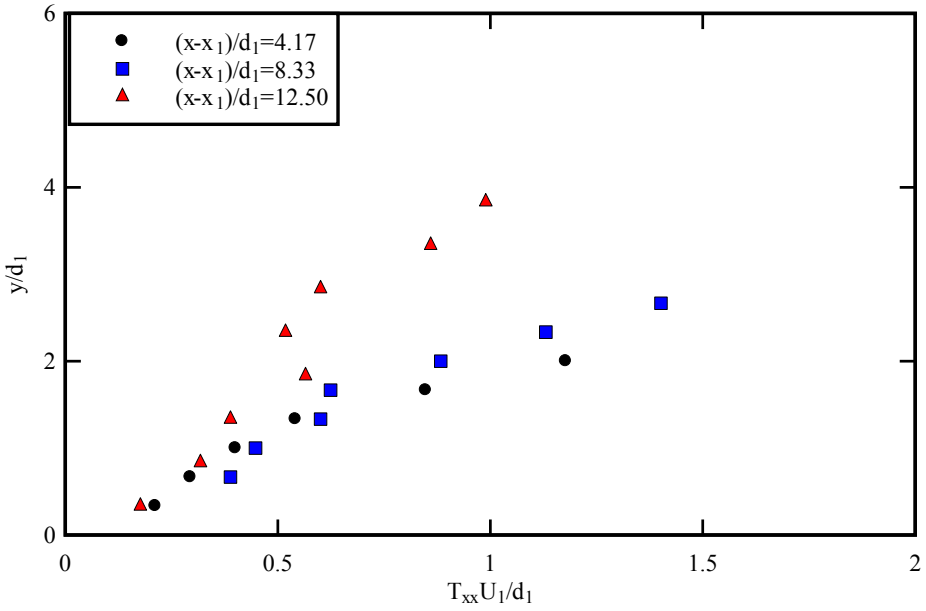

(B) *Fr* = 7.6

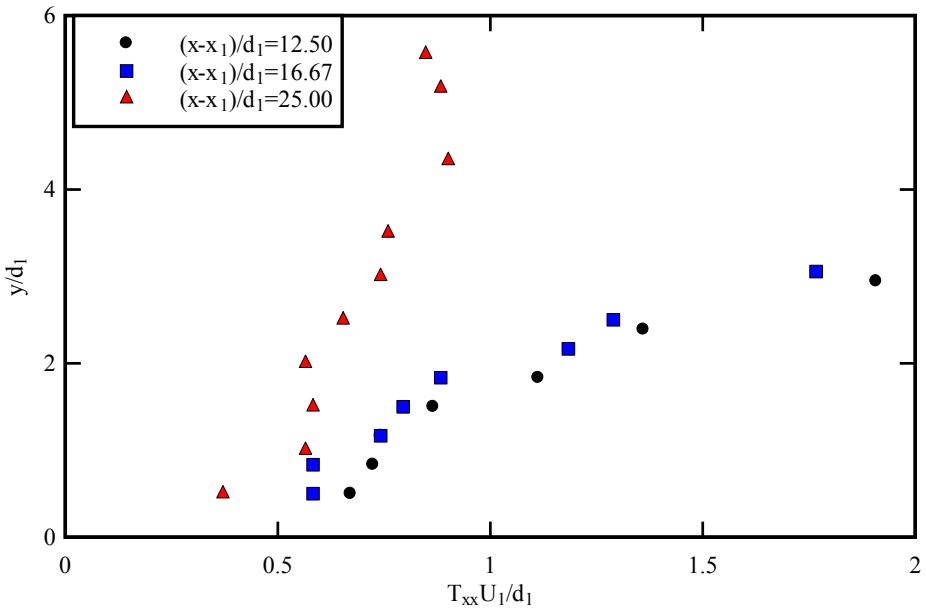

(C) *Fr* = 8.3 (Present study) and 8.6 (CHANSON 2006)

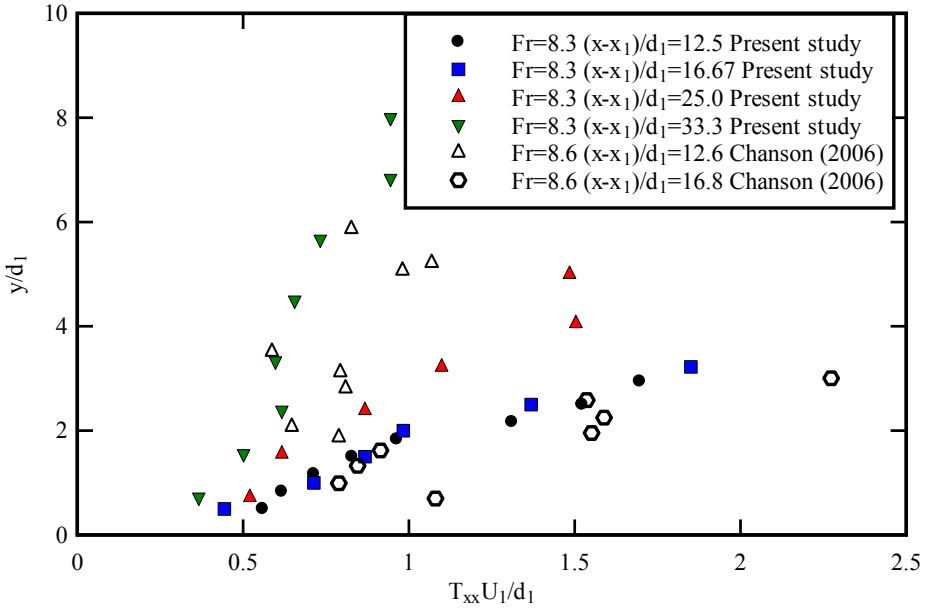

3.2.4 Probability distribution functions of bubble chord times

Further information on the air-water flow properties included the probability density functions (PDF) of bubble chord times. The bubble chord time is defined as the time spent by the bubble on the probe tip. It is thus proportional to the bubble chord length and inversely proportional to the bubble velocity. Herein, the focus was on the PDFs of bubble chord time at two characteristic

relative elevations (y_{Cmax}/d_1 and y_{Fmax}/d_1) corresponding respectively to the positions of the maximum void fraction and bubble count rate in the developing shear layer (Fig. 1-1).

Typical results are presented in Figure 3.24, where all the graphs have the same horizontal and vertical scales. For each graph, the caption and legend provide the location (x-x_1, y/d_1), local air-water flow properties (C, F), and number of recorded bubbles N_{ab} while the horizontal axis lists the chord time interval in milliseconds. The histogram columns represent each the normalised probability of bubble chord time in a 0.5 millisecond chord time interval. For example, the probability of bubble chord time from 1 to 1.5 ms is represented by the column labeled 1. Bubble chord times larger than 15 ms are regrouped in the last column (> 15).

The results highlighted first the broad spectrum of bubble chord times at each location with a predominance for small bubble chord times compared to the mean. The range extended from less than 0.5 ms to more than 15 ms. Further, when Froude number increased, the PDFs became more skewed with a longer upper chord size tail, and a larger proportion of small bubbles with increasing Froude number. Overall the findings were in agreement with the earlier experimental observations of CHANSON (2006,2007) and KUCUKALI and CHANSON (2007) (Table 3.3).

Fig. 3.24 - Bubble chord time distributions at two characteristic relative elevations (y_{Cmax}/d_1 and y_{Fmax}/d_1) in the bubbly flow region of hydraulic jumps

(A) Fr = 5.1

(A1) (x-x_1)/d_1 = 4.17

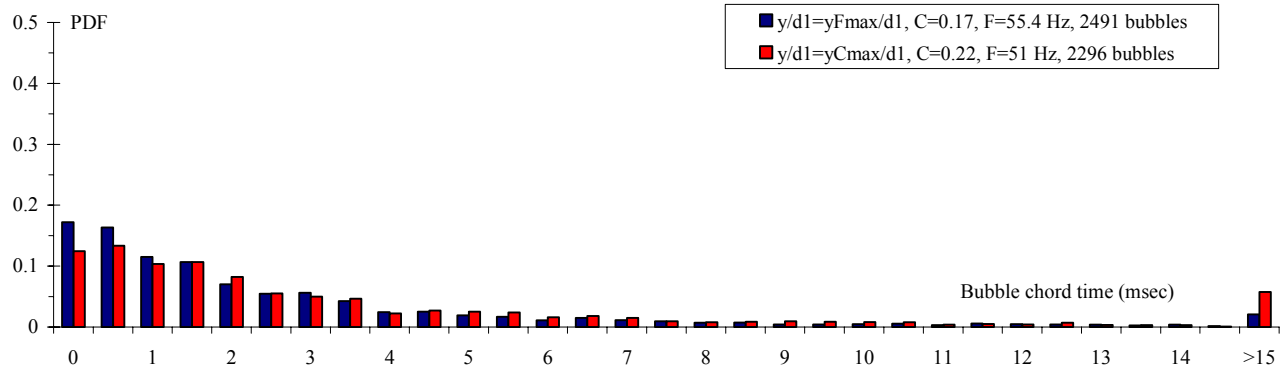

(A2) (x-x_1)/d_1 = 8.33

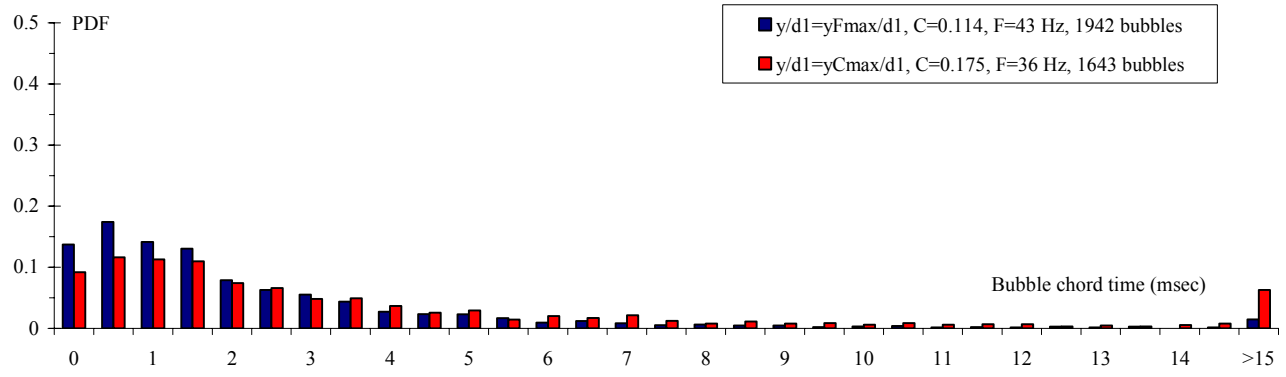

(A3) $(x\text{-}x_1)/d_1 = 12.5$

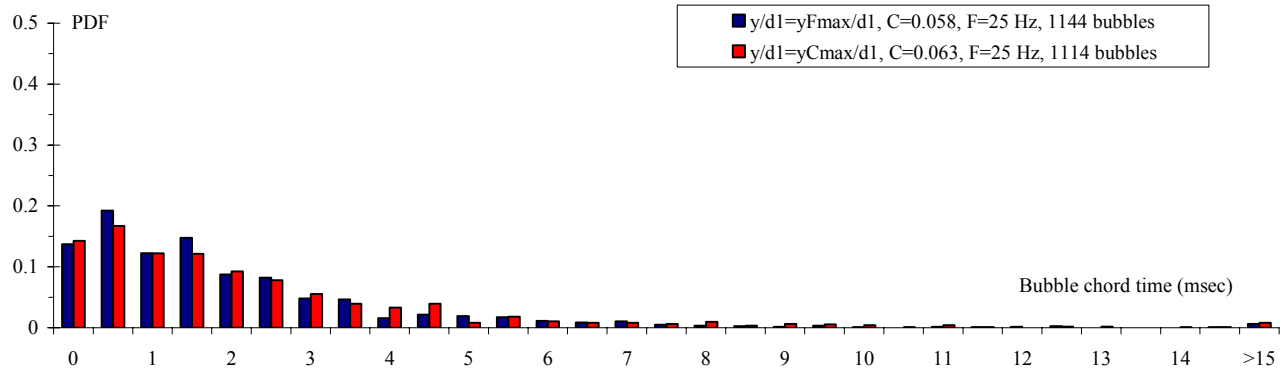

(B) $Fr = 7.6$

(B1) $(x\text{-}x_1)/d_1 = 12.5$

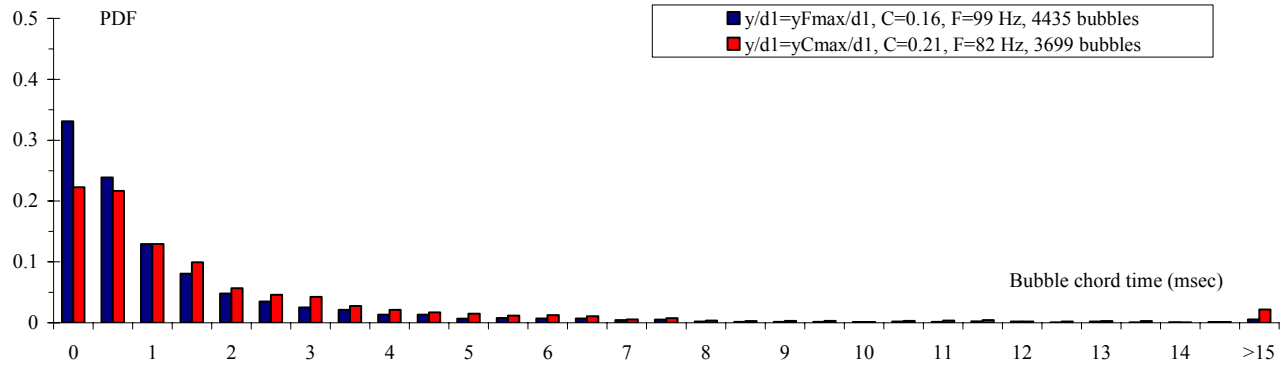

(B2) $(x\text{-}x_1)/d_1 = 16.67$

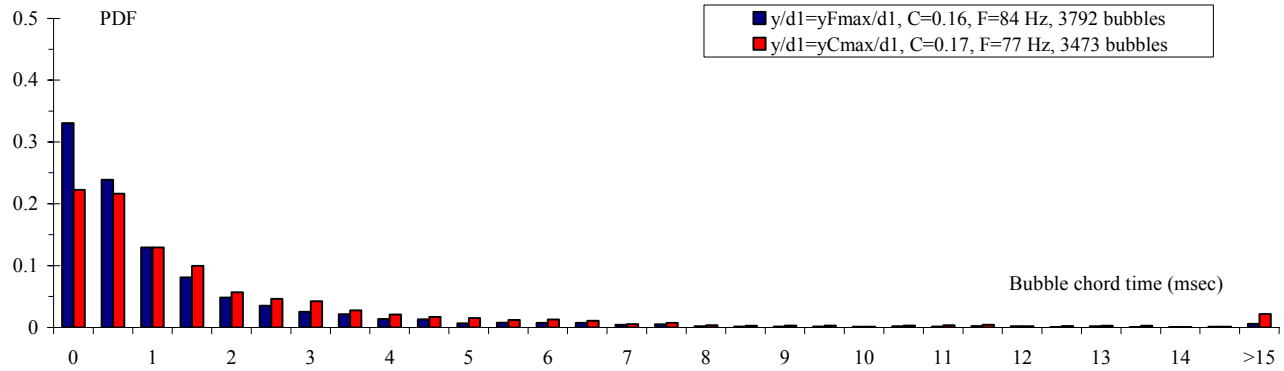

(B3) $(x\text{-}x_1)/d_1 = 25$

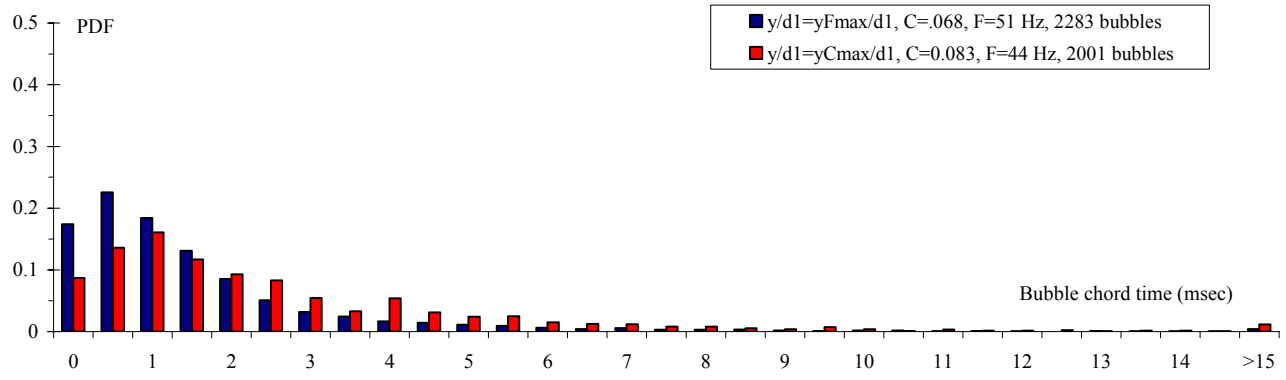

(C) $Fr = 8.3$

(C1) $(x\text{-}x_1)/d_1 = 12.5$

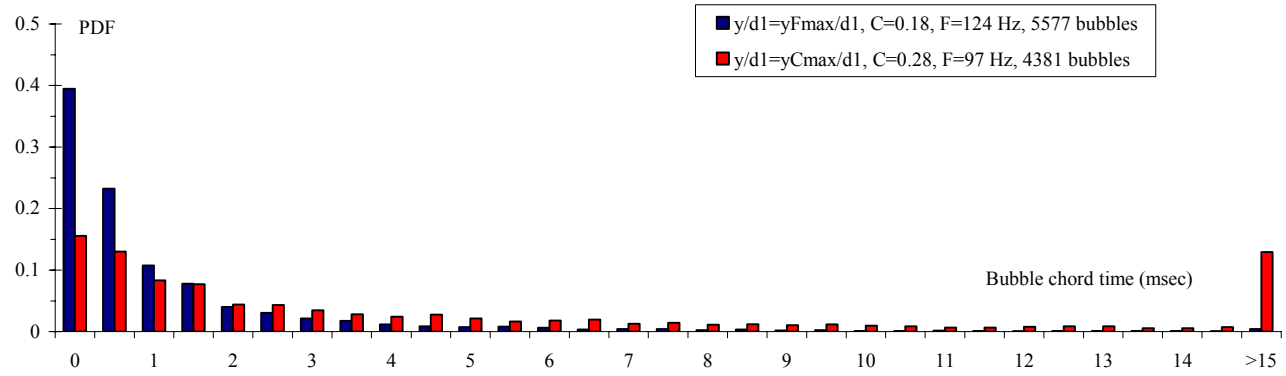

(C2) $(x\text{-}x_1)/d_1 = 16.7$

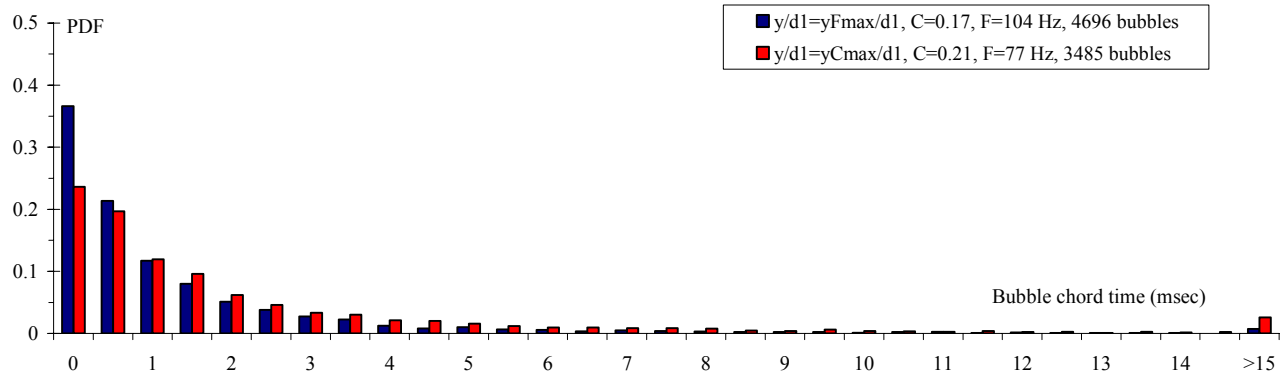

(C3) $(x\text{-}x_1)/d_1 = 25$

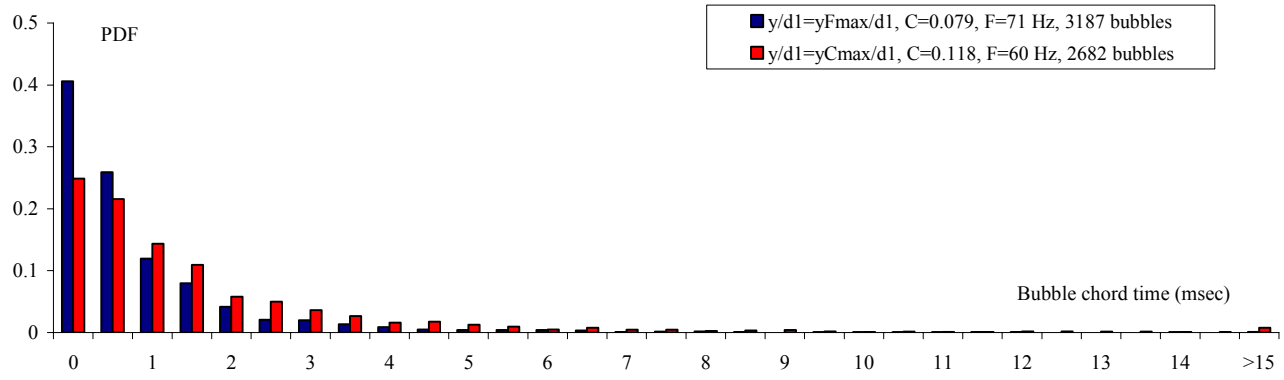

4. SIMULTANEOUS MEASUREMENTS OF FREE SURFACE AND BUBBLY FLOW PROPERTIES

4.1 Principle and experimental arrangements

Simultaneous measurements of free surface fluctuations and air-water flow properties were conducted using respectively an acoustic displacement meter and the dual-tip conductivity probe. The goal was to study whether a relationship could be found between frequency ranges of the free surface and the bubbly flow properties. Figure 4.1 illustrates the experimental setup. The experimental conditions are summarised in Table 4.1. Note that only one Froude number was investigated (Fr = 5.1). At larger Froude numbers, the acoustic displacement sensor was regularly covered by spray and splashing, limiting an accurate comparative signal analysis.

For each experiment, two acoustic displacement sensors were used. One was set upstream of the jump toe while the other was aligned in the vertical direction with the dual-tip conductivity probe leading sensor (Fig. 4.1). The sampling rate was fixed at 5,000 Hz and the acquisition duration was 12 s. Altogether 60,000 samples were collected for both free surface and bubbly flow sensors. Although several data acquisitions were made at different vertical elevations of the conductivity probe sensor, the comparative results are focused herein on the air-water flow properties at the vertical elevations where $C \approx 0.3$ (i.e. $y = y_{30}$) and on the acoustic displacement meter located immediately above the conductivity probe leading tip.

Fig. 4.1 - Photograph of the experimental setup - Flow conditions: Fr = 4.7, flow from foreground to background, shutter speed: 1/800 s

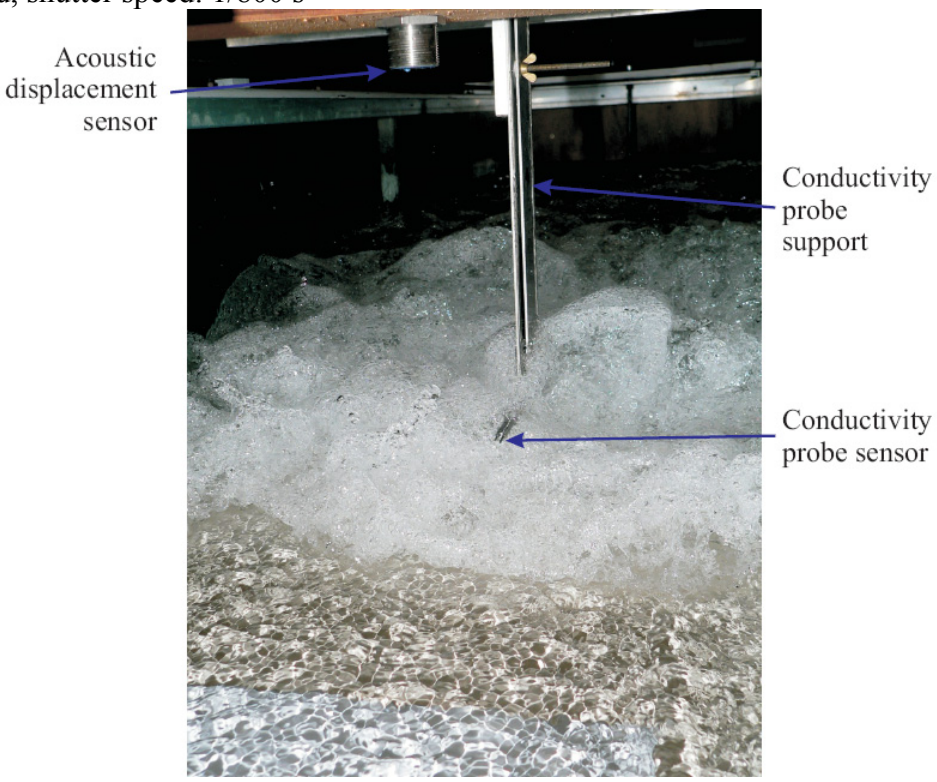

Table 4.1 - Experimental conditions for simultaneous measurements of free surface fluctuations and bubbly flow properties

Fr	d_1 (m)	x_1 (m)	x-x_1 (m)	$(x$-$x_1)/d_1$	Number of measurement points	y_{30}/d_1
5.1	0.018	0.75	0.090	5.0	10	3.50
			0.165	9.17	9	4.83
			0.240	13.33	9	5.67

Spectral analyses were performed for both conductivity probe and free surface output signals. The original output signal of the conductivity probe (Figure 4.2A) was converted into a binary file of instantaneous void fraction being 0 for water and 1 for air (Figure 4.2B). The signal was then filtered using a band pass (0-25 Hz). The filtering aimed to remove electrical noise and any high-frequency signal component with a frequency greater than the dynamic response of the sensor. The low-pass filtered signal was averaged (over 100 points) (Fig. 4.2C). Lastly the output was linearly interpolated using a constant interval time (0.02 s) to facilitate spectral analyses. The spectral analysis was performed on the resulting processed/filtered signal. A typical result of the fast Fourier transform (FFT) is shown in Figure 4.3 for the signal output shown in Figure 4.2. The same technique was applied to the acoustic displacement sensor signal output.

Figure 4.2 - Simultaneous measurement of air-water flow properties and free-surface fluctuations - Conductivity probe output signal - Flow conditions: Fr = 5.1, $(x$-$x_1)/d_1$ = 5.0, y/d_1 = 3.5
(A) Raw voltage output

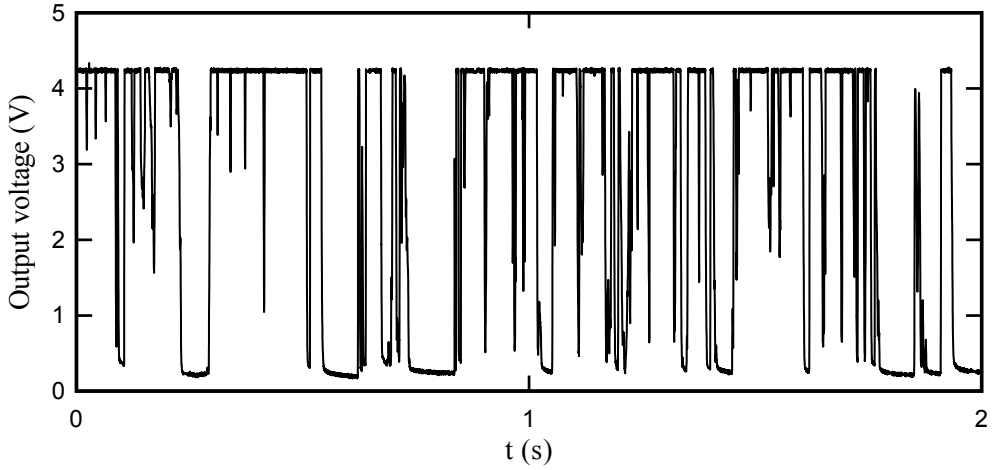

(B) Binary output signal, or instantaneous void fraction

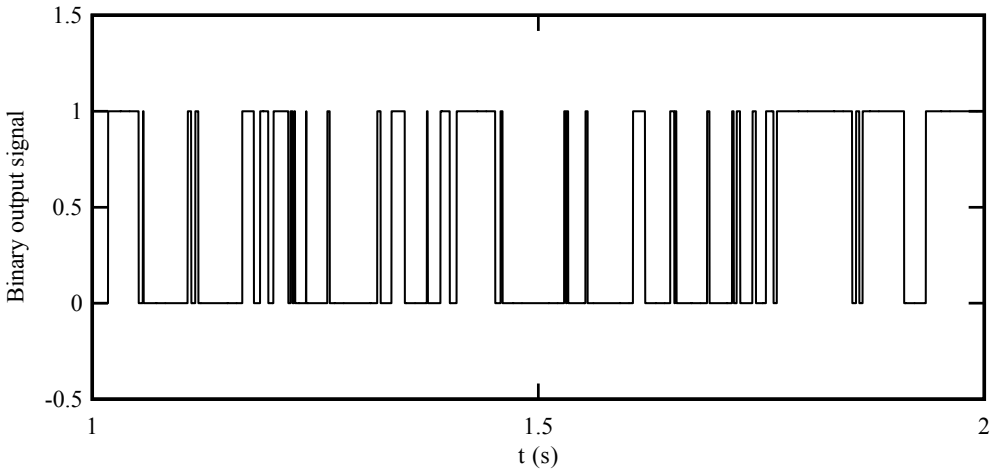

(C) Averaged signal (average over 100 points) with equal interval (0.02 s) of the low-pass filtered signal component (Band pass 0-25 Hz)

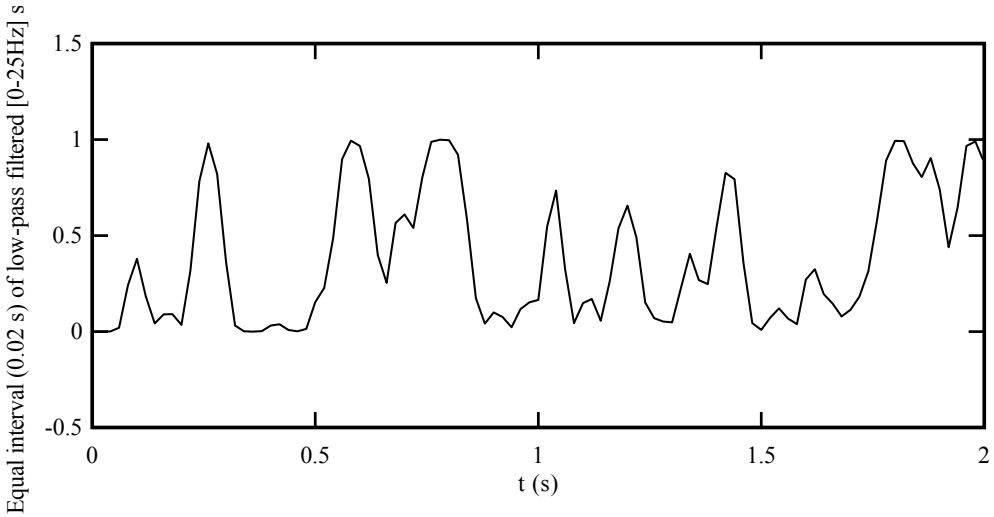

Figure 4.3 - Spectral analysis FFT of the low-pass filtered conductivity probe signal component - Flow conditions: Fr = 5.1, $(x\text{-}x_1)/d_1$ = 5.0, y/d_1 = 3.5

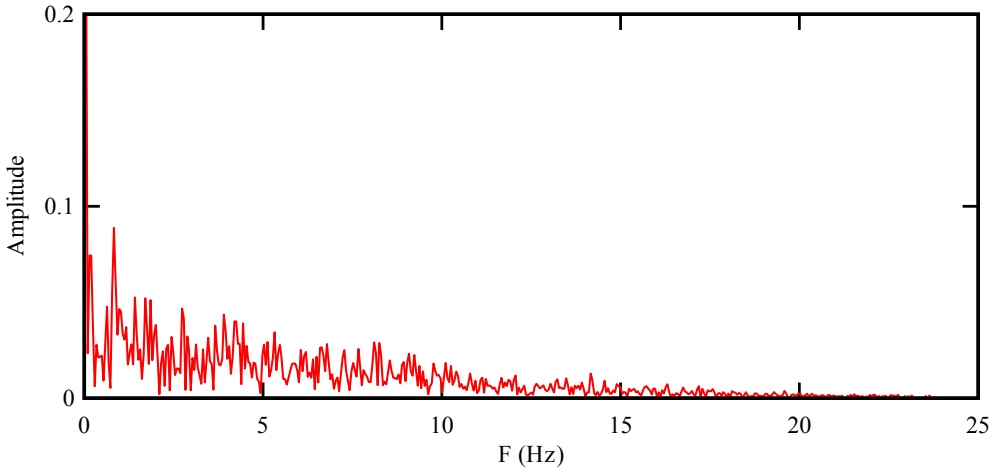

4.2 Preliminary results: spectral and cross-correlation analyses

Typical results of spectral analyses are presented in Figure 4.4 for Fr = 5.1. For each figure, the FFT analysis of the conductivity probe signal is on the left and that of the free-surface signal on the right. The results showed that the dominant frequencies were less than 5 Hz for both conductivity probe and acoustic displacement sensors (Fig. 4.4). The acoustic displacement meter results were consistent with the results presented in paragraph 3.1.4. The findings implied further that the bubble generation and free surface vertical motion might be dependant processes. Figure 4.5 illustrates the time-series of simultaneous processed signals.

A cross-correlation analysis was performed on the processed signals of both conductivity probe and acoustic sensor. The cross correlation functions for the three conditions shown in Figure 4.5 are presented on Figure 4.6. In Figure 4.6, the vertical axis is the normalised coefficient of correlation R_{xz} where x is the conductivity probe signal and z is the free-surface fluctuation signal. The results exhibited some large negative and positive values with some periodic shape (Fig. 4.6). A spectral analysis of these cross-correlation functions revealed that their main frequencies were 1.12 Hz, 1.56 Hz and 2.34 Hz for $(x\text{-}x_1)/d_1$ = 5.0, 9.17 and 13.3 respectively. These were consistent with earlier results presented herein. Further developments may be required to gain a clearer picture of the complex interactions between air entrainment and free-surface fluctuations. This topic was discussed by BROCCHINI and PEREGRINE (2001) and TOOMBES and CHANSON (2007).

Figure 4.4 - Spectral analyses (FFT) of both conductivity probe and acoustic displacement sensor signals - Flow conditions: $Fr = 5.1$

(A) $(x\text{-}x_1)/d_1 = 5.0$, $y/d_1 = 3.5$

(Left) conductivity probe signal; (Right) acoustic displacement sensor signal

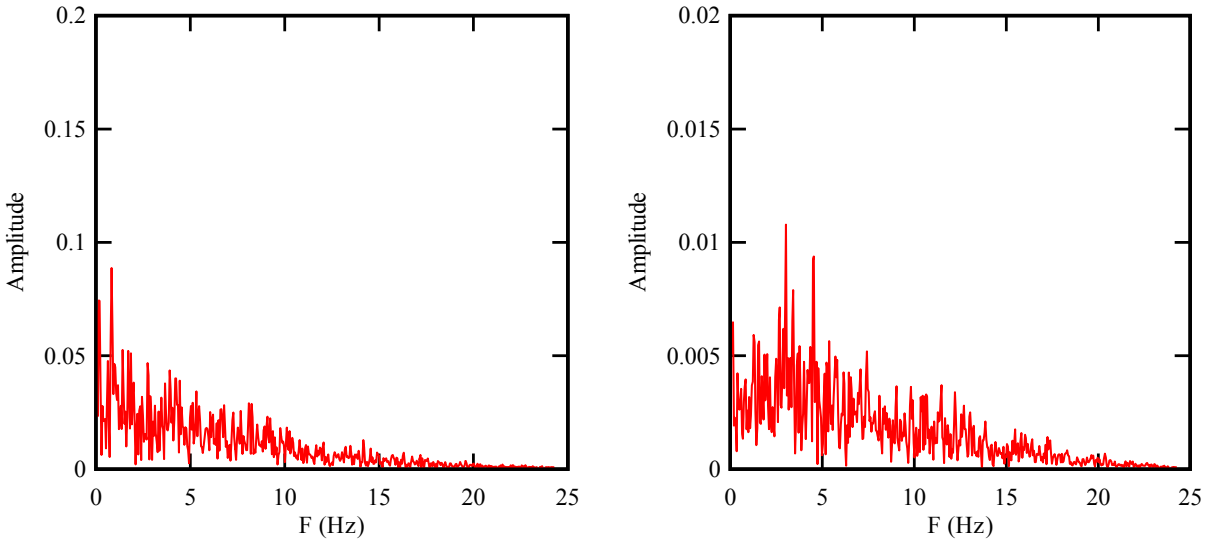

(B) $(x\text{-}x_1)/d_1 = 9.17$, $y/d_1 = 4.83$

(Left) conductivity probe signal; (Right) acoustic displacement sensor signal

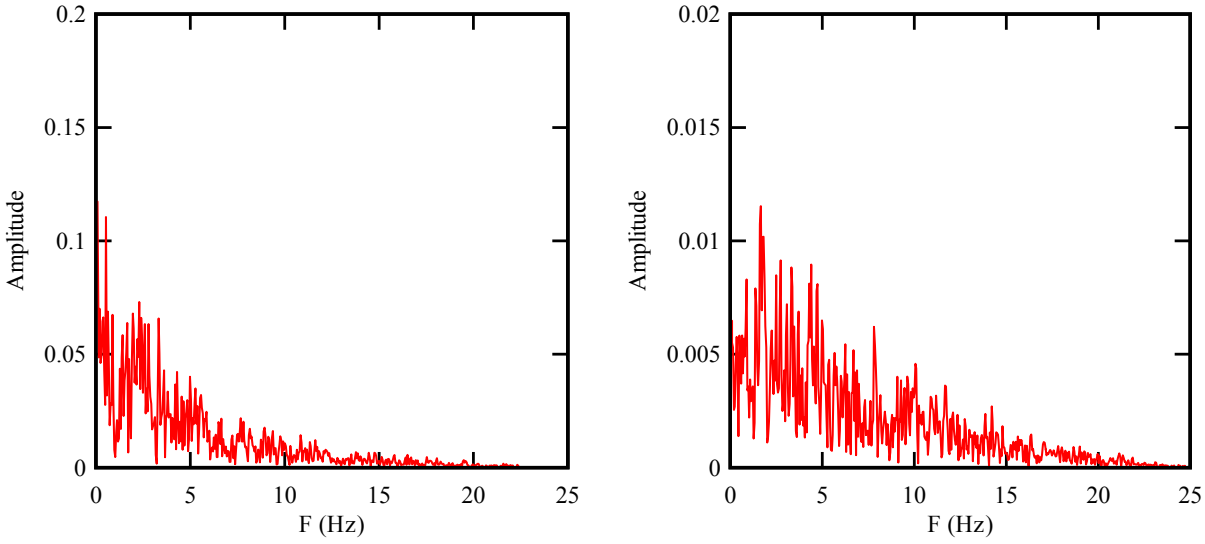

(C) $(x\text{-}x_1)/d_1 = 13.33$, $y/d_1 = 5.67$

(Left) conductivity probe signal; (Right) acoustic displacement sensor signal

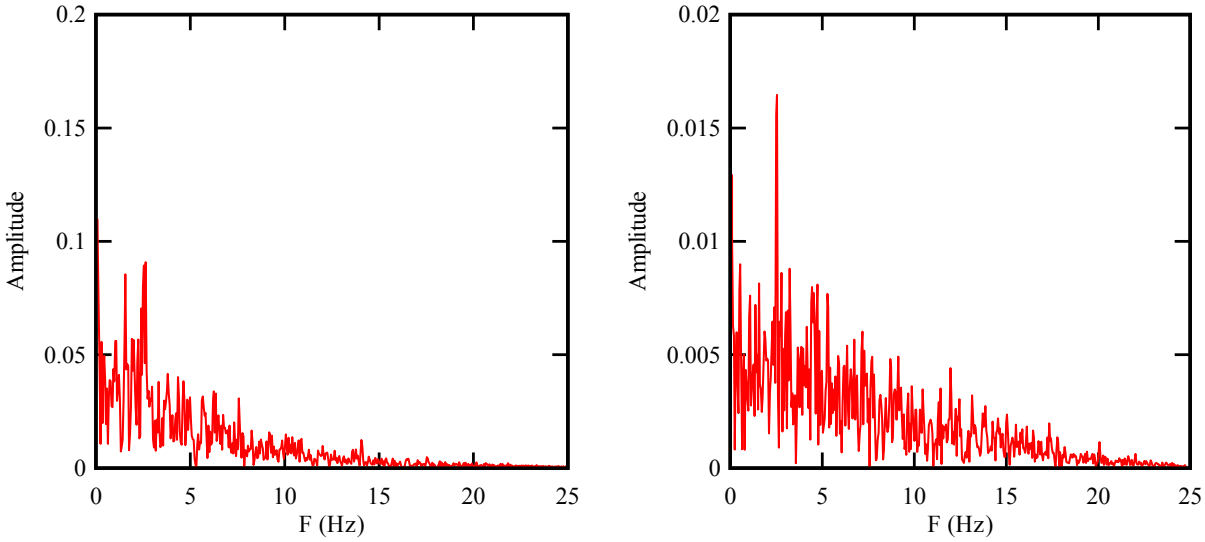

Fig 4.5 - Simultaneous processed/filtered signals of conductivity probe and acoustic displacement sensor - Flow conditions: $Fr = 5.1$

(A) $(x\text{-}x_1)/d_1 = 5.0$, $y/d_1 = 3.50$

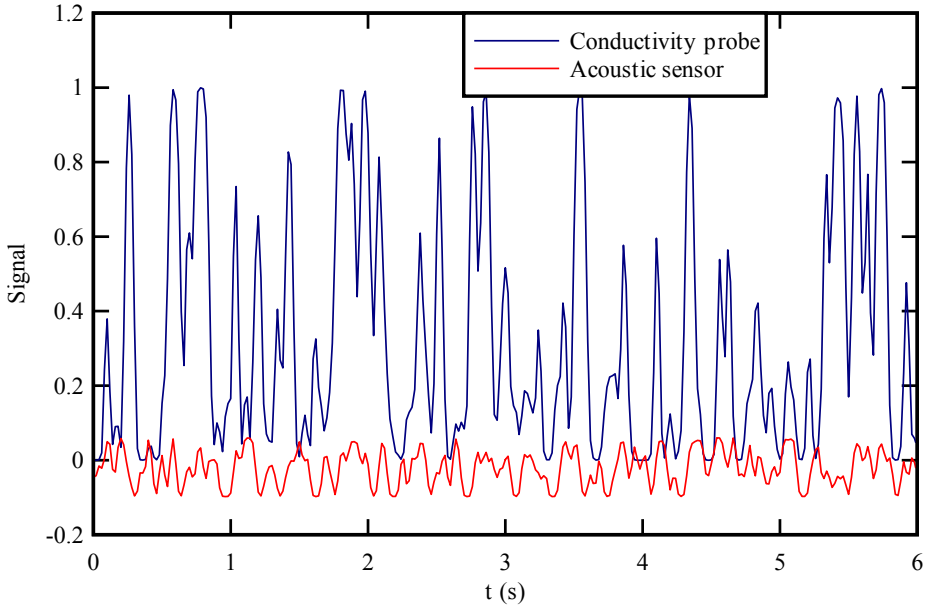

(B) $(x\text{-}x_1)/d_1 = 9.17$, $y/d_1 = 4.83$

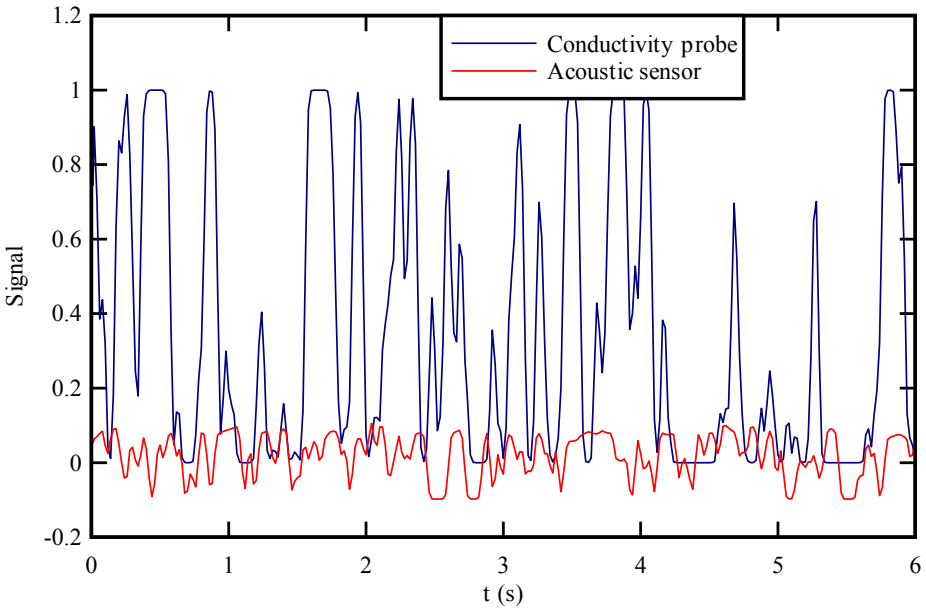

(C) $(x\text{-}x_1)/d_1 = 13.33$, $y/d_1 = 5.67$

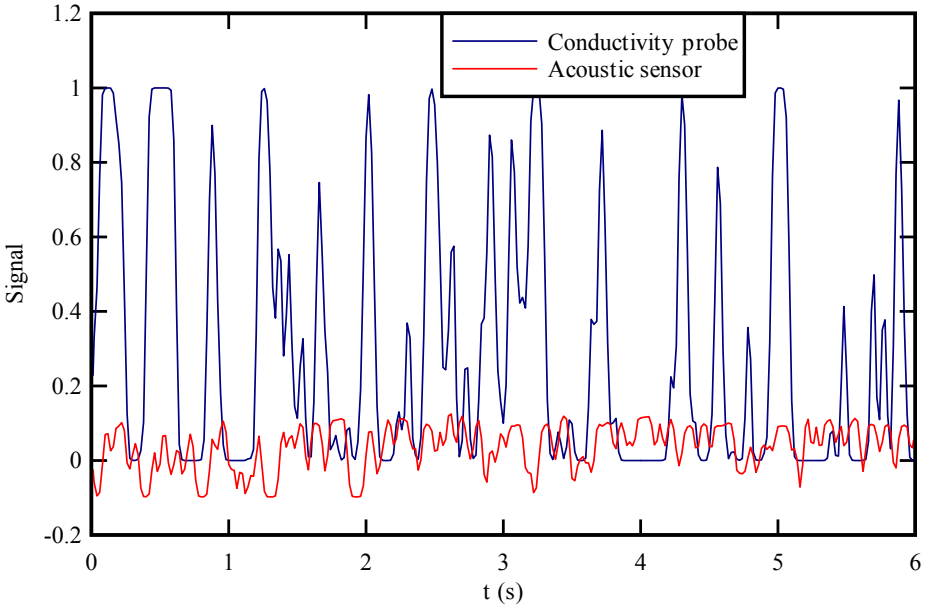

Fig 4.6 - Normalised cross-correlation functions between the conductivity probe signal and acoustic displacement meter sensor - Flow conditions : *Fr* = 5.1

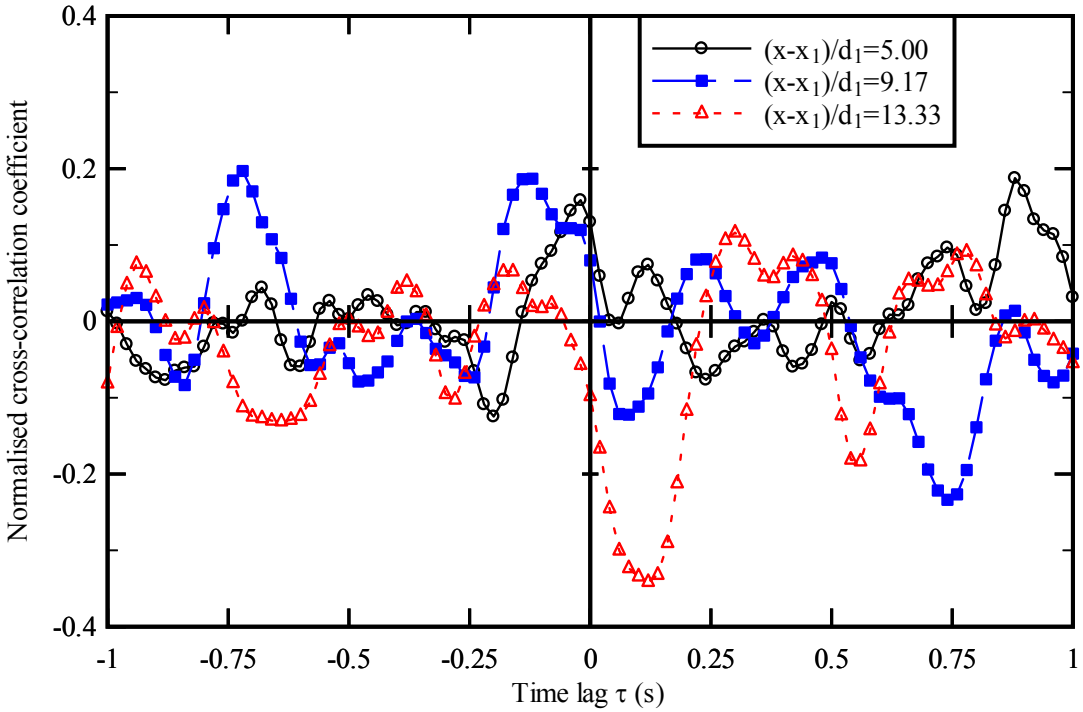

5. DISCUSSION: SCALE EFFECTS AFFECTING AIR BUBBLE ENTRAINMENT IN HYDRAULIC JUMPS

5.1 PRESENTATION

Theoretical and numerical studies of air bubble entrainment in hydraulic jumps are difficult because of the large number of relevant equations (CHANSON 1997,2007c). Experimental investigations of air-water flows are performed with geometrically similar models based upon a dimensional analysis and dynamic similitude. In the study of open channel flows including the hydraulic jump, a Froude similitude is commonly used because the gravity effects are dominant (e.g. HENDERSON 1966, CHANSON 1999,2004). That is, the model and prototype Froude numbers must be equal. However the entrapment of air bubbles and the mechanisms of air bubble breakup and coalescence are dominated by surface tension effects, while turbulent processes in the shear region are dominated by viscous forces (WOOD 1991, CHANSON 1997). Dynamic similarity of air bubble entrainment in open channel flows becomes impossible because of too many relevant parameters (Froude, Reynolds and Morton numbers). For example, with the same fluids (air and water) in model and prototype, the air entrainment process is adversely affected by significant scale effects in small size models, with drastically lesser air entrainment in small models (KOBUS 1984).

For a hydraulic jump in a horizontal, rectangular channel, a simplified dimensional analysis showed that the parameters affecting the air-water flow properties at a position (x, y, z) include : (a) the fluid properties including the air and water densities ρ_{air} and ρ, the air and water dynamic viscosities μ_{air} and μ, the surface tension σ, and the gravity acceleration g, (b) the channel properties including the width W, and, (c) the inflow properties such as the inflow depth d_1, the inflow velocity U_1, a characteristic turbulent velocity u'_1, and the boundary layer thickness δ (CHANSON 2006,2007c). The air-water flow properties at a location (x, y, z) within the jump may be expressed as :

$$C, F, V, u', d_{ab} \ ... \ = F_1(x, y, z, d_1, U_1, u_1', x_1, \delta, W, g, \rho_{air}, \rho, \mu_{air}, \mu, \sigma, ...) \quad (5.1)$$

where C is the void fraction, F is the bubble count rate, V is the velocity, u' is a characteristic turbulent velocity, d_{ab} is a bubble size, x is the coordinate in the flow direction measured from the nozzle, y is the vertical coordinate, z is the transverse coordinate measured from the channel centreline, and x_1 is the distance from the upstream gate (Fig. 1-1A). In addition, biochemical properties of the water solution must be considered and may have some significant effect (e.g. CHANSON et al. 2002,2006). If the local void fraction C is known, the density and viscosity of the air-water mixture may be expressed in terms of the water properties and void fraction only; hence the parameters ρ_{air} and μ_{air} may be ignored.

Equation (5.1) may be rewritten in dimensionless terms :

$$C, \frac{F\,d_1}{V_1}, \frac{V}{\sqrt{g\,d_1}}, \frac{u'}{V_1}, \frac{d_{ab}}{d_1} ... = F_2\left(\frac{x}{d_1}, \frac{y}{d_1} \frac{z}{d_1}, Fr, \frac{u_1'}{V_1}, \text{Re} \ , Mo, \frac{x_1}{d_1}, \frac{\delta}{d_1}, \frac{W}{d_1}\right) \quad (5.2)$$

In Equation (5.2), the dimensionless air-water flow properties (left handside terms) at a dimensionless position (x/d_1, y/d_1, z/d_1) within the jump are expressed as functions of the dimensionless inflow properties and channel geometry. In the right handside of Equation (5.2), the fourth, sixth and seventh terms are the inflow Froude, inflow Reynolds and Morton numbers

respectively. Any combination of these numbers is also dimensionless and may be used to replace one of the combinations. In Equation (5.2), the Weber *We* was replaced by the Morton number *Mo* = $g\ \mu^4/(\rho\ \sigma^3)$ since :

$$Mo = \frac{We^3}{Fr^2\ \mathrm{Re}^4} \tag{5.3}$$

The Morton number is a function only of fluid properties and gravity constant, and it becomes an invariant if the same fluids (air and water) are used in both model and prototype, as in the present study (WOOD 1991, CHANSON 1997).

The first systematic study of dynamic similarity and scale effects affecting the two-phase flow properties in hydraulic jumps was the work of CHANSON (2006,2007c). For two inflow Froude numbers (*Fr* = 5.1 & 8.5), the experiments tested the validity of the Froude similitude and the effects of the inflow Reynolds number, with all other relevant parameters being constant (Table 5.1). That is:

$$C, \frac{F\,d_1}{V_1}, \frac{V}{\sqrt{g\,d_1}}, \frac{u'}{V_1}, \frac{d_{ab}}{d_1} ... = F_3(\mathrm{Re}) \qquad \text{study of CHANSON (2006,2007c)} \tag{5.4}$$

where the Froude number *Fr* and the relative channel width W/d_1 were constant : i.e., *Fr* = 5.1 and 8.5, W/d_1 = 20 (Table 5.1). The results of the Froude-similar experiments showed some drastic scale effects in the smaller hydraulic jumps in terms of void fraction, bubble count rate and bubble chord time distributions. The void fraction distributions implied comparatively greater detrainment at low Reynolds numbers yielding to lesser overall aeration of the jump roller. The dimensionless bubble count rates were significantly lower in the smaller channel, especially in the mixing layer. The bubble chord times were quantitatively close in both channels, and they were not scaled according to a Froude similitude.

In the same study, CHANSON (2006,2007c) tested the effect of the relative width W/d_1,with all other relevant parameters being constant. That is:

$$C, \frac{F\,d_1}{V_1}, \frac{V}{\sqrt{g\,d_1}}, \frac{u'}{V_1}, \frac{d_{ab}}{d_1} ... = F_3\left(\frac{W}{d_1}\right) \qquad \text{study of CHANSON (2006,2007c)} \tag{5.5}$$

where the inflow Froude and Reynolds numbers were constant : i.e., *Fr* = 5.1 and 8.5, Re = 70,000 to 95,000 (Table 5.1). The results showed that the relative channel width had no effect on the air-water flow properties, including the void fraction, bubble count rate and bubble chord time distributions, for :

$$\frac{W}{d_1} \geq 10 \qquad \text{no effect of channel width} \tag{5.6}$$

In the present study, two experiments were conducted with the same inflow Froude numbers as the study of CHANSON (2006,2007c) (Table 5.1). A systematic comparison between that study and the present data may provide new information on the validity of the Froude similarity to study air bubble entrainment in hydraulic jumps, particularly with reference to the effects of the inflow Reynolds numbers. Note that the present study was conducted with a relative channel width W/d_1 =

28 which satisfied Equation (5.6).

Table 5.1 - Physical modelling of two-phase flow properties in hydraulic jumps based upon an undistorted Froude similitude with air and water

Reference	x_1 (m)	d_1 (m)	Fr	Re	W (m)	Instrumentation	Sensor size (mm)	Sampling rate (Hz)	Sampling time (s)
CHANSON (2006,2007c)	1.0	0.024	5.1 8.6	68,000 98,000	0.50	Single-tip conductivity	0.35	20,000	45
Present study	0.75	0.018	5.1 8.3	38,000 62,000	0.50	Dual-tip conductivity	0.25	20,000	45
CHANSON (2006,2007c)	0.5	0.012	5.1 8.4	25,000 38,000	0.25	Single-tip conductivity	0.35	20,000	45
CHANSON (2006,2007c)	1.0	0.024	5.0 8.0	77,000 95,00	0.25	Single-tip conductivity	0.35	20,000	45

Note : Hydraulic jumps with partially-developed inflow conditions

5.2 COMPARATIVE ANALYSES

The three series of experiments were designed to be geometrically similar based upon a Froude similitude with undistorted scale (Table 5.1). The geometric scaling ratio was $L_{scale} = 2.0$ between the smallest and largest series of experiments, where L_{scale} is the geometric scaling ratio defined as the ratio of prototype to model dimensions, and $L_{scale} = 1.33$ between the largest series of experiments and the present study. Similar experiments were conducted for identical Froude numbers $Fr = U_1 / \sqrt{g\,d_1}$ with identical upstream distance x_1/d_1 between gate and jump toe, where U_1 is the supercritical upstream flow velocity and d_1 is the inflow depth. For a given Froude number, the air-water flow measurements were performed in the developing air-water flow region at identical cross-sections $(x\text{-}x_1)/d_1 \leq 20$.

The comparative analyses were conducted for two inflow Froude numbers $Fr = 5.1$ and 8.5, with inflow Reynolds numbers Re ranging from 25,000 to 98,000. Typical results are presented in Figures 5.1 and 5.2 for $Fr = 5.1$ and 8.5 respectively.

Fig. 5.1 - Effects of the inflow Reynolds number on the dimensionless distributions of void fraction and bubble count rate for Fr = 5.1, x_1/d_1 = 42, $W/d_1 \geq 20$ and $(x\text{-}x_1)/d_1$ = 8, Re = 25,000, 38,000 & 68,000 - Experimental data : CHANSON (2006,2007c) and Present study

(A) Dimensionless distributions of void fraction - Comparison with Equation (3.4)

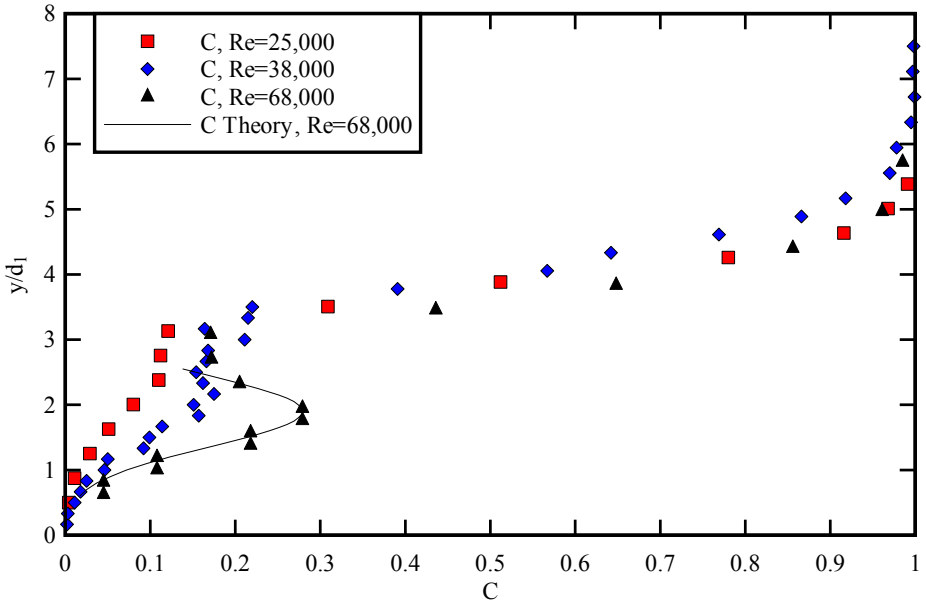

(B) Dimensionless distributions of bubble count rate $F\ d_1/U_1$

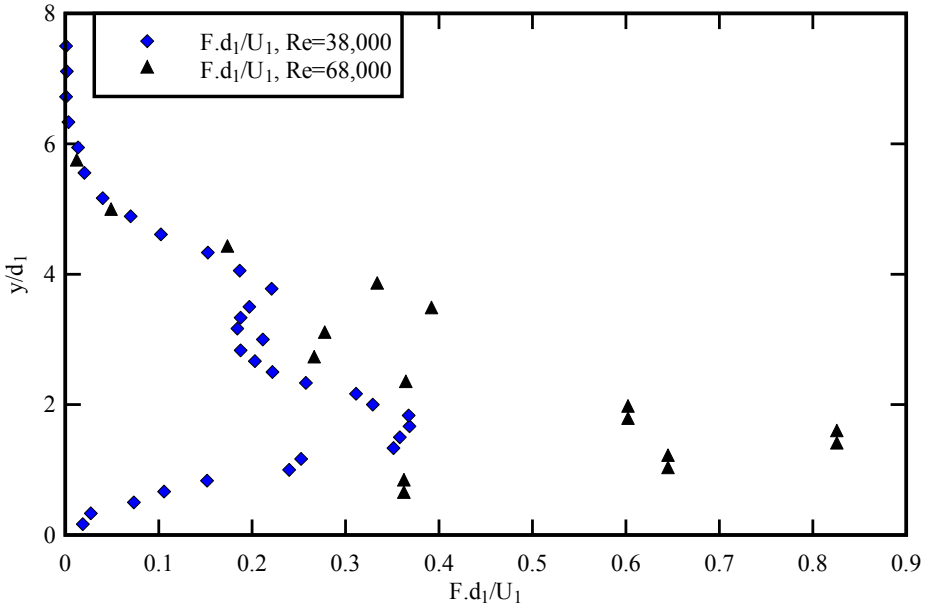

Fig. 5.2 - Effects of the inflow Reynolds number on the dimensionless distributions of void fraction and bubble count rate for Fr = 8.5, x_1/d_1 = 42, $W/d_1 \geq 20$ and $(x\text{-}x_1)/d_1$ = 12, Re = 38,000, 62,000 & 98,000 - Experimental data : CHANSON (2006,2007c) and Present study

(A) Dimensionless distributions of void fraction - Comparison with Equation (3.4)

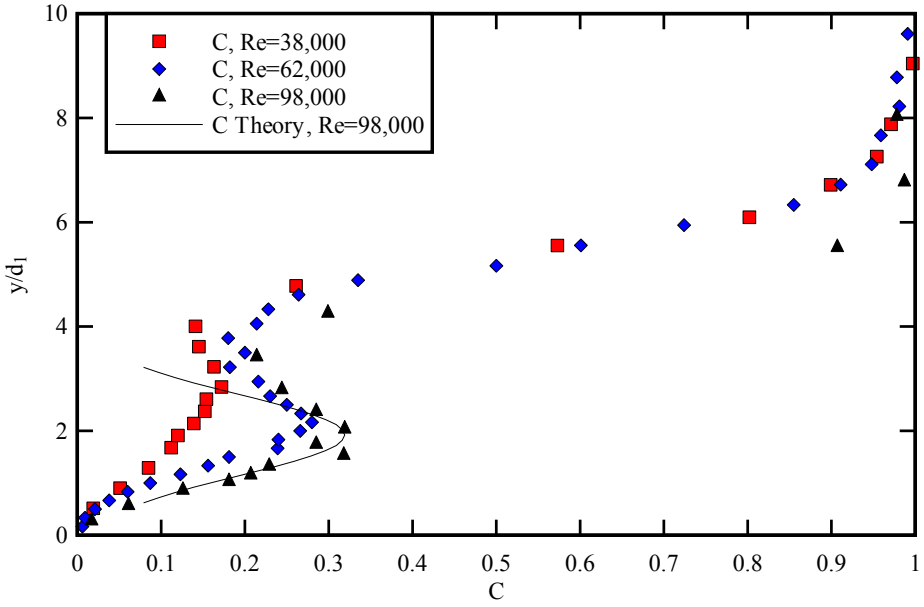

(B) Dimensionless distributions of bubble count rate $F\ d_1/U_1$

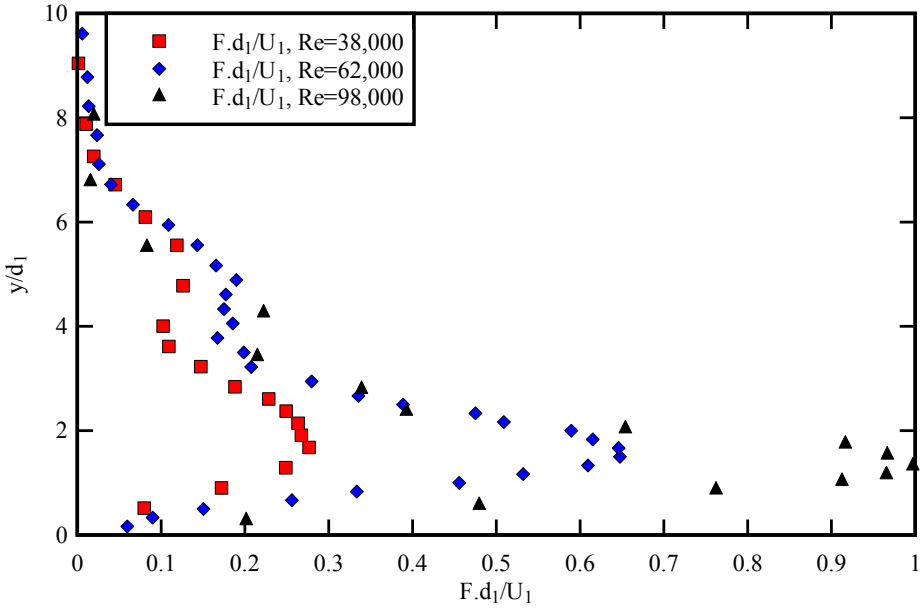

The comparative results showed drastic scale effects in the smaller hydraulic jumps in terms of void fraction, bubble count rate and bubble chord time distributions. The results highlighted consistently a more rapid de-aeration of the jump roller with decreasing Reynolds number for a given inflow Froude number, an absence of self-similarity of the void fraction profiles in the developing shear layer for Re < 40,000 for Fr = 5.1 (Fig. 5.1A), and an increasing dimensionless bubble count rate with increasing Reynolds number for a given inflow Froude number (Fig. 5.1B and 5.2B). The bubble chord time distributions were more skewed with increasing Reynolds number for a given inflow Froude number, and the bubble chord times were not scaled according to a Froude similitude.

For a given inflow Froude number, the effects of the Reynolds number on the two-phase flow properties were particularly marked in the developed shear layer. This is illustrated in Figure 5.3 showing the maximum void fraction C_{max} and maximum dimensionless bubble count rate $F_{max}d_1/U_1$ in the shear layer for a given inflow Froude number *Fr* as functions of the inflow Reynolds number Re. Figure 5.3A presents the relationship between C_{max} and Re, and Figure 5.3B shows the relationship between $F_{max}d_1/U_1$ and Re. Figure 5.3C presents a definition sketch illustrating the definition of C_{max} and F_{max}. The results indicated some monotonic increase in maximum void fraction and maximum dimensionless bubble count rate in the mixing layer with increasing Reynolds number. No asymptotic limit was observed within the range of the experiments (Table 5.1). Further the rate of increase was about the same for both inflow Froude numbers *Fr* = 5.1 and 8.5. The growths in maximum void fraction and bubble count rate with increasing Reynolds number were correlated by :

$$C_{max} = \frac{0.745\ \mathrm{Re}}{\mathrm{Re} + 1.20\ 10^5} \qquad 2\ 10^4 < \mathrm{Re} < 10^5 \quad (5.7)$$

$$\frac{F_{max}\ d_1}{V_1} = 0.73 \times Ln(\mathrm{Re}) - 7.38 \qquad 2\ 10^4 < \mathrm{Re} < 10^5 \quad (5.8)$$

with a normalised coefficient of correlation of 0.978 and 0.984 respectively.

The comparative analysis highlighted that the present data sets with inflow Reynolds numbers up to 98,000 cannot be extrapolated to large-size prototype structures without significant scale effects in terms of void fraction, bubble count rate and bubble chord time distributions. This result has important implications in terms of civil, environmental and sanitary engineering design. In hydraulic structures, storm water systems and water treatment facilities, hydraulics jumps may be experienced with inflow Reynolds numbers ranging from 10^6 to over 10^8. Figure 5.4 illustrates two prototype flow situations with hydraulic jump Reynolds numbers between 10^6 and 10^7.

In a physical model, the flow conditions are said to be similar to those in the prototype if the model displays similarity of form (geometric similarity), similarity of motion (kinematic similarity) and similarity of forces (dynamic similarity) (CHANSON 1999). Scale effects may exist when one or more relevant dimensionless parameters have different values in the model and prototype. Equation (5.2) highlighted that the study of air bubble entrainment in hydraulic jumps required a large number of relevant parameters (CHANSON 2006,2007c). The present comparative analysis

demonstrated further that dynamic similarity of two-phase flows in hydraulic jumps cannot be achieved with a Froude similitude unless working at full-scale (1:1). In experimental facilities with Reynolds numbers up to 10^5, some viscous scale effects were observed in terms of the rate of entrained air (void fraction), air-water interfacial area (bubble count rate) and bubble size populations (bubble chord time distributions) (e.g. Fig. 5.1 to 5.3).

Fig. 5.3 - Effects of the inflow Reynolds number on the maximum void fraction C_{max} and maximum dimensionless bubble count rate $F_{max}d_1/U_1$ for a given inflow Froude number Fr - Experimental data : CHANSON (2006,2007c) and Present study
(A) Effects of the inflow Reynolds number on the maximum void fraction C_{max} - Comparison with Equation (5.7)

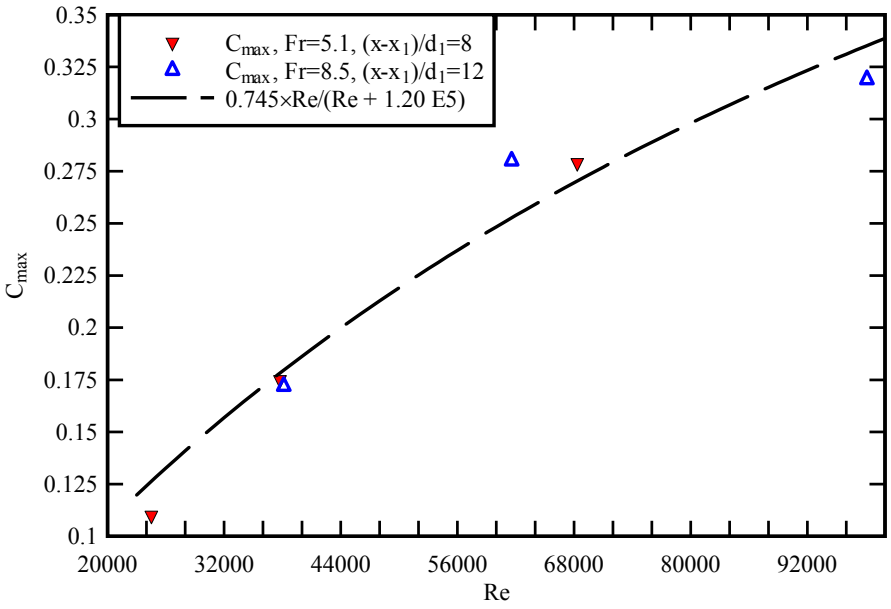

(B) Effects of the inflow Reynolds number on the maximum dimensionless bubble count rate $F_{max}d_1/U_1$ - Comparison with Equation (5.8)

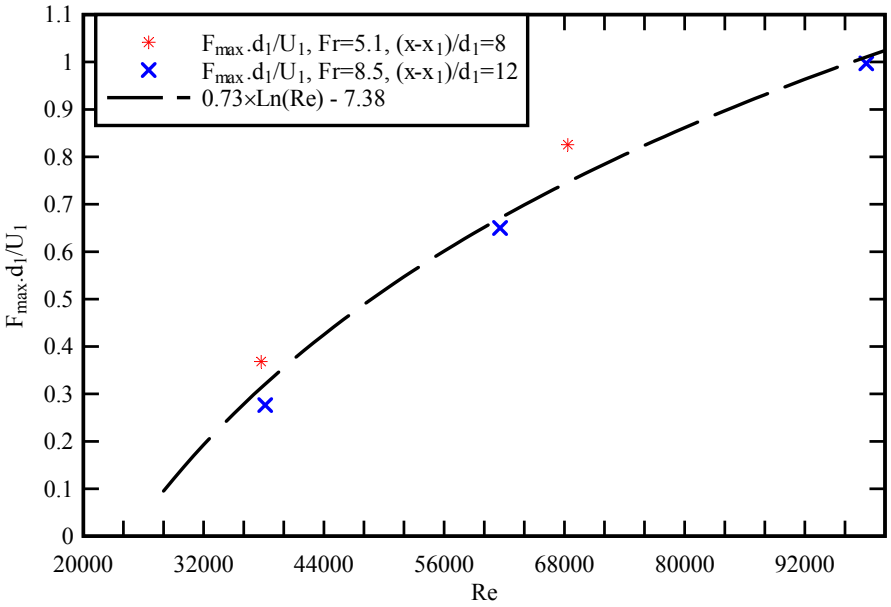

(C) Definition sketch

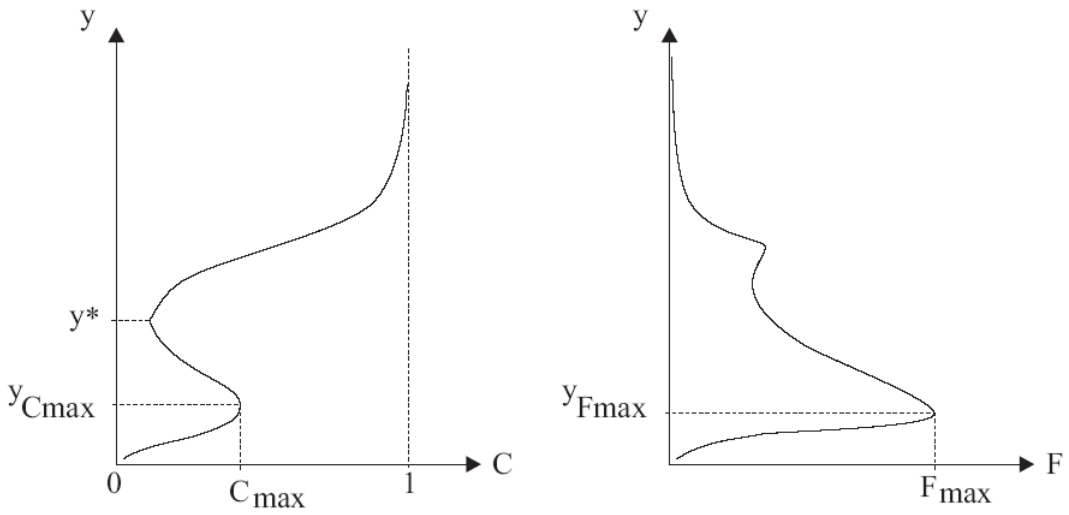

Fig. 5.4 - Prototype hydraulic jumps
(A) Hydraulic jump downstream of the Clermont M.E.L. weir (Clermont QLD, Australia) during a flood in 1992 or 1993 (Courtesy of A.J. HOLMES) - Flow from left to right

(B) Hydraulic jump energy dissipator in operation (Courtesy of John REMI) - Pine Coulee dam spillway during floods in South Alberta, Canada in June 2005 - Flood flow from left to right

5.3 DISCUSSION

5.3.1 Effects of sensor size on physical modelling results

It is worth commenting that the above analysis did not account for the characteristics of the

instrumentation. The size of the probe sensor, the sampling rate and possibly other probe characteristics do affect the minimum bubble size detectable by the measurement system. To date, most systematic studies of scale effects affecting air entrainment processes were conducted with the same instrumentation and sensor size in all experiments. The probe sensor size was not scaled down in the small size models. The present study was no exception and it is acknowledged that this aspect might become a limitation.

It is believed that the only systematic investigation on the effects of the probe sensor size is a series of two studies of air entrainment in skimming flows in stepped spillways (CHANSON and TOOMBES 2002b, CAROSI and CHANSON 2006). In each case, the air-water flow measurements were repeated with identical flow conditions and chute geometry, but different instrumentation. Some comparison was conducted on the performances of phase-detection conductivity probes using two sensors sizes : 25 μm (0.025 mm) and 350 μm (0.35 mm) with the same sampling rates. The results indicated consistently larger bubble count rate measurements with the smaller 0.025 mm sensor probe and a broader range of bubble/droplet sizes detected by the 0.025 mm sensor probe than by the 0.35 mm sensor probe. For example, with a dimensionless flow rate d_c/h = 1.18 and Re = 126,000 where h is the step height, the bubble chord sizes measured with the 0.35 mm sensor were typically 18 to 50% larger (28% in average) than the chord lengths measured with the 0.025 mm sensor (CAROSI and CHANSON 2006).

5.3.2 Reynolds similitude in hydraulic jumps

The present results demonstrated that the dynamic similarity of air bubble entrainment in hydraulic jump was not satisfied with a Froude similitude and Reynolds numbers up to 98,000. Significantly smaller bubble count rates and comparatively larger bubble chord times were observed in a small channel operating at lower Reynolds number for an identical inflow Froude number. Are there other scaling criteria beside the Froude similitude ?

Table 5.1 summarised some studies performed with only one dependant variable, namely the Reynolds number Re. All the other dependant parameters were controlled and maintained constant including the inflow Froude number Fr, the Morton number Mo, the relative width W/d_1, the inflow conditions x_1/d_1 and δ/x_1, and the measurement location ($(x-x_1)/d_1$, y/d_1, z/d_1=0).

An alternative approach could be based upon a Reynolds similitude. ROUSE et al. (1959) conducted such a relevant hydraulic jump study in a wind tunnel. In this study, the air flow was selected to conduct turbulence measurements with a hot-wire probe in the shear flow. While the findings of ROUSE et al. (1959) were important, it was argued that their air model did not reproduce all the main features of the hydraulic jump (RAJARATNAM 1965). A comparison between the air flow results of ROUSE et al. (1959) and the water flow data of RESCH and LEUTHEUSSER (1972b) highlighted some differences in terms of distributions of normal and tangential Reynolds stresses in the jump flow (CHANSON 2007c).

The dynamic similarity of air entrainment in hydraulic jumps is characterised by a large number of relevant parameters. Neither the Froude similitude nor Reynolds similitude are free of scale effects, unless the physical modelling is conducted at full-scale.

6. CONCLUDING REMARKS

Experimental studies of multiphase flows are difficult and complex. But the relevant range of applications is broad encompassing chemical engineering, pollutant transport in the environment, beach dynamics, hydraulic structures, mixing processes... In many applications, the multiphase flows are characterised by some mixing of air, water and/or solid particles. For the scientists, the hydraulic jump is one most interesting, fascinating two-phase flow situation with a free-surface. Despite nearly two centuries of studies, there is still a lack of knowledge on the fluid dynamics of the turbulent shear layer, the roller and the region next to the air-water interface. Particularly, the turbulence structure of the flow needs some better understanding.

In the present study, new series of experimental measurements were conducted in hydraulic jumps with Froude numbers between 3.1 and 8.5, and inflow Reynolds numbers between 24,000 and 62,000. Two experimental techniques were used. Dynamic free surface measurements were performed with acoustic displacement meters to gain some information on the mean and turbulent surface profiles, integral time scales and frequency range. For the two-phase flow measurements, a dual-tip conductivity probe was selected. Some new analysis was performed to characterise the turbulence in this highly-aerated shear flow. Further, instantaneous free surface and void fraction data were simultaneously recorded to study some correlation between their respective frequency ranges.

A detailed study of the free surface behaviour was conducted for Fr = 3.1 to 8.5. The shape of the mean free surface profile was well defined and in agreement with visual observations. The turbulent fluctuation profiles highlighted a distinct peak of turbulent intensity in the first part of the jump roller. Far downstream of the impingement point, a dissipation area was observed where the turbulence decayed gradually. The peak of free-surface fluctuation levels increased with increasing Froude number. The free-surface fluctuation frequencies were typically between 1 and 4 Hz, with a dominant frequency for a given Froude number. The dominant frequency was typically higher in the roller than in the downstream flow. This result was consistent with visual observations. A comparison between the acoustic sensor signals and conductivity probe data suggested that the air-water "free-surface" detected by the acoustic sensor corresponded to about the boundary between the turbulent shear layer and the upper free-surface layer ($y \sim y^*$).

The two-phase flow properties were investigated for Fr = 5.1 to 8.3. The vertical profiles of void fraction showed two distinct regions, namely the turbulent shear region in the lower part of the flow and an upper free-surface region. In the air-water shear region, the void fraction and bubble count rate distributions exhibited marked peaks : i.e., C_{max} and F_{max} respectively. The maximum of void fraction (C_{max}) was always found above the location of the maximum bubble count rate (F_{max}). The quantitative values were functions both Froude number and streamwise position, illustrating the influence of the Froude number on the air entrainment processes. The data analysis showed also that the mean bubble chord length in the turbulent shear layer was between 1 mm and 6 mm. These basics results were in good agreement with previous experimental studies.

The distributions of interfacial velocity, turbulence intensity and integral turbulence time scales were documented. The dimensionless distributions of interfacial velocity compared favourably with

some wall-jet flow equations. The turbulence intensity data highlighted a decay of the turbulent level with increasing distance from the impingement point, while lower intensities were observed close to the bottom. The boundary condition at the bottom of the channel was believed to be responsible of the latter result. The vertical distributions of auto-correlation integral time scales showed some increase with increasing distance from the bed. Further the integral time scales decreased with increasing distance from the jump toe, and the vertical profiles became nearly uniform near the downstream end of the roller with $T_{xx}U_1/d_1 \sim 0.7$. The probability distribution functions (PDF) of bubble chord time illustrated a broad spectrum with predominance to small bubble chord times (less than 2-3 ms).

Simultaneous measurements of free surface and bubbly flow fluctuations for $Fr = 5.1$ were performed. Spectral analyses indicated that the frequency ranges of both sensors were similar ($F < 5$ Hz) whatever the position downstream of the toe. The signal cross correlations showed some large positive and negative values implying with some periodic shapes.

A comparative analysis of Froude similar experiments was conducted with Reynolds numbers between 25,000 and 98,000, inflow depths of 0.012, 0.018 and 0.024 m, and two Froude numbers ($Fr = 5.1$ and 8.5). The results implied that the experimental data obtained with inflow Reynolds numbers up to 98,000 cannot be extrapolated to large-size prototype structures without significant scale effects in terms of void fraction, bubble count rate and bubble chord time distributions. This result has important implications in terms of civil, environmental and sanitary engineering structures because the prototype Reynolds numbers range typically from 10^6 to over 10^8.

It is believed that the present results bring new information on the fluid dynamics of hydraulic jumps. They revealed the turbulent nature of this complex two-phase flow with large turbulence intensities and complex motions. The results will need further developments. For instance, experimental studies with larger Froude numbers could be undertaken as well as some analysis of bubble clustering. In that way, all data of the present study are available. Numerical modelling of hydraulic jumps may also be a future research topic. The large amount of data collected up to date provides a nice calibration database. This computing approach will not be easy because the hydraulic jump flows encompass many challenges including two-phase flow, turbulence, free surface…

7. ACKNOWLEDGEMENTS

The writers thank Dr Nicolas RIVIERE (INSA Lyon, France) and Dr Marti SANCHEZ-JUNY (UPC, Spain) for their expert review of the report and valuable comments.

They thank further Graham ILLIDGE and Clive BOOTH (The University of Queensland) for their technical assistance.

The first writer acknowledges the financial support of the ESTACA and particularly François STEPHAN (Head of Department). He thanks Sho-ichi FURUYAMA, Stephan FELDER, Mark TREVETHAN and people from the School of Civil Engineering at The University of Queensland at Brisbane during his visit in May-June 2007. Lastly he thanks Claire and Clémence for their support.

APPENDIX A – PHOTOGRAPHS OF AIR BUBBLE ENTRAINMENT IN HYDRAULIC JUMPS

Fig. A.1 - General view of the experimental facility at the University of Queensland
(A) Experimental channel used for experiments at the University of Queensland, flow bottom right to upper left

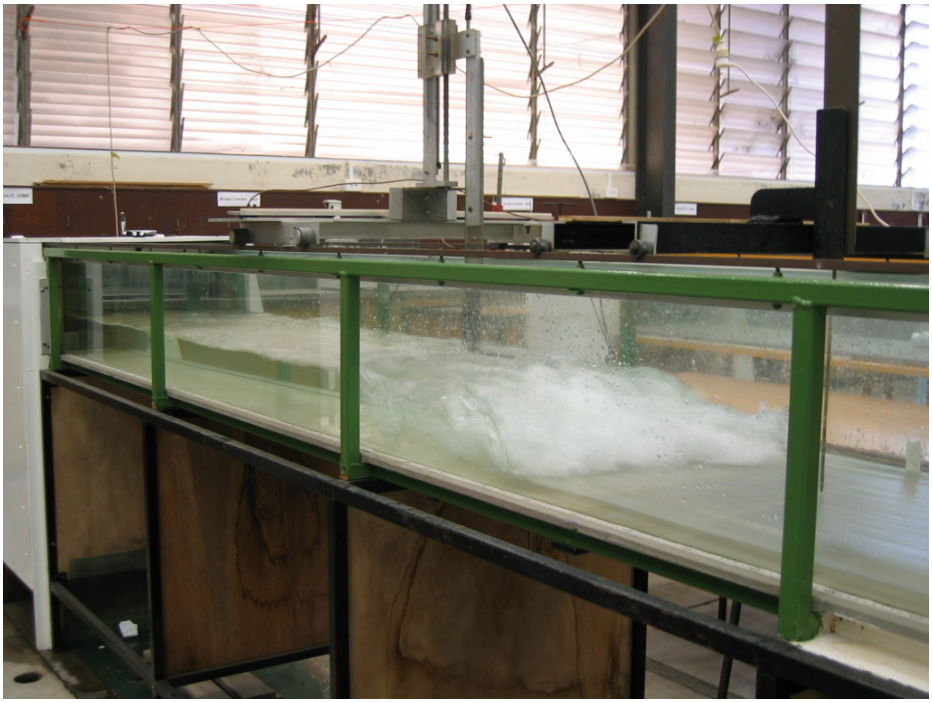

(B) Flow conditions: Fr = 5.1, x_1 = 0.75 m, d_1 = 0.018 m, shutter speed: 1/40 s, flow from right to left

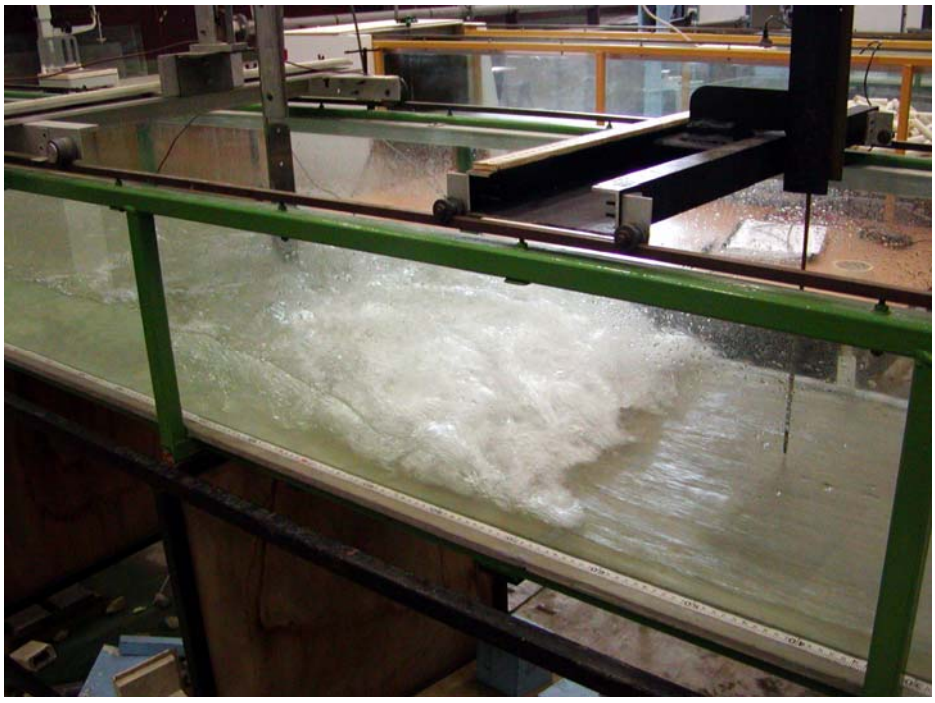

(C) Flow conditions: Fr = 7.6, x_1 = 0.75 m, d_1 = 0.018 m, shutter speed: 1/40 s, flow from right to left

(D) Flow conditions: Fr = 8.3, x_1 = 0.75 m, d_1 = 0.018 m, shutter speed: 1/20 s, flow from right to left

Fig. A.2 - Side view of air bubble entrainment in hydraulic jumps
(A) Jump to - Flow conditions: Fr = 5.1, x_1 = 0.75 m, d_1 = 0.018 m, shutter speed: 1/320 s, flow from right to left

(B) Flow conditions: Fr = 7.6, x_1 = 0.75 m, d_1 = 0.018 m, shutter speed: 1/80 s, flow from left to right

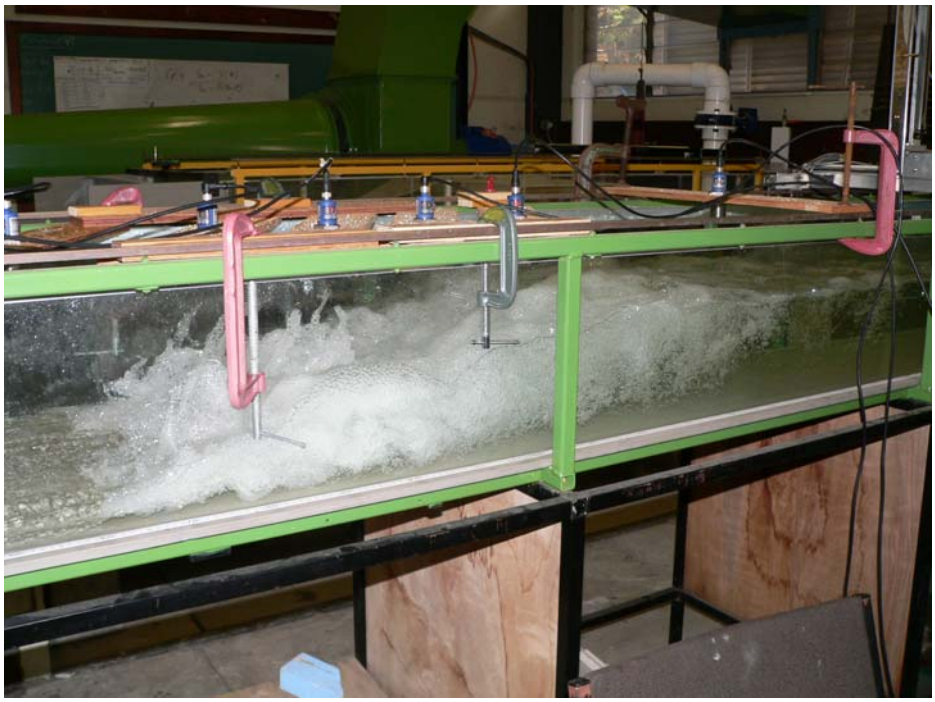

(C) Flow conditions: Fr = 8.3, x_1 = 0.75 m, d_1 = 0.018 m, shutter speed: 1/80 s, flow from right to left

Fig. A.3 - Details of the air-water flow structures above the hydraulic jump
(A) Jump toe - Flow conditions: Fr = 5.1, x_1 = 0.75 m, d_1 = 0.018 m, shutter speed: 1/320 s, flow from foreground to background

(B) Free-surface region - Flow conditions: Fr = 7.6, x_1 = 0.75m, d_1 = 0.018m, shutter speed: 1/250 s, flow from right to left

(C) Jump toe and roller - Flow conditions: Fr = 8.3, x_1 = 0.75m, d_1 = 0.018m, shutter speed: 1/250 s, flow from right to left

APPENDIX B - METROLOGY AND MEASUREMENTS OF TURBULENT FREE-SURFACE FLUCTUATIONS IN HYDRAULICS

B.1 Presentation

New experiments were carried out in the Gordon McKAY Hydraulic Laboratory at the University of Queensland (Australia) (Table B.1). The measurements were conducted in a horizontal rectangular flume (0.50 m in width, 0.45 m in depth and 3.2 m in length) with long glass sidewalls and a PVC bed. Photographs are shown in Appendix A. It was previously used by CHANSON (2001,2005,2007) and KUCUKALI and CHANSON (2007).

The water discharge was measured with a Venturi meter located in the supply line and which was calibrated on-site with a large V-notch weir. The discharge measurements were accurate within +/- 2%. The upstream and downstream conjugate flow depths were measured using rail mounted point gauges with a 0.2 mm accuracy.

The free-surface fluctuations were recorded using six ultrasonic displacement meters. 5 Microsonic™ Mic+25/IU/TC ultrasonic displacement meters were used above the jump roller (locations S2 to S6, Fig. B.1), with an accuracy of 0.18 mm and a response time of 50 ms. An Microsonic™ Mic+35/IU/TC ultrasonic displacement meter was used to record the inflow depth fluctuations (location S1, Fig. B.1), with an accuracy of 0.18 mm and a response time of 70 ms. Further details on the displacement meters are given in Table B.2. The displacement meters were mounted above the flow and scanned downward the air-water flow "pseudo" free-surface as illustrated in Figure B.1. Each probe signal output was scanned at 50 Hz per sensor for 10 minutes. Note that each sensor was set with no filter and for multiplex mode.

Fig. B.1 - Experimental set-up with ultrasonic 6 displacement meters above the flow

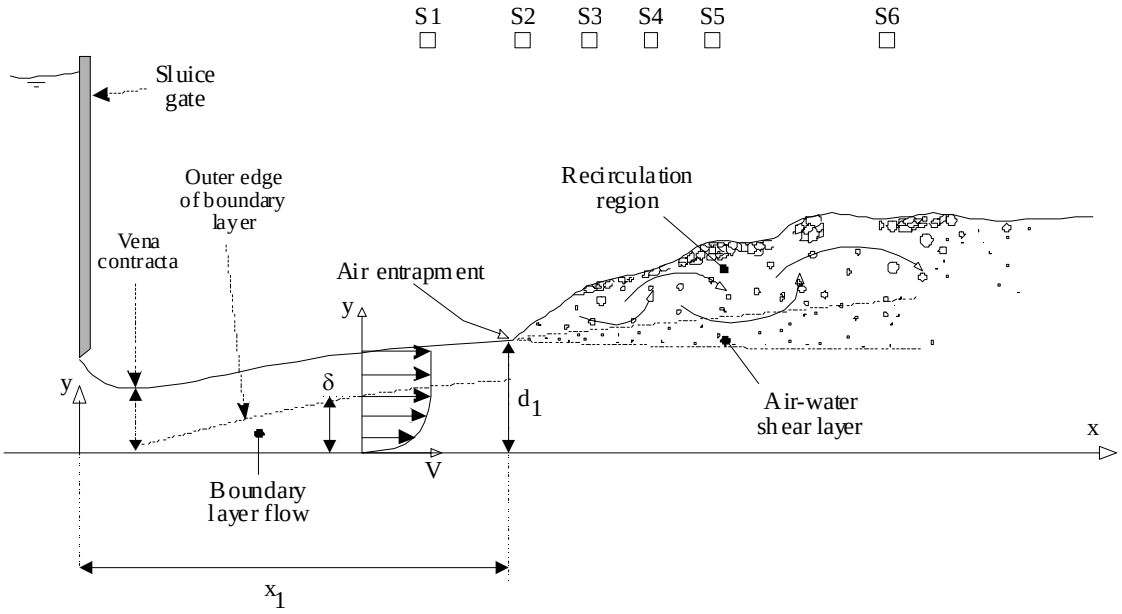

Table B.1 - Experimental flow conditions

		x	d_1	U_1	Fr	Re	S1 x-x_1	S2 x-x_1	S3 x-x_1	S4 x-x_1	S5 x-x_1	S6 x-x_1
	(m^3/s)	(m)	(m)	(m/s)			(m)	(m)	(m)	(m)	(m)	(m)
1	0.012	0.75	0.018	1.32	3.1	23,750	-0.20	0.06	0.24	0.41	0.58	1.06
2	0.016	0.75	0.018	1.77	4.2	31,850	-0.20	0.06	0.24	0.41	0.58	1.06
3	0.020	0.75	0.018	2.21	5.3	39,800	-0.20	0.06	0.24	0.41	0.58	1.06
4	0.024	0.75	0.018	2.70	6.4	48,600	-0.20	0.06	0.24	0.41	0.58	1.06
5	0.028	0.75	0.018	3.17	7.6	57,050	-0.20	0.06	0.24	0.41	0.58	1.06
6	0.032	0.75	0.018	3.56	8.5	64,100	-0.20	0.06	0.24	0.41	0.58	1.06

Table B.2 - Characteristics of the ultrasonic acoustic displacement meters (Ref. Microsonic™ (http://www.microsonic.de))

	Microsonic™ Mic+25/IU/TC	Microsonic™ Mic+35/IU/TC	Units
Accuracy	0.18	0.18	mm
Response time	50	70	ms
Ultrasonic frequency	320	400	Hz
Wave length (at 20 C)	1.1	0.9	mm
Detection zone radius at operating range	22	37.5	mm
Blind zone :	30	60	mm
Operating range	250	350	mm
Maximum range :	350	600	mm

The principle of the acoustic displacement meters is based upon an acoustic beam emitted in air by the sensitive part of the acoustic displacement meter. The beam propagates downward perpendicular to the free-surface. Once it hits the air-water interface, the beam is reflected back to the sensor. From the knowledge of the sound celerity in air, a simple measure of the travel time provides the distance between the sensor and the free surface. Herein the ultrasonic displacement probes were calibrated in clear water at rest against pointer gauge measurements for a range of water depths shortly before each experiment, using the same procedure as KOCH and CHANSON (2005) and KUCUKALI and CHANSON (2007). The calibration lasted 5 seconds and 250 samples were recorded.

With any ultrasonic displacement meter, the signal output is a function of the strength of the acoustic signal reflected by the "free-surface". Hence some erroneous points may be recorded for various reasons and must be eliminated (see chapter 2). CHANSON et al. (1999, 2002) tested an ultrasonic displacement meter Keyence™ UD300 in a bubbly column with up to 10% void fraction. Their results suggested that the ultrasonic probe readings corresponded to about y_{50} to $\underline{y}_{60}$ where y_{xx} is the elevation where the void fraction is xx %.

During the present study, it was observed that the ultrasonic probe reading gave a depth corresponding to a level just above the turbulent shear layer in the hydraulic jump roller : i.e., $y \approx y^*$ where y* is a characteristic depth where the void fraction distribution exhibits a marked change between a Gaussian bell-shape in the turbulent shear layer, and a Gaussian error function in the free-surface region (Fig. 1.1B)

Notation

C	void fraction defined as the volume of air per unit volume of air and water; it is also called air concentration or local air content;
d	water depth (m);
d_1	flow depth (m) measured immediately upstream of the hydraulic jump;
d_2	flow depth (m) measured immediately downstream of the hydraulic jump;
d_{asw}	distance (m) above still water for the calibration of the sensor
d_b	distance (m) from the sensor tto the bottom
Fr	upstream Froude number: $Fr = \frac{q}{\sqrt{g{d_1}^3}}$;
g	gravity acceleration (m/s^2) : $g = 9.80 m/s^2$ in Brisbane (Australia);
L_r	hydraulic jump length (m);
Q	water discharge (m^3/s);
q	water discharge per unit width (m^2/s): $q = Q/W$;
Re	inflow Reynolds number : $Re = \rho \frac{U_1 d_1}{\mu}$;
U_1	upstream flow velocity (m/s): $U_1 = \frac{q}{d_1}$;
W	channel width (m);
x	longitudinal distance from the sluice gate (m);
x_1	longitudinal distance from the gate to the jump toe (m);
y	distance (m) measured normal to the flow direction;
y_{50}	characteristic depth (m) where C = 0.50;
y_{60}	characteristic depth (m) where C = 0.60;
y_{80}	characteristic depth (m) where C = 0.80;
η	water depth (m);
η'	root mean square of the water depth (m);
μ	dynamic viscosity (Pa.s) of water;
ν	kinematic viscosity (m^2/s) of water: ν = μ/ρ;
ρ	density (kg/m^3) of water;

Subscript

1	upstream flow conditions;
2	downstream flow conditions

Abbreviations

Kurt kurtosis (or excess kurtosis);

Skew skewness;

Std standard deviation.

B.2 - Calibration of the acoustic displacement meters

Prior to each experiment, the acoustic displacement meters were calibrated in still water for 3 different distances above the still water (d_{asw}). Herein the corresponding output voltages are given, with the linear relationship between the output voltage and the distance to the free surface from the sensor. Finally, a relation is given for each sensor which links the output voltage to the water depth (Table B.2).

Table B.2 - Calibration of the acoustic displacement meters

Sensor 1 (x=0.55m)		Sensor 2 (x=0.81m)		Sensor 3 (x=0.99m)	
Distance to bottom: d_b=0.265m		Distance to bottom: d_b=0.266m		Distance to bottom:d_b=0.263m	
d_{asw} (m)	Voltage output (V)	d_{asw} (m)	Voltage output (V)	d_{asw} (m)	Voltage output (V)
0.218	8.59	0.219	8.75	0.217	8.62
0.168	6.31	0.169	6.56	0.167	6.49
0.118	4.03	0.118	4.35	0.116	4.27
Relation distance/voltage: d(m)=0.0219V+0.0296		Relation distance/voltage: d(m)=0.0230V+0.0182		Relation distance/voltage: d(m)=0.0232V+0.0296	
Relation output voltage/water depth η(m)=0.265-(0.0219V+0.0296)		Relation output voltage/water depth η(m)=0.266-(0.0230V+0.0182)		Relation output voltage/water depth η(m)=0.263-(0.0232V+0.0167)	

Sensor 4 (x=1.16m)		Sensor 5 (x=1.33m)		Sensor 6 (x=1.81m)	
Distance to bottom: d_b=0.267m		Distance to bottom: d_b=0.265m		Distance to bottom: d_b=0.297m	
d_{asw} (m)	Voltage output (V)	d_{asw} (m)	Voltage output (V)	d_{asw} (m)	Voltage output (V)
0.220	6.26	0.218	8.43	0.250	6.80
0.170	4.74	0.167	6.26	0.200	5.10
0.120	3.22	0.116	4.05	0.149	3.39
Relation distance/voltage: d(m)=0.0329V+0.0141		Relation distance/voltage: d(m)=0.0233V+0.0215		Relation distance/voltage: d(m)=0.0296V+0.0487	
Relation output voltage/water depth η(m)=0.267-(0.0329V+0.0141)		Relation output voltage/water depth η(m)=0.265-(0.0233V+0.0215)		Relation output voltage/water depth η(m)=0.297-(0.0296V+0.0487)	

B.3 - Free-surface fluctuation measurements

B.3.1 Fr = 3.1

Location :	The University of Queensland (Australia)
Date :	May 2007
Experiments by :	F. MURZYN
Data processing by:	F. MURZYN
Data analysis by :	F.MURZYN and H. CHANSON
Experiment characteristics :	Channel: Length=3.2m, Width=0.50m, Slope=0º (horizontal). Open channel with glass sidewalls and PVC bottom. Q = 0.012m^3/s, x_1=0.75m, d_1=0.018 m, Fr=3.1, Re=23,750

Instrumentation :	Ultrasonic displacement meters Microsonic™ Mic+25/IU/TC and Mic+35/IU/TC x=0.55, 0.81, 0.99, 1.16, 1.33 and 1.81 m Scan rate: 50 Hz per probe sensor Sampling duration: 600 sec (10 minutes)
Comments :	Initial conditions : partially-developed inflow. Each ultrasonic displacement meter was set with no filter and for multiplex mode. Experiments: 070522

x (m)	0.55	0.81	0.99	1.16	1.33	1.81
$(x-x_1)/d_1$	-11.11	3.33	13.33	22.78	32.22	58.89
Mean value η (m)	0.017	0.060	0.072	0.077	0.076	0.077
Root mean square η' (m)	0.0003	0.0060	0.0027	0.0024	0.0021	0.0017
η/d_1	0.94	3.33	4.00	4.28	4.22	4.28
η'/d_1	0.017	0.333	0.150	0.133	0.117	0.094

B.3.2 Fr = 4.2

Location :	The University of Queensland (Australia)
Date :	May 2007
Experiments by :	F. MURZYN
Data processing by:	F. MURZYN
Data analysis by :	F.MURZYN and H. CHANSON
Experiment characteristics :	Channel: Length=3.2m, Width=0.50m, Slope=0º (horizontal). Open channel with glass sidewalls and PVC bottom. Q = 0.016m^3/s, x_1=0.75m, d_1=0.018 m, Fr=4.2, Re=31,850
Instrumentation :	Ultrasonic displacement meters Microsonic™ Mic+25/IU/TC and Mic+35/IU/TC x=0.55, 0.81, 0.99, 1.16, 1.33 and 1.81 m Scan rate: 50 Hz per probe sensor Sampling duration: 600 sec (10 minutes)
Comments :	Initial conditions : partially-developed inflow. Each ultrasonic displacement meter was set with no filter and for multiplex mode. Experiments: 070522

x (m)	0.55	0.81	0.99	1.16	1.33	1.81
$(x-x_1)/d_1$	-11.11	3.33	13.33	22.78	32.22	58.89
Mean value η (m)	0.017	0.064	0.095	0.106	0.104	0.106
Root mean square η' (m)	0.0003	0.0098	0.0070	0.0043	0.0035	0.0024
η/d_1	0.94	3.56	5.28	5.89	5.78	5.89
η'/d_1	0.017	0.544	0.389	0.239	0.194	0.133

B.3.3 Fr = 5.3

Location :	The University of Queensland (Australia)
Date :	May 2007

Experiments by :	F. MURZYN
Data processing by:	F. MURZYN
Data analysis by :	F.MURZYN and H. CHANSON
Experiment characteristics :	Channel: Length=3.2m, Width=0.50m, Slope=0º (horizontal). Open channel with glass sidewalls and PVC bottom. Q = 0.020m^3/s, x_1=0.75m, d_1=0.018 m, Fr=5.3, Re=39,800
Instrumentation :	Ultrasonic displacement meters Microsonic™ Mic+25/IU/TC and Mic+35/IU/TC x=0.55, 0.81, 0.99, 1.16, 1.33 and 1.81 m Scan rate: 50 Hz per probe sensor Sampling duration: 600 sec (10 minutes)
Comments :	Initial conditions : partially-developed inflow. Each ultrasonic displacement meter was set with no filter and for multiplex mode. Experiments: 070522

x (m)	0.55	0.81	0.99	1.16	1.33	1.81
$(x-x_1)/d_1$	-11.11	3.33	13.33	22.78	32.22	58.89
Mean value η (m)	0.018	0.056	0.102	0.129	0.131	0.144
Root mean square η' (m)	0.0004	0.0125	0.0122	0.0083	0.0060	0.0039
η/d_1	1.00	3.11	5.67	7.17	7.28	8.00
η'/d_1	0.022	0.694	0.678	0.461	0.333	0.217

B.3.4 Fr = 6.4

Location :	The University of Queensland (Australia)
Date :	May 2007
Experiments by :	F. MURZYN
Data processing by:	F. MURZYN
Data analysis by :	F.MURZYN and H. CHANSON
Experiment characteristics :	Channel: Length=3.2m, Width=0.50m, Slope=0º (horizontal). Open channel with glass sidewalls and PVC bottom. Q = 0.024m^3/s, x_1=0.75m, d_1=0.018 m, Fr=6.4, Re=48,600
Instrumentation :	Ultrasonic displacement meters Microsonic™ Mic+25/IU/TC and Mic+35/IU/TC x=0.55, 0.81, 0.99, 1.16, 1.33 and 1.81 m Scan rate: 50 Hz per probe sensor Sampling duration: 600 sec (10 minutes)
Comments :	Initial conditions : partially-developed inflow. Each ultrasonic displacement meter was set with no filter and for multiplex mode. Experiments: 070522

x (m)	0.55	0.81	0.99	1.16	1.33	1.81
$(x-x_1)/d_1$	-11.11	3.33	13.33	22.78	32.22	58.89
Mean value η (m)	0.018	0.066	0.114	0.150	0.159	0.163
Root mean square η' (m)	0.0005	0.0141	0.0154	0.0122	0.0100	0.0059
η/d_1	1.00	3.67	6.33	8.33	8.83	9.06
η'/d_1	0.028	0.783	0.856	0.678	0.556	0.328

B.3.5 Fr = 7.6

Location :	The University of Queensland (Australia)
Date :	May 2007
Experiments by :	F. MURZYN
Data processing by:	F. MURZYN
Data analysis by :	F.MURZYN and H. CHANSON
Experiment characteristics :	Channel: Length=3.2m, Width=0.50m, Slope=0º (horizontal). Open channel with glass sidewalls and PVC bottom. Q = 0.028m^3/s, x_1=0.75m, d_1=0.018 m, Fr=7.6, ,Re=57,050
Instrumentation :	Ultrasonic displacement meters Microsonic™ Mic+25/IU/TC and Mic+35/IU/TC x=0.55, 0.81, 0.99, 1.16, 1.33 and 1.81 m Scan rate: 50 Hz per probe sensor Sampling duration: 600 sec (10 minutes)
Comments :	Initial conditions : partially-developed inflow. Each ultrasonic displacement meter was set with no filter and for multiplex mode. Experiments: 070522

x (m)	0.55	0.81	0.99	1.16	1.33	1.81
$(x-x_1)/d_1$	-11.11	3.33	13.33	22.78	32.22	58.89
Mean value η (m)	0.020	0.056	0.107	0.143	0.172	0.192
Root mean square η' (m)	0.0008	0.0141	0.0187	0.0186	0.0182	0.0095
η/d_1	1.11	3.11	5.94	7.94	9.56	10.67
η'/d_1	0.044	0.783	1.039	1.033	1.011	0.528

B.3.6 Fr = 8.5

Location :	The University of Queensland (Australia)
Date :	May 2007
Experiments by :	F. MURZYN
Data processing by:	F. MURZYN
Data analysis by :	F.MURZYN and H. CHANSON
Experiment characteristics :	Channel: Length=3.2m, Width=0.50m, Slope=0º (horizontal). Open channel with glass sidewalls and PVC bottom. Q = 0.032m^3/s, x_1=0.75m, d_1=0.018 m, Fr=8.5, Re=64,100
Instrumentation :	Ultrasonic displacement meters Microsonic™ Mic+25/IU/TC and Mic+35/IU/TC x=0.55, 0.81, 0.99, 1.16, 1.33 and 1.81 m Scan rate: 50 Hz per probe sensor Sampling duration: 600 sec (10 minutes)
Comments :	Initial conditions : partially-developed inflow. Each ultrasonic displacement meter was set with no filter and for multiplex mode. Experiments: 070522

x (m)	0.55	0.81	0.99	1.16	1.33	1.81

$(x\text{-}x_1)/d_1$	-11.11	3.33	13.33	22.78	32.22	58.89
Mean value η (m)	0.020	N/A	0.088	0.137	0.156	0.214
Root mean square η' (m)	0.0013	N/A	0.0159	0.0219	0.0264	0.0123
η/d_1	1.11	N/A	4.89	7.61	8.67	11.89
η'/d_1	0.072	N/A	0.883	1.217	1.467	0.683

APPENDIX C - AIR-WATER MEASUREMENTS IN HYDRAULIC JUMPS WITH PARTIALLY-DEVELOPED INFLOW CONDITIONS

C.1 Presentation

New experiments were carried out in the Gordon McKAY Hydraulic Laboratory at the University of Queensland (Australia). The measurements were conducted in a horizontal rectangular flume (0.50 m wide, 0.45 m high and 3.2 m long) with glass sidewalls and a PVC bed. (Photographs of the experimental facility are presented in Appendix A.) This channel was previously used by CHANSON (2001,2005,2007) and KUCUKALI and CHANSON (2007).

The water discharge was measured with a Venturi meter located in the supply line and it was calibrated on-site with a large V-notch weir. The discharge measurement was accurate within $\pm 2\%$. The clear-water flow depths were measured using rail mounted point gauges with a 0.2 mm accuracy.

The air-water flow properties were measured with a double-tip conductivity probe. The probe sensor size was 0.25 mm and the longitudinal separation distance between sensors was Δx = 7.0 mm. The probe was manufactured at the University of Queensland and it was excited by an electronic system (Ref. UQ82.518) designed with a response time of less than 10 μs. The probe and electronics were previously used by CHANSON (2005b), CHANSON and CAROSI (2007) and KUCUKALI and CHANSON (2007). During the present experiments, each probe sensor was sampled at 20 kHz for 45 s. The probe displacement in the vertical direction was controlled by a fine adjustment system connected to a Mitutoyo™ digimatic scale unit with a vertical accuracy Δy of less than 0.1 mm. Table C.1 summarises the experimental flow conditions.

Table C.1 - Experimental flow conditions for air water measurements

	Q (m^3/s)	x_1 (m)	d_1 (m)	U_1 (m/s)	Fr	Re	x-x_1 Profile 1 (m)	x-x_1 Profile 2 (m)	x-x_1 Profile 3 (m)	x-x_1 Profile 4 (m)
1	0.019	0.75	0.018	2.12	5.1	38150	0.075	0.150	0.225	--
2	0.029	0.75	0.018	3.18	7.6	57250	0.225	0.300	0.450	--
3	0.031	0.75	0.018	3.47	8.3	62250	0.225	0.300	0.450	0.600

Discussion

The flow conditions corresponded to a partially-developed flow at the jump toe (Table C.1). That is, the ratio of bottom boundary layer thickness to inflow depth was less than unity.

Herein the velocity measurements were not conducted in the recirculation region because the phase-detection intrusive probes cannot discriminate the direction nor magnitude of the velocity in complicated turbulent flows. Indeed intrusive probes, including the phase-detection dual-tip probe used herein, are designed to measure positive velocities only and the probe sensor would be affected by wake effects during flow reversal.

Simply the velocity data signal processing could only be performed at locations where the correlation calculations were meaningful (e.g. CHANSON 2006, CAROSI and CHANSON 2006). At some sampling locations, especially in the recirculation region, the calculations were unsuccessful. Problems included some flat cross-correlation functions without a distinctive peak, non-zero crossing of the correlation function(s) with the horizontal axis, correlation functions with several peaks, meaningless correlation trends ... While most correlation calculations can be automated, some human intervention is essential to validate each calculation step. Herein most calculations were performed by hand and all meaningless results were rejected.

Notation

C void fraction defined as the volume of air per unit volume of air and water; it is also called air concentration or local air content;

ch_{mbc} mean bubble chord length (m)

d water depth (m);

d_1 flow depth (m) measured immediately upstream of the hydraulic jump;

Fr upstream Froude number: $Fr = \frac{q}{\sqrt{g d_1^3}}$;

g gravity acceleration (m/s^2) : g = 9.80 m/s^2 in Brisbane (Australia);

L_r hydraulic jump length (m);

Q water discharge (m^3/s);

q water discharge per unit width (m^2/s): $q = Q/W$;

Re inflow Reynolds number : $\text{Re} = \rho \frac{U_1 d_1}{\mu}$;

T average air-water interfacial travel time between the two probe sensors (s);

T_{xx} auto-correlation integral time scale (s): $T_{xx} = \int_{\tau=0}^{\tau=\tau(R_{xx}=0)} R_{xx} d\tau$;

U_1 upstream flow velocity (m/s): $U_1 = \frac{q}{d_1}$;

W channel width (m);

x longitudinal distance from the sluice gate (m);

x_1 longitudinal distance from the gate to the jump toe (m);

y distance (m) measured normal to the flow direction;

η water depth (m);

μ Dynamic viscosity (Pa.s) of water;

ν kinematic viscosity (m^2/s) of water: $\nu = \mu/\rho$;

ρ density (kg/m^3) of water;

Subscript

1 upstream flow conditions;

2 downstream flow conditions

Abbreviations

Kurt kurtosis (or excess kurtosis);

Skew skewness;

Std standard deviation.

C.2 Measurements of void fraction, bubble count rate, bubble diameter and velocity

C.2.1 $Fr = 5.1$

Location :	The University of Queensland (Australia)
Date :	May 2007
Experiments by :	F. MURZYN
Data processing by:	F. MURZYN
Data analysis by :	F. MURZYN and H. CHANSON
Experiment characteristics :	Channel: Length=3.2m, Width=0.50m, Slope=0º (horizontal). Open channel with glass sidewalls and PVC bottom. Q=0.019m^3/s, x_1=0.75 m, d_1=0.018 m, Fr=5.1, Re=38,150
Instrumentation :	Double-tip conductivity probe (∅=0.25 mm, Δx=7mm). Scan rate: 20kHz per probe sensor, sampling duration: 45 sec.
Comments :	Initial conditions : partially-developed inflow Experiments 070528

$x - x_1 = 0.075m$

y (mm)	C	F (Hz)	ch_{mbc} (mm)	V (m/s)
3	0.000	0.6	1.09	1.69
6	0.003	2.9	1.27	1.28
9	0.007	6.2	1.89	1.57
12	0.013	11.5	1.93	1.67
15	0.029	21.0	1.95	1.43
18	0.052	33.2	2.51	1.59
21	0.086	46.1	2.76	1.47
24	0.130	54.1	3.57	1.48
27	0.170	55.4	4.48	1.46
30	0.218	51.0	5.58	1.31
33	0.216	42.6	6.70	1.32
36	0.222	32.2	7.85	1.14
39	0.236	29.2	12.18	1.51
42	0.236	26.6	54.03	N/A
45	0.266	25.5	60.91	N/A
48	0.293	29.1	61.25	N/A
51	0.450	26.7	102.6	N/A
54	0.501	25.6	119.2	N/A
57	0.664	20.5	197.4	N/A
60	0.802	13.3	366.1	N/A
63	0.897	7.7	712.2	N/A
68	0.949	3.8	1529.3	N/A
73	0.968	2.5	760.2	N/A
78	0.962	2.5	2372.7	N/A
83	0.987	1.2	5199.9	N/A
90	0.994	0.6	1838.7	1.07

97	0.994	0.5	11824.6	N/A

$x - x_1 = 0.150m$

y (mm)	C	F (Hz)	ch_{mbc} (mm)	V (m/s)
3	0.002	2.2	1.34	1.47
6	0.003	3.2	1.22	1.25
9	0.011	8.6	1.95	1.52
12	0.018	12.4	2.13	1.51
15	0.025	17.8	2.21	1.56
18	0.046	28.1	2.61	1.59
21	0.050	29.6	2.24	1.32
24	0.092	41.2	2.93	1.31
27	0.099	42.0	3.07	1.30
30	0.114	43.2	3.57	1.35
33	0.157	43.1	5.06	1.39
36	0.151	38.6	5.12	1.31
39	0.175	36.5	5.55	1.16
42	0.162	30.2	8.24	1.54
45	0.154	26.0	11.68	1.97
48	0.166	23.8	19.11	N/A
51	0.168	22.0	46.71	N/A
54	0.211	24.8	51.73	N/A
57	0.164	21.6	46.09	N/A
60	0.215	22.0	43.96	N/A
63	0.22	23.1	58.09	N/A
68	0.391	25.9	91.88	N/A
73	0.567	21.9	157.82	N/A
78	0.642	17.9	218.3	N/A
83	0.769	12.0	389.9	N/A
88	0.866	8.2	639.2	N/A
93	0.918	4.7	1090.6	N/A
100	0.970	2.4	1441.2	N/A
107	0.978	1.6	1425.7	N/A
114	0.995	0.4	5268.4	N/A
121	0.999	0.1	77702.8	N/A
128	0.997	0.2	16112.3	N/A
135	0.998	0.1	15188.6	N/A

$x - x_1 = 0.225m$

y (mm)	C	F (Hz)	ch_{mbc} (mm)	V (m/s)
3	0.004	2.5	1.69	1.03
6	0.006	4.4	1.55	1.07
9	0.011	7.2	1.69	1.07
12	0.016	9.3	1.88	1.10
15	0.022	12.4	1.93	1.09
18	0.025	14.3	1.78	1.01
21	0.033	18.0	1.88	1.03
24	0.040	20.3	2.17	1.11
27	0.044	20.4	2.32	1.07
30	0.058	25.4	2.50	1.09
33	0.059	24.9	2.67	1.13
36	0.063	24.8	2.84	1.11
39	0.051	20.4	2.55	1.01
42	0.057	20.4	2.83	1.01

45	0.052	18.7	2.85	1.01
48	0.052	17.3	3.06	1.01
51	0.058	17.5	4.34	1.32
54	0.058	16.2	3.63	1.01
57	0.063	16.6	22.97	N/A
60	0.059	15.0	4.00	1.01
63	0.057	12.6	4.60	1.01
66	0.068	12.0	21.63	N/A
69	0.058	11.3	5.25	1.01
72	0.053	10.3	19.65	N/A
75	0.082	12.0	11.48	N/A
78	0.067	11.2	36.33	N/A
83	0.150	12.4	15.98	1.32
88	0.194	14.8	13.24	1.01
93	0.425	16.9	49.55	N/A
98	0.524	15.7	36.25	1.09
103	0.736	12.0	64.60	1.05
110	0.867	6.2	141.9	1.01
117	0.954	2.7	356.9	1.01
124	0.984	1.0	2347.7	N/A
131	0.997	0.2	17260.6	N/A
138	0.999	N/A	22805.7	1.01
145	0.99	N/A	N/A	N/A
152	0.99	N/A	N/A	N/A

C.2.2 $Fr = 7.6$

Location :	The University of Queensland (Australia)
Date :	May 2007
Experiments by :	F. MURZYN
Data processing by:	F. MURZYN
Data analysis by :	F. MURZYN and H. CHANSON
Experiment characteristics :	Channel: Length=3.2m, Width=0.50m, Slope=0º (horizontal). Open channel with glass sidewalls and PVC bottom. Q=0.029m^3/s, x_1=0.75m, d_1=0.018m, Fr=7.6, Re =57,250
Instrumentation :	Double-tip conductivity probe (∅=0.25 mm, Δx=7mm). Scan rate: 20 kHz per probe sensor, sampling duration: 45 sec.
Comments :	Initial conditions : partially-developed inflow Experiments 070523-24

$x - x_1 = 0.225m$

y (mm)	C	F (Hz)	ch_{mbc} (mm)	V (m/s)
3	0.007	12.0	1.21	2.09
6	0.017	24.0	1.38	1.97
9	0.033	40.4	1.81	2.19
12	0.046	50.8	2.01	2.22
15	0.070	66.8	2.28	2.19
18	0.093	77.4	2.72	2.26
21	0.122	92.1	2.78	2.09
24	0.129	92.7	2.64	1.89
27	0.161	98.6	3.27	2.00
30	0.164	96.3	3.13	1.84
33	0.194	93.0	3.84	1.84
38	0.208	82.2	4.60	1.82

43	0.190	69.7	4.66	1.71
48	0.186	56.7	4.94	1.51
53	0.179	43.6	9.76	2.37
58	0.172	33.6	19.95	3.89
63	0.151	31.7	21.48	4.52
68	0.134	27.3	29.92	N/A
73	0.134	25.0	32.69	N/A
80	0.217	32.1	41.20	N/A
87	0.253	34.0	45.30	N/A
94	0.478	30.6	95.03	N/A
101	0.601	27.4	133.35	N/A
108	0.750	19.3	236.4	N/A
115	0.878	10.7	500.9	N/A
122	0.923	6.6	848.6	N/A
129	0.956	3.9	1496.4	N/A
136	0.972	3.4	1717.0	N/A
143	0.973	2.4	2468.9	N/A

$x - x_1 = 0.300m$

y (mm)	C	F (Hz)	ch_{mbc} (mm)	V (m/s)
3	0.021	27.7	1.48	1.97
6	0.010	15.4	1.26	1.97
9	0.031	37.1	1.50	1.82
12	0.044	47.2	1.85	1.97
15	0.051	57.7	1.69	1.89
18	0.061	58.6	1.97	1.89
21	0.079	68.7	2.14	1.87
24	0.092	76.0	2.50	2.06
27	0.101	78.0	2.59	2.00
30	0.114	82.5	2.80	2.03
33	0.131	80.7	2.92	1.80
36	0.157	84.3	3.67	1.97
39	0.167	77.2	3.64	1.69
42	0.154	72.0	3.37	1.57
45	0.159	63.8	3.83	1.54
50	0.157	54.6	4.37	1.52
55	0.169	48.2	5.70	1.63
60	0.137	42.0	11.71	3.59
65	0.119	29.7	24.38	N/A
70	0.128	27.4	8.74	1.87
75	0.109	22.0	30.23	N/A
80	0.117	24.4	29.35	N/A
85	0.148	26.3	34.37	N/A
92	0.188	29.8	38.37	N/A
99	0.338	33.6	61.23	N/A
106	0.571	27.2	127.61	N/A
113	0.714	20.4	212.89	N/A
120	0.744	17.8	253.80	N/A
127	0.882	10.6	508.64	N/A
134	0.934	5.8	973.14	N/A
141	0.948	4.7	1224.9	N/A
148	0.962	3.1	908.5	2.92
155	0.983	1.1	5496.8	N/A
162	0.990	1.0	6027.3	N/A

169	0.985	1.3	4382.7	N/A
176	0.996	0.4	3353.9	1.27
183	0.996	0.4	3754.3	1.59
193	0.999	0.2	6053.3	1.08
203	1.000	0.2	2059.8	0.50

$x - x_1 = 0.450m$

y (mm)	C	F (Hz)	ch_{mbc} (mm)	V (m/s)
3	0.007	8.4	0.91	1.17
6	0.016	17.0	1.23	1.28
9	0.022	23.8	1.48	1.63
12	0.032	32.8	1.81	1.87
15	0.039	35.8	1.58	1.46
18	0.043	37.5	1.97	1.73
21	0.048	41.2	1.49	1.28
24	0.056	44.5	1.87	1.49
27	0.054	44.7	1.96	1.63
30	0.059	46.7	1.83	1.44
33	0.068	50.7	1.84	1.37
36	0.057	41.2	2.09	1.51
39	0.07	45.5	2.19	1.43
42	0.071	45.3	2.35	1.49
45	0.071	43.4	1.88	1.15
48	0.071	43.1	1.84	1.12
51	0.083	44.5	2.95	1.57
54	0.077	42.2	2.76	1.52
57	0.081	41.8	2.80	1.44
60	0.080	40.9	2.10	1.07
63	0.073	38.6	2.01	1.05
68	0.074	36.1	2.35	1.15
73	0.074	31.4	2.90	1.24
78	0.072	28.8	2.66	1.06
83	0.067	25.5	11.78	N/A
88	0.066	23.4	2.57	1.01
93	0.052	18.3	10.15	N/A
98	0.044	13.7	3.54	1.11
103	0.049	17.7	3.61	1.31
108	0.036	11.9	4.20	1.40
113	0.039	12.0	19.61	N/A
118	0.042	12.0	2.41	1.46
123	0.047	11.3	20.22	N/A
130	0.057	11.4	30.39	N/A
137	0.0167	15.2	23.95	N/A
144	0.297	19.0	50.75	N/A
151	0.383	18.5	55.73	N/A
158	0.665	13.7	295.2	N/A
165	0.667	13.7	296.8	N/A
172	0.867	7.7	449.6	N/A
179	0.919	3.7	548.3	N/A
186	0.970	2.6	462.3	1.25
193	0.973	1.5	976.1	1.54
203	0.996	0.4	4238.5	1.89
213	0.999	0.1	35977.8	N/A
223	1.000	N/A	11327.5	1.01

233	0.99_	0.4	2386.9	1.09
243	0.998	N/A	N/A	1.03

C.2.3 $Fr = 8.3$

Location :	The University of Queensland (Australia)
Date :	May 2007
Experiments by :	F. MURZYN
Data processing by:	F. MURZYN
Data analysis by :	F. MURZYN and H. CHANSON
Experiment characteristics :	Channel: Length=3.2m, Width=0.50m, Slope=0º (horizontal). Open channel with glass sidewalls and PVC bottom. Q=0.031m^3/s, x_1=0.75m, d_1=0.018m, Fr=8.3, Re=62,250
Instrumentation :	Double-tip conductivity probe (∅=0.25 mm, Δx=7mm). Scan rate: 20 kHz per probe sensor, sampling duration: 45 sec.
Comments :	Initial conditions : partially-developed inflow Experiments 070529-30

$x - x_1 = 0.225m$

y (mm)	C	F (Hz)	ch_{mbc} (mm)	V (m/s)
3	0.006	11.4	1.31	2.46
6	0.009	17.2	1.34	2.46
9	0.021	28.8	2.00	2.69
12	0.038	49.0	2.16	2.80
15	0.060	63.8	2.54	2.69
18	0.087	87.2	2.68	2.69
21	0.123	101.8	3.13	2.59
24	0.156	116.6	3.47	2.59
27	0.181	123.9	3.72	2.55
30	0.239	123.6	4.51	2.33
33	0.240	117.7	4.76	2.33
36	0.266	112.8	5.33	2.26
39	0.280	97.4	5.83	2.03
42	0.267	90.9	5.80	1.97
45	0.250	74.4	7.84	2.33
48	0.230	64.2	6.60	1.84
53	0.216	53.5	7.34	1.82
58	0.182	39.7	9.86	2.15
63	0.200	38.0	32.01	N/A
68	0.180	32.0	34.21	N/A
73	0.214	35.5	36.68	N/A
78	0.228	33.5	41.46	N/A
83	0.264	33.9	47.43	N/A
88	0.335	36.3	56.20	N/A
93	0.500	31.7	96.05	N/A
100	0.601	27.4	133.8	N/A
107	0.724	20.8	211.5	N/A
114	0.855	12.7	410.9	N/A
121	0.911	7.7	723.1	N/A
128	0.948	4.9	1169.1	N/A
138	0.959	4.5	1288.3	N/A
148	0.981	2.6	2336.1	N/A
158	0.978	2.3	2575.3	N/A

173	0.991	1.1	5539.7	N/A

$x - x_1 = 0.300m$

y (mm)	C	F (Hz)	ch_{mbc} (mm)	V (m/s)
3	0.005	8.6	1.39	2.46
6	0.007	12.1	1.43	2.41
9	0.023	34.1	1.59	2.37
12	0.034	46.1	1.93	2.59
15	0.051	62.0	2.13	2.59
18	0.073	72.9	2.50	2.50
21	0.089	82.4	2.48	2.30
24	0.105	92.6	2.70	2.37
27	0.134	100.0	2.98	2.22
30	0.152	103.6	3.21	2.19
33	0.168	104.4	3.63	2.26
36	0.177	101.6	3.34	1.92
39	0.192	95.5	4.21	2.09
42	0.207	87.4	4.54	1.92
45	0.212	77.4	5.79	2.12
48	0.206	70.4	5.25	1.80
53	0.184	64.0	4.78	1.67
58	0.179	44.5	9.23	2.30
63	0.177	42.4	9.89	2.37
68	0.161	33.3	19.38	N/A
73	0.128	26.0	23.81	N/A
78	0.141	25.6	33.56	N/A
83	0.108	22.2	29.69	N/A
90	0.189	26.4	43.76	N/A
97	0.268	30.6	53.27	N/A
104	0.297	31.5	57.42	N/A
111	0.475	27.4	105.8	N/A
118	0.612	24.8	150.2	N/A
125	0.743	17.8	253.4	N/A
132	0.884	10.0	539.1	N/A
139	0.873	9.1	585.8	N/A
146	0.918	6.9	808.9	N/A
153	0.957	3.5	1649.1	N/A
160	0.977	1.7	3475.8	N/A
167	0.976	2.0	2905.4	N/A
177	0.995	0.8	7169.6	N/A
187	0.991	0.8	7142.7	N/A
197	0.995	0.4	3521.6	N/A
207	0.999	0.1	57716.0	N/A

$x - x_1 = 0.450m$

y (mm)	C	F (Hz)	ch_{mbc} (mm)	V (m/s)
3	0.004	7.5	0.86	1.56
8	0.018	26.3	1.32	1.94
13	0.020	22.9	1.94	2.22
18	0.040	47.5	1.75	2.06
23	0.056	57.5	1.98	2.03
28	0.066	63.1	1.87	1.80

33	0.079	70.8	2.23	2.00
38	0.086	67.7	2.19	1.73
43	0.106	70.0	2.94	1.94
48	0.109	66.1	3.17	1.92
53	0.113	64.2	3.43	1.94
58	0.118	59.6	3.45	1.75
63	0.100	44.9	3.42	1.54
68	0.116	45.8	3.20	1.26
73	0.110	39.1	4.34	1.54
78	0.089	32.9	5.62	2.09
83	0.084	25.7	10.94	N/A
90	0.073	22.5	19.70	N/A
97	0.060	19.3	18.90	N/A
104	0.062	16.1	7.47	N/A
111	0.047	12.9	22.00	N/A
118	0.055	14.3	23.23	N/A
125	0.105	17.5	36.59	N/A
132	0.211	22.1	58.17	N/A
139	0.296	21.2	84.95	N/A
146	0.489	22.6	131.54	N/A
153	0.566	19.6	175.3	N/A
160	0.747	13.7	331.6	N/A
167	0.834	9.7	525.4	N/A
174	0.903	6.6	827.1	N/A
181	0.924	5.4	287.6	N/A
188	0.965	2.4	2470.2	N/A
195	0.979	1.8	3395.5	N/A
202	0.988	1.0	1989.5	N/A
212	0.988	1.0	1455.9	N/A
222	0.996	0.3	5095.4	N/A
232	0.998	0.3	11643.1	N/A
242	0.999	0.2	5069.5	N/A

$x - x_1 = 0.600m$

y (mm)	C	F (Hz)	ch_{mbc} (mm)	V (m/s)
3	0.008	9.3	0.96	1.05
8	0.015	14.6	1.44	1.39
13	0.022	20.1	1.47	1.37
18	0.032	29.3	1.59	1.47
23	0.038	34.2	1.73	1.56
28	0.045	38.2	1.55	1.32
33	0.044	34.7	2.26	1.80
38	0.050	35.6	1.67	1.20
43	0.067	47.1	1.96	1.39
48	0.063	43.4	1.83	1.26
53	0.066	40.3	2.95	1.80
60	0.055	35.0	1.68	1.06
67	0.070	39.4	2.44	1.37
74	0.073	37.9	3.10	1.61
81	0.066	33.3	2.15	1.09
88	0.073	31.5	3.26	1.40
95	0.059	25.6	3.08	1.33
102	0.058	24.6	2.37	1.01
109	0.056	22.5	2.66	1.07

116	0.060	22.2	3.02	1.12
123	0.049	17.1	3.23	1.12
130	0.038	12.7	5.41	1.82
137	0.036	12.7	8.81	N/A
144	0.043	13.6	8.55	N/A
151	0.082	16.4	17.17	N/A
158	0.081	12.7	21.26	N/A
165	0.154	19.1	48.97	N/A
172	0.221	15.8	85.30	N/A
179	0.478	19.4	86.18	N/A
186	0.664	15.4	263.24	N/A
193	0.747	11.4	105.91	N/A
200	0.888	6.9	181.2	N/A
207	0.932	3.8	406.5	N/A
214	0.956	2.5	1718.6	N/A
224	0.985	1.2	4420.6	N/A
234	0.992	1.0	2691.5	N/A
244	0.999	0.2	30396.5	N/A
254	1.000	0.1	91292	N/A

B.3 Measurements of turbulence intensity

B.3.1 Fr=5.1

Location :	The University of Queensland (Australia)
Date :	May 2007
Experiments by :	F. MURZYN
Data processing by:	F. MURZYN
Data analysis by :	F. MURZYN and H. CHANSON
Experiment characteristics :	Channel: Length=3.2m, Width=0.50m, Slope=0º (horizontal). Open channel with glass sidewalls and PVC bottom. Q=0.019m^3/s, x_1=0.75 m, d_1=0.018 m, Fr=5.1, Re=38,150
Instrumentation :	Double-tip conductivity probe (∅=0.25 mm, Δx=7mm). Scan rate: 20kHz per probe sensor, sampling duration: 45 sec.
Comments :	Initial conditions : partially-developed inflow Experiments 070528

x-x_1= 0.075 m		x-x_1= 0.150 m		x-x_1= 0.225 m	
y (mm)	Tu	y (mm)	Tu	y (mm)	Tu
12	0.73	12	0.37	6	0.21
18	1.05	18	1.40	15	0.38
24	1.26	24	1.21	24	0.52
30	1.49	30	1.47	33	0.84
36	2.83	36	1.98	42	0.55
--	--	42	3.60	51	0.78
--	--	--	--	60	0.61
--	--	--	--	69	0.5

B.3.2 Fr=7.6

Location :	The University of Queensland (Australia)
Date :	May 2007
Experiments by :	F. MURZYN

Data processing by:	F. MURZYN
Data analysis by :	F. MURZYN and H. CHANSON
Experiment characteristics :	Channel: Length=3.2m, Width=0.50m, Slope=0º (horizontal). Open channel with glass sidewalls and PVC bottom. Q=0.029m^3/s, x_1=0.75m, d_1=0.018m, Fr=7.6, Re =57,250
Instrumentation :	Double-tip conductivity probe (∅=0.25 mm, Δx=7mm). Scan rate: 20 kHz per probe sensor, sampling duration: 45 sec.
Comments :	Initial conditions : partially-developed inflow Experiments 070523-24

x-x_1= 0.225 m		x-x_1= 0.300 m		x-x_1= 0.450 m	
y (mm)	Tu	y (mm)	Tu	y (mm)	Tu
9	1.16	9	1.02	9	0.53
15	1.26	15	1.13	18	0.93
21	1.41	21	1.31	27	1.30
27	1.58	27	1.42	36	1.07
33	2.14	33	1.44	45	0.81
43	2.61	39	2.15	54	1.78
--	--	45	2.11	63	0.72
--	--	55	3.36	78	1.17

B.3.3 Fr=8.3

Location :	The University of Queensland (Australia)
Date :	May 2007
Experiments by :	F. MURZYN
Data processing by:	F. MURZYN
Data analysis by :	F. MURZYN and H. CHANSON
Experiment characteristics :	Channel: Length=3.2m, Width=0.50m, Slope=0º (horizontal). Open channel with glass sidewalls and PVC bottom. Q=0.031m^3/s, x_1=0.75m, d_1=0.018m, Fr=8.3, Re=62,250
Instrumentation :	Double-tip conductivity probe (∅=0.25 mm, Δx=7mm). Scan rate: 20 kHz per probe sensor, sampling duration: 45 sec.
Comments :	Initial conditions : partially-developed inflow Experiments 070529-30

x-x_1= 0.225 m		x-x_1= 0.300 m		x-x_1= 0.450 m		x-x_1= 0.600 m	
y (mm)	Tu	y (mm)	Tu	y (mm)	Tu	y (mm)	Tu
9	1.02	9	0.95	13	1.20	13	0.42
15	1.47	18	1.07	28	1.20	28	0.82
21	1.53	27	1.67	43	1.79	43	1.28
27	1.67	36	1.86	58	2.49	60	0.77
33	1.93	45	2.46	73	2.75	81	1.12
39	2.74	58	3.64	90	*10.9*	102	1.02
45	2.58	--	--	--	--	123	0.42
53	4.20	--	--	--	--	144	1.24

B.4 Measurements of auto-correlation integral time scale

B.4.1 Fr=5.1

Location :	The University of Queensland (Australia)

Date :	May 2007
Experiments by :	F. MURZYN
Data processing by:	F. MURZYN
Data analysis by :	F. MURZYN and H. CHANSON
Experiment characteristics :	Channel: Length=3.2m, Width=0.50m, Slope=0º (horizontal). Open channel with glass sidewalls and PVC bottom. Q=0.019m^3/s, x_1=0.75 m, d_1=0.018 m, Fr=5.1, Re=38,150
Instrumentation :	Double-tip conductivity probe (∅=0.25 mm, Δx=7mm). Scan rate: 20kHz per probe sensor, sampling duration: 45 sec.
Comments :	Initial conditions : partially-developed inflow Experiments 070528

Fr=	5.1
d_1 (m) =	0.018

$(x-x_1)/d_1$=	4.17	$(x-x_1)/d_1$=	8.33	$(x-x_1)/d_1$=	12.5
y/d_1	T_{xx} s	y/d_1	T_{xx} s	y/d_1	T_{xx} s
0.33	0.0018	0.67	0.0033	0.33	0.0015
0.67	0.0025	1.00	0.0038	0.83	0.0027
1.00	0.0034	1.33	0.0051	1.33	0.0033
1.33	0.0046	1.67	0.0053	1.83	0.0048
1.67	0.0072	2.00	0.0075	2.33	0.0044
2.00	0.0100	2.33	0.0096	2.83	0.0051
--	--	2.67	0.0119	3.33	0.0073
--	--	--	--	3.83	0.0084

B.4.2 Fr=7.6

Location :	The University of Queensland (Australia)
Date :	May 2007
Experiments by :	F. MURZYN
Data processing by:	F. MURZYN
Data analysis by :	F. MURZYN and H. CHANSON
Experiment characteristics :	Channel: Length=3.2m, Width=0.50m, Slope=0º (horizontal). Open channel with glass sidewalls and PVC bottom. Q=0.029m^3/s, x_1=0.75m, d_1=0.018m, Fr=7.6, Re =57,250
Instrumentation :	Double-tip conductivity probe (∅=0.25 mm, Δx=7mm). Scan rate: 20 kHz per probe sensor, sampling duration: 45 sec.
Comments :	Initial conditions : partially-developed inflow Experiments 070523-24

Fr=	7.6
d_1 (m) =	0.018

$(x-x_1)/d_1$=	12.5	$(x-x_1)/d_1$=	16.67	$(x-x_1)/d_1$=	25.00
y/d_1	T_{xx} s	y/d_1	T_{xx} s	y/d_1	T_{xx} s
0.50	0.0038	0.50	0.0033	0.50	0.0021
0.83	0.0041	0.83	0.0033	1.00	0.0032
1.17	0.0042	1.17	0.0042	1.50	0.0033
1.50	0.0049	1.50	0.0045	2.00	0.0032
1.83	0.0063	1.83	0.0050	2.50	0.0037
2.39	0.0077	2.17	0.0067	3.00	0.0042

2.94	0.0108	2.50	0.0073	3.50	0.0043
--	--	3.06	0.0100	4.33	0.0051
--	--	--	--	5.17	0.0050
--	--	--	--	5.56	0.0048

B.4.3 Fr=8.3

Location :	The University of Queensland (Australia)
Date :	May 2007
Experiments by :	F. MURZYN
Data processing by:	F. MURZYN
Data analysis by :	F. MURZYN and H. CHANSON
Experiment characteristics :	Channel: Length=3.2m, Width=0.50m, Slope=0º (horizontal). Open channel with glass sidewalls and PVC bottom. Q=0.031m^3/s, x_1=0.75m, d_1=0.018m, Fr=8.3, Re=62,250
Instrumentation :	Double-tip conductivity probe (∅=0.25 mm, Δx=7mm). Scan rate: 20 kHz per probe sensor, sampling duration: 45 sec.
Comments :	Initial conditions : partially-developed inflow Experiments 070529-30

Fr=	8.30
d_1 (m) =	0.018

$(x-x_1)/d_1$=	12.5	$(x-x_1)/d_1$=	16.67	$(x-x_1)/d_1$=	25.00	$(x-x_1)/d_1$=	33.33
y/d_1	T_{xx} s	y/d_1	T_{xx} s	y/d_1	T_{xx} s	y/d_1	T_{xx} s
0.50	0.0029	0.50	0.0023	0.72	0.0027	0.72	0.0019
0.83	0.0032	1.00	0.0037	1.56	0.0032	1.56	0.0026
1.17	0.0037	1.50	0.0045	2.39	0.0045	2.39	0.0032
1.50	0.0043	2.00	0.0051	3.22	0.0057	3.33	0.0031
1.83	0.0050	2.50	0.0071	4.06	0.0078	4.50	0.0034
2.17	0.0068	3.22	0.0096	5.00	0.0077	5.67	0.0038
2.50	0.0079	--	--	--	--	6.83	0.0049
2.94	0.0088	--	--	--	--	8.00	0.0049

APPENDIX D - CHARACTERISTIC PROPERTIES OF VOID FRACTION, BUBBLE COUNT RATE AND VELOCITY DISTRIBUTIONS IN HYDRAULIC JUMPS WITH PARTIALLY-DEVELOPED INFLOW CONDITIONS

Run	d_1 m	Fr	x_1 m	x-x_1 m	Y_{Cmax} m	C_{max}	Y_{Fmax} m	F_{max} Hz	V_{max} m/s	y_{Vmax} m
1	0.018	5.1	0.75	0.075	0.03	0.218	0.027	55.4	1.69	0.003
				0.15	0.039	0.175	0.03	43.2	1.59	0.018
				0.225	0.036	0.063	0.03	25.4	1.13	0.033
2	0.018	7.6	0.75	0.225	0.038	0.208	0.027	98.6	2.26	0.018
				0.30	0.039	0.167	0.036	84.3	2.06	0.024
				0.45	0.051	0.083	0.033	50.7	1.87	0.012
3	0.018	8.3	0.75	0.225	0.039	0.280	0.027	123.9	2.80	0.012
				0.30	0.045	0.212	0.033	104.4	2.59	0.012
				0.45	0.058	0.118	0.033	70.8	2.22	0.013
				0.60	0.074	0.073	0.043	47.1	1.795	0.033

Notation

C void fraction defined as the volume of air per unit volume of air and water; it is also called air concentration or local air content;

C_{max} maximum void fraction in the air bubble diffusion layer;

d water depth (m);

d_1 flow depth (m) measured immediately upstream of the hydraulic jump;

Fr upstream Froude number: $Fr = \frac{q}{\sqrt{g d_1^3}}$;

F_{max} maximum bubble count rate (Hz) at a given cross-section;

g gravity acceleration (m/s^2) : g = 9.80 m/s^2 in Brisbane (Australia);

Q water discharge (m^3/s);

q water discharge per unit width (m^2/s): $q = Q/W$;

V_{max} maximum velocity (m/s) in the wall jet;

W channel width (m);

x longitudinal distance from the sluice gate (m);

x_1 longitudinal distance from the gate to the jump toe (m);

y distance (m) measured normal to the channel bed;

y_{Cmax} distance (m) normal to the jet support where $C = C_{max}$;

y_{Fmax} distance (m) normal to the jet support where $F = F_{max}$;

y_{Vmax} distance (m) from invert where $V = V_{max}$;

Subscript

1 upstream flow conditions.

REFERENCES

AMADOR, A., SANCHEZ-JUNY, M., and DOLZ, J. (2006). "Characterization of the Nonaerated Flow Region in a Stepped Spillway by PIV." *Journal of Fluids Engineering*, Trans. ASME, Vol. 128, No. 6, pp. 1266-1273.

BELANGER, J.B. (1828). "Essai sur la Solution Numérique de quelques Problèmes Relatifs au Mouvement Permanent des Eaux Courantes." ('Essay on the Numerical Solution of Some Problems relative to Steady Flow of Water.') *Carilian-Goeury*, Paris, France (in French).

BROCCHINI, M., and PEREGRINE, D.H. (2001). "The Dynamics of Strong Turbulence at Free Surfaces. Part 1. Description." *Journal of Fluid Mechanics*, Vol. 449, pp. 225-254.

CAROSI, G., and CHANSON, H. (2006). "Air-Water Time and Length Scales in Skimming Flows on a Stepped Spillway. Application to the Spray Characterisation." *Report No. CH59/06*, Div. of Civil Engineering, The University of Queensland, Brisbane, Australia, July, 142 pages (ISBN 1864998601).

CHANSON, H. (1995). "Air Entrainment in Two-Dimensional Turbulent Shear Flows with Partially Developed Inflow Conditions." *International Journal of Multiphase Flow*, Vol. 21, No. 6, pp. 1107-1121.

CHANSON, H. (1997). "*Air Bubble Entrainment in Free-Surface Turbulent Shear Flows*." *Academic Press*, London, UK, 401 pages.

CHANSON, H. (1999). "The Hydraulics of Open Channel Flow : An Introduction." *Edward Arnold*, London, UK, 512 pages (ISBN 0 340 74067 1).

CHANSON, H. (2001). "Flow Field in a Tidal Bore : a Physical Model." *Proc. 29th IAHR Congress*, Beijing, China, Theme E, Tsinghua University Press, Beijing, G. LI Ed., pp. 365-373. (CD-ROM, Tsinghua University Press.)

CHANSON, H. (2002). "Air-Water Flow Measurements with Intrusive Phase-Detection Probes. Can we Improve their Interpretation ?" *Journal of Hydraulic Engineering*, Trans. ASCE, Vol. 128, No. 3, pp. 252-255

CHANSON, H. (2004). "The Hydraulics of Open Channel Flow : An Introduction." *Butterworth-Heinemann*, Oxford, UK, 2nd edition, 630 pages (ISBN 978 0 7506 5978 9).

CHANSON, H. (2004). "Air-Water Flows in Water Engineering and Hydraulic Structures. Basic Processes and Metrology." *Proc. Intl Conf. on Hydraulics of Dams and River Structures*, Tehran, Iran, Keynote lecture, Balkema Publ., The Netherlands, F. YAZDANDOOST and J. ATTARI Ed., pp. 3-16 (ISBN 978-90-5809-632-6). (Also CD-ROM, Taylor & Francis, ISBN 90 5809 683 4.)

CHANSON, H. (2005). "Physical Modelling of the Flow Field in an Undular Tidal Bore." *Journal of Hydraulic Research*, IAHR, Vol. 43, No. 3, pp. 234-244.

CHANSON, H. (2005b). "Air-Water and Momentum Exchanges in Unsteady Surging Waters : an Experimental Study." *Experimental Thermal and Fluid Science*, Vol. 30, No. 1, pp. 37-47.

CHANSON, H. (2006). "Air Bubble Entrainment in Hydraulic Jumps. Similitude and Scale Effects." *Report No. CH57/05*, Dept. of Civil Engineering, The University of Queensland, Brisbane, Australia, Jan., 119 pages (ISBN 1864998423).

CHANSON, H. (2007). "Bubbly Flow Structure in Hydraulic Jump." *European Journal of Mechanics B/Fluids*, Vol. 26, No. 3, pp.367-384 (DOI:10.1016/j.euromechflu.2006.08.001).

CHANSON, H. (2007b). "Advective Diffusion of Air Bubbles in Turbulent Water Flows." in "Fluid Mechanics of Environmental Interfaces", *Taylor & Francis*, Leiden, The Netherlands, C. GUALTIERI and D.T. MIHAILOVIC Editors (ISBN 978-0-415-44669-3).

CHANSON, H. (2007c). "Dynamic Similarity and Scale Effects Affecting Air Bubble Entrainment in Hydraulic Jumps." *Proc. 6th International Conference on Multiphase Flow ICMF 2007*, Leipzig, Germany, July 9-13, M. SOMMERFIELD Editor, Session 7, Paper S7_Mon_B_S7_Mon_B_3, 11 pages (CD-ROM) (ISBN 978-3-86010-913-7).

CHANSON, H., AOKI, S., and HOQUE, A. (2002). "Scaling Bubble Entrainment and Dispersion in Vertical Circular Plunging Jet Flows: Freshwater versus Seawater." *Proc. 5th Intl Conf. on Hydrodynamics ICHD 2002*, Tainan, Taiwan, H.H. HWUNG, J.F. LEE & K.S. HWANG Editors, pp. 431-436.

CHANSON, H., AOKI, S., and HOQUE, A. (2006). "Bubble Entrainment and Dispersion in Plunging Jet Flows: Freshwater versus Seawater." *Journal of Coastal Research*, Vol. 22, No. 3, May, pp. 664-677.

CHANSON, H., AOKI, S., and MARUYAMA, M. (1999). "Air Bubble Entrainment at Plunging Breakers and its Effect on Long Period Waves: an Experimental study." *Coastal/Ocean Engineering Report*, No. COE99-1, Dept. of Architecture and Civil Eng., Toyohashi University of Technology, Japan, July, 41 pages.

CHANSON, H., AOKI, S., and MARUYAMA, M. (2002). "Unsteady Air Bubble Entrainment and Detrainment at a Plunging Breaker: Dominant Time Scales and Similarity of Water Level Variations." *Coastal Engineering*, Vol. 46, No. 2, pp. 139-157.

CHANSON, H., and BRATTBERG, T. (1997). "Experimental Investigations of Air Bubble Entrainment in Developing Shear Layers." *Report CH48/97*, Dept. of Civil Engineering, University of Queensland, Australia, Oct., 309 pages (ISBN 0 86776 748 0).

CHANSON, H., and BRATTBERG, T. (2000). "Experimental Study of the Air-Water Shear Flow in a Hydraulic Jump." *International Journal of Multiphase Flow*, Vol. 26, No. 4, pp. 583-607.

CHANSON, H., and CAROSI, G. (2006a). "Advanced Post-Processing and Correlation Analyses in High-Velocity Air-Water Flows. 1- Macroscopic Properties." *Proceedings of the International Junior Researcher and Engineer Workshop on Hydraulic Structures (IJREWHS'06)*, Montemor-o-Novo, Jorge MATOS and Hubert CHANSON Eds., Report CH61/06, Div. of Civil Engineering, The University of Queensland, Brisbane, Australia, Dec., pp 139-148 (ISBN 1864998687).

CHANSON, H., and CAROSI, G. (2006b). "Advanced Post-Processing and Correlation Analyses in High-Velocity Air-Water Flows. 2- Microscopic Properties." *Proceedings of the International Junior Researcher and Engineer Workshop on Hydraulic Structures (IJREWHS'06)*, Montemor-

o-Novo, Jorge MATOS and Hubert CHANSON Eds., Report CH61/06, Div. of Civil Engineering, The University of Queensland, Brisbane, Australia, Dec., pp 149-158 (ISBN 1864998687).

CHANSON, H., and CAROSI, G. (2007). "Turbulent Time and Length Scale Measurements in High-Velocity Open Channel Flows." *Experiments in Fluids*, Vol. 42, No. 3, pp. 385-401 (DOI 10.1007/s00348-006-0246-2).

CHANSON, H., and TOOMBES, L. (2002). "Air-Water Flows down Stepped chutes : Turbulence and Flow Structure Observations." *International Journal of Multiphase Flow*, Vol. 28, No. 11, pp. 1737-1761.

CHANSON, H., and TOOMBES, L. (2002b). "Experimental Study of Gas-Liquid Interfacial Properties in a Stepped Cascade Flow." *Environmental Fluid Mechanics*, Vol. 2, No. 3, pp. 241-263.

CHOW, V.T. (1959). "Open Channel Hydraulics." *McGraw-Hill*, New York, USA.

CROWE, C., SOMMERFIELD, M., and TSUJI, Y. (1998). "Multiphase Flows with Droplets and Particles." *CRC Press*, Boca Raton, USA, 471 pages.

ERVINE, D.A., and FALVEY, H.T. (1987). "Behaviour of Turbulent Water Jets in the Atmosphere and in Plunge Pools." *Proc. Instn Civ. Engrs., London*, Part 2, Mar. 1987, 83, pp. 295-314. Discussion : Part 2, Mar.-June 1988, 85, pp. 359-363.

GUALTIERI, C., and CHANSON, H. (2007). "Experimental Analysis of Froude Number Effect on Air Entrainment in the Hydraulic Jump." *Environmental Fluid Mechanics*, Vol. 5, pp. 217-238, (DOI:10.1007/s10654-006-9016-1).

HAGER, W.H., BREMEN, R., and KAWAGOSHI, N. (1990). "Classical Hydraulic Jump : Length of Roller." *Journal of Hydraulic Research*, IAHR, Vol. 28, No. 5, pp. 591-608.

HENDERSON, F.M. (1966). "Open Channel Flow." *MacMillan Company*, New York, USA.

KOBUS, H. (1984). "Scale Effects in Modelling Hydraulic Structures." *Proc. Intl Symp. on Scale Effects in Modelling Hydraulic Structures*, IAHR, Esslingen, Germany.

KOCH, C., and CHANSON, H. (2005). "An Experimental Study of Tidal Bores and Positive Surges: Hydrodynamics and Turbulence of the Bore Front." *Report No. CH56/05*, Dept. of Civil Engineering, The University of Queensland, Brisbane, Australia, July, 170 pages (ISBN 978-1-86499-824-5).

KUCUKALI, S., and CHANSON, H. (2007). "Turbulence in hydraulic jumps: experimental measurements", *Research Report No. CH62/07*, Dept. of Civil Engineering, The University of Queensland, Brisbane, Australia, July, 40 pages (ISBN 9781864998825).

LIU, M., RAJARATNAM, N., and ZHU, D.Z. (2004). "Turbulent Structure of Hydraulic Jumps of Low Froude Numbers." *Journal of Hydraulic Engrg*, Trans. ASCE, Vol. 130, No. 6, pp. 511-520.

MADSEN, P.A. (1981). "A Model for a Turbulent Bore." *Ph.D. thesis*, Tech. Univ. of Denmark, Inst. of Hydrodyamics and Hyd. Eng., Copenhager, Denmark, 149 pages. (also Series Paper No. 28, Tech. Univ. of Denmark, Inst. of Hydrodyamics and Hyd. Eng., Copenhager, Denmark, 149 pages.)

MOSSA, M., TOLVE, U. (1998). "Flow Visualization in Bubbly Two Phase Hydraulic Jumps." *Journal of Fluids Engineering*, Trans. ASME, Vol. 120, ppP 160-165.

MOUAZE, D., MURZYN, F., and CHAPLIN, J.R. (2004). "Turbulence at Free surface in Hydraulic Jumps." *Proceedings of 2004 ASME Heat Transfer / Fluids Engineering Summer Conference*, Charlotte (NC), USA, Paper No. 56077, 5 pages.

MOUAZE, D., MURZYN, F., and CHAPLIN, J.R. (2005). "Free Surface Length Scale Estimation in Hydraulic Jumps." *Journal of Fluids Engineering*, Trans. ASME, Vol. 127, pp. 1191-1193.

MURZYN, F., (2002). "Etude Experimentale de l'Influence d'une Onde sur les Echelles de Turbulence. Application à la Houle." *Ph.D. thesis*, Université de Caen-Basse Normandie, 201 pages (in French).

MURZYN, F., MOUAZE, D., and CHAPLIN, J.R. (2005). "Optical Fibre Probe Measurements of Bubbly Flow in Hydraulic Jumps." *International Journal of Multiphase Flow*, Vol. 31, No. 1, pp. 141-154.

MURZYN, F., MOUAZE, D., and CHAPLIN, J.R. (2007). "Air-Water Interface Dynamic and Free Surface Features in Hydraulic Jumps." *Journal of Hydraulic Research*, IAHR, Vol. 45, No. 5, pp. 679-685.

RAJARATNAM, N. (1962). "An Experimental Study of Air Entrainment Characteristics of the Hydraulic Jump." *Journal of Instn. Eng. India*, Vol. 42, No. 7, March, pp. 247-273.

RAJARATNAM, N. (1965). "The Hydraulic Jump as a Wall Jet." *Journal of Hydraulic Division*, ASCE, Vol. 91, No. HY5, pp. 107-132. Discussion : Vol. 92, No. HY3, pp. 110-123 & Vol. 93, No. HY1, pp. 74-76.

RESCH, F.J., and LEUTHEUSSER, H.J. (1972). "Le Ressaut Hydraulique : mesure de Turbulence dans la Région Diphasique. " ('The Hydraulic Jump : Turbulence Measurements in the Two-Phase Flow Region.'), *La Houille Blanche*, No. 4, pp. 279-293 (in French).

RESCH, F.J., and LEUTHEUSSER, H.J. (1972b). "Reynolds Stress Measurements in Hydraulic Jumps." *Journal of Hydraulic Research*, IAHR, Vol. 10, No. 4, pp. 409-429.

ROUSE, H., SIAO, T.T., and NAGARATNAM, S. **(**1959). "Turbulence Characteristics of the Hydraulic Jump." *Transactions*, ASCE, Vol. 124, pp. 926-966.

RYU, Y., CHANG, K.A., and LIM, H.J. (2005). "Use of Bubble imaging Velocimetry for Measurement of Plunging wave Impinging on Structure and Associated Greenwater." *Measurement Science Technology*, Vol. 16, No. 10, pp. 1945-1953.

TENNEKES, H., and LUMLEY, J.L. (1997). "A First Course in Turbulence." *MIT Press*, USA, 16th edition.

TOOMBES, L., and CHANSON, H. (2007). "Surface Waves and Roughness in Self-Aerated Supercritical Flow." *Environmental Fluid Mechanics*, Vol. 5, No. 3, pp. 259-270 (DOI 10.1007/s10652-007-9022-y).

WOOD, I.R. (1991). "Air Entrainment in Free-Surface Flows." *IAHR Hydraulic Structures Design Manual No. 4*, Hydraulic Design Considerations, Balkema Publ., Rotterdam, The Netherlands, 149 pages.

OTHERS REFERENCES

INTERNET REFERENCES

Air entrainment on chute and stepped spillways	{http://www.uq.edu.au/~e2hchans/self_aer.html}
Air entraiment at a circular plunging jet: physical and acoustic characteristics - Internet Database	{http://www.uq.edu.au/~e2hchans/bubble/}
Air entrainment in the developing flow region of two-dimensional plunging jets - Databank	{http://www.uq.edu.au/~e2hchans/data/jfe97.html}

Open Access Repositories

EprintsUq	{http://eprint.uq.edu.au/}
OAIster	{http://www.oaister.org/}
UQeSpace	{http://espace.library.uq.edu.au/}

BIBLIOGRAPHIC REFERENCE OF THE REPORT CH63/07

The Hydraulic Model research report series CH is a refereed publication published by the Division of Civil Engineering at the University of Queensland, Brisbane, Australia.

The bibliographic reference of the present report is :

MURZYN, F., and CHANSON, H. (2007). "Free Surface, Bubbly Flow and Turbulence Measurements in Hydraulic Jumps." *Report No. CH63/07*, Div. of Civil Engineering, The University of Queensland, Brisbane, Australia, July, 116 pages (ISBN 9781864998917).

The Report CH63/07 is available, in the present form, as a PDF file on the Internet at UQeSpace :

http://espace.library.uq.edu.au/

It is listed at :

http://espace.library.uq.edu.au/list.php?browse=author&author_id=193

HYDRAULIC MODEL RESEARCH REPORT CH

The Hydraulic Model Report CH series is published by the Division of Civil Engineering at the University of Queensland. Orders of any of the Hydraulic Model Reports should be addressed to the Departmental Secretary.

Departmental Secretary, Div. of Civil Engineering, The University of Queensland
Brisbane 4072, Australia - Tel.: (61 7) 3365 3619 - Fax : (61 7) 3365 4599
Url: http://www.eng.uq.edu.au/civil/ Email: hodciveng@uq.edu.au

Report CH	**Unit price**	Quantity	**Total price**
MURZYN, F., and CHANSON, H. (2007). "Free Surface, Bubbly flow and Turbulence Measurements in Hydraulic Jumps." *Report No. CH63/07*, Div. of Civil Engineering, The University of Queensland, Brisbane, Australia, July, 116 pages (ISBN 9781864998917).	AUD$60.00		
KUCUKALI, S., and CHANSON, H. (2007). "Turbulence in Hydraulic Jumps: Experimental Measurements." *Report No. CH62/07*, Div. of Civil Engineering, The University of Queensland, Brisbane, Australia, July, 96 pages (ISBN 9781864998825).	AUD$60.00		
MATOS, J., and CHANSON, H. (2006). "Hydraulic Structures: a Challenge to Engineers and Researchers." Proc. Intl Junior Researcher and Engineer Workshop on Hydraulic Structures (IJREWHS'06), 2-4 Sept., Montemor-o-Novo, Portugal, Report No. CH61/06, Div. of Civil Engineering, The University of Queensland, Brisbane, Australia, Dec., 205 pages (ISBN 1864998687).	AUD$100		
CHANSON, H., TAKEUCHI, M, and TREVETHAN, M. (2006). "Using Turbidity and Acoustic Backscatter Intensity as Surrogate Measures of Suspended Sediment Concentration. Application to a Sub-Tropical Estuary (Eprapah Creek)." *Report No. CH60/06*, Div. of Civil Engineering, The University of Queensland, Brisbane, Australia, July (ISBN 1864998628).	AUD$60.00		
CAROSI, G., and CHANSON, H. (2006). "Air-Water Time and Length Scales in Skimming Flows on a Stepped Spillway. Application to the Spray Characterisation." *Report No. CH59/06*, Div. of Civil Engineering, The University of Queensland, Brisbane, Australia, July (ISBN 1864998601).	AUD$60.00		
TREVETHAN, M., CHANSON, H., and BROWN, R. (2006). "Two Series of Detailed Turbulence Measurements in a Small Sub-Tropical Estuarine System." *Report No. CH58/06*, Div. of Civil Engineering, The University of Queensland, Brisbane, Australia, Mar. (ISBN 1864998520).	AUD$60.00		
KOCH, C., and CHANSON, H. (2005). "An Experimental Study of Tidal Bores and Positive Surges: Hydrodynamics and Turbulence of the Bore Front." *Report No. CH56/05*, Dept. of Civil Engineering, The University of Queensland, Brisbane, Australia, July (ISBN 1864998245).	AUD$60.00		
CHANSON, H. (2005). "Applications of the Saint-Venant Equations and Method of Characteristics to the Dam Break Wave Problem." *Report No. CH55/05*, Dept. of Civil Engineering, The University of Queensland, Brisbane, Australia, May (ISBN 1864997966).	AUD$60.00		
CHANSON, H., COUSSOT, P., JARNY, S., and TOQUER, L. (2004). "A Study of Dam Break Wave of Thixotropic Fluid: Bentonite Surges down an Inclined plane." *Report No. CH54/04*, Dept. of Civil Engineering, The University of Queensland, Brisbane, Australia, June, 90 pages (ISBN 1864997710).	AUD$60.00		

CHANSON, H. (2003). "A Hydraulic, Environmental and Ecological Assessment of a Sub-tropical Stream in Eastern Australia: Eprapah Creek, Victoria Point QLD on 4 April 2003." *Report No. CH52/03*, Dept. of Civil Engineering, The University of Queensland, Brisbane, Australia, June, 189 pages (ISBN 1864997044).	AUD$90.00		
CHANSON, H. (2003). "Sudden Flood Release down a Stepped Cascade. Unsteady Air-Water Flow Measurements. Applications to Wave Run-up, Flash Flood and Dam Break Wave." *Report CH51/03*, Dept of Civil Eng., Univ. of Queensland, Brisbane, Australia, 142 pages (ISBN 1864996552).	AUD$60.00		
CHANSON, H,. (2002). "An Experimental Study of Roman Dropshaft Operation : Hydraulics, Two-Phase Flow, Acoustics." *Report CH50/02*, Dept of Civil Eng., Univ. of Queensland, Brisbane, Australia, 99 pages (ISBN 1864996544).	AUD$60.00		
CHANSON, H., and BRATTBERG, T. (1997). "Experimental Investigations of Air Bubble Entrainment in Developing Shear Layers." *Report CH48/97*, Dept. of Civil Engineering, University of Queensland, Australia, Oct., 309 pages (ISBN 0 86776 748 0).	AUD$90.00		
CHANSON, H. (1996). "Some Hydraulic Aspects during Overflow above Inflatable Flexible Membrane Dam." *Report CH47/96*, Dept. of Civil Engineering, University of Queensland, Australia, May, 60 pages (ISBN 0 86776 644 1).	AUD$60.00		
CHANSON, H. (1995). "Flow Characteristics of Undular Hydraulic Jumps. Comparison with Near-Critical Flows." *Report CH45/95*, Dept. of Civil Engineering, University of Queensland, Australia, June, 202 pages (ISBN 0 86776 612 3).	AUD$60.00		
CHANSON, H. (1995). "Air Bubble Entrainment in Free-surface Turbulent Flows. Experimental Investigations." *Report CH46/95*, Dept. of Civil Engineering, University of Queensland, Australia, June, 368 pages (ISBN 0 86776 611 5).	AUD$80.00		
CHANSON, H. (1994). "Hydraulic Design of Stepped Channels and Spillways." *Report CH43/94*, Dept. of Civil Engineering, University of Queensland, Australia, Feb., 169 pages (ISBN 0 86776 560 7).	AUD$60.00		
POSTAGE & HANDLING (per report)	AUD$10.00		
GRAND TOTAL			

OTHER HYDRAULIC RESEARCH REPORTS

Reports/Theses	Unit price	Quantity	Total price
GONZALEZ, C.A. (2005). "An Experimental Study of Free-Surface Aeration on Embankment Stepped Chutes." *Ph.D. thesis*, Dept of Civil Engineering, The University of Queensland, Brisbane, Australia, 240 pages.	AUD$80.00		
TOOMBES, L. (2002). "Experimental Study of Air-Water Flow Properties on Low-Gradient Stepped Cascades." *Ph.D. thesis*, Dept of Civil Engineering, The University of Queensland, Brisbane, Australia.	AUD$120.00		
CHANSON, H. (1988). "A Study of Air Entrainment and Aeration Devices on a Spillway Model." *Ph.D. thesis*, University of Canterbury, New Zealand.	AUD$60.00		
POSTAGE & HANDLING (per report)	AUD$10.00		
GRAND TOTAL			

CIVIL ENGINEERING RESEARCH REPORT CE

The Civil Engineering Research Report CE series is published by the Division of Civil Engineering at the University of Queensland. Orders of any of the Civil Engineering Research Report CE should be addressed to the Departmental Secretary.

Departmental Secretary, Dept. of Civil Engineering, The University of Queensland
Brisbane 4072, Australia
Tel.: (61 7) 3365 3619 Fax : (61 7) 3365 4599
Url: http://www.eng.uq.edu.au/civil/ Email: hodciveng@uq.edu.au

Recent Research Report CE	Unit price	Quantity	Total price
CALLAGHAN, D. P., NIELSEN, P. and CARTWRIGHT, N. (2006). "Data and Analysis Report: Manihiki and Rakahanga, Northern Cook Islands - For February and October/November 2004 Research Trips." *Research Report No. CE161*, Division of Civil Engineering, The University of Queensland, Brisbane, Australia (ISBN 1864998318).	AUD$40.00		
GONZALEZ, C.A., TAKAHASHI, M., and CHANSON, H. (2005). "Effects of Step Roughness in Skimming Flows: an Experimental Study." *Research Report No. CE160*, Dept. of Civil Engineering, The University of Queensland, Brisbane, Australia, July (ISBN 1864998105).	AUD$40.00		
CHANSON, H., and TOOMBES, L. (2001). "Experimental Investigations of Air Entrainment in Transition and Skimming Flows down a Stepped Chute. Application to Embankment Overflow Stepped Spillways." *Research Report No. CE158*, Dept. of Civil Engineering, The University of Queensland, Brisbane, Australia, July, 74 pages (ISBN 1 864995297).	AUD$40.00		
HANDLING (per order)	AUD$10.00		
GRAND TOTAL			

Note: Prices include postages and processing.

PAYMENT INFORMATION

1- VISA Card

Name on the card :	
Visa card number :	
Expiry date :	

Amount :	AUD$ .....

2- Cheque/remittance payable to : THE UNIVERSITY OF QUEENSLAND and crossed "Not Negotiable".

N.B. For overseas buyers, cheque payable in Australian Dollars drawn on an office in Australia of a bank operating in Australia, payable to: THE UNIVERSITY OF QUEENSLAND and crossed "Not Negotiable".

Orders of any Research Report should be addressed to the Departmental Secretary.

Departmental Secretary, Div. of Civil Engineering, The University of Queensland
Brisbane 4072, Australia - Tel.: (61 7) 3365 3619 - Fax : (61 7) 3365 4599
Url: http://www.eng.uq.edu.au/civil/ Email: hodciveng@uq.edu.au